THERMODYNAMIC ANALYSIS AND MODELING STUDY OF AN INTERMITTENT SOLAR ADSORPTION REFRIGERATION SYSTEM

BY

NAEF QASEM

A Thesis Presented to the
DEANSHIP OF GRADUATE STUDIES

KING FAHD UNIVERSITY OF PETROLEUM & MINERALS

DHAHRAN, SAUDI ARABIA

In Partial Fulfillment of the
Requirements for the Degree of

MASTER OF SCIENCE

In

MECHANICAL ENGINEERING

MAY, 2013

KING FAHD UNIVERSITY OF PETROLEUM & MINERALS

DHAHRAN- 31261, SAUDI ARABIA

DEANSHIP OF GRADUATE STUDIES

This thesis, written by **NAEF ABDULJALIL ABDULRAHMAN QASEM** under the direction his thesis advisor and approved by his thesis committee, has been presented and accepted by the Dean of Graduate Studies, in partial fulfillment of the requirements for the degree of **MASTER OF SCIENCE IN MECHANICAL ENGINEERING.**

Dr. Maged A. I. El-Shaarawi
(Advisor)

Dr. Zuhair M. Gasem
Department Chairman

Dr. Syed A. M. Said
(Member)

Dr. Salam A. Zummo
Dean of Graduate Studies

Dr. Amro M. Al-Qutub
(Member)

19/5/13

Date

Dedication

To my beloved parents, wife, brothers, sisters and my small daughter.

ACKNOWLEDGMENTS

Thanks and all praise be to Allah (azzawagal) who created me, blessed me with health and who grant me success.

I would like to state my deep appreciation and gratitude to my thesis advisor Prof. Maged A. I. El-Shaarawi who has always been providing kindest support, continual encouragement and supervision.

I also would like to acknowledge my committee members: Prof. Syed A. M. Said and Prof. Amro M. Al-Qutub for their valuable advices and guidance.

I also acknowledge KFUPM and Mechanical Engineering Department (ME) as well as the all faculties who taught and helped me.

Finally, I acknowledge Kingdom of Saudi Arabia for providing me MS scholarship and for all different facilitations.

TABLE OF CONTENTS

LIST OF TABLES

LIST OF FIGURES

NOMENCLATURE

A	area (m^2)
COP	Coefficient of Performance
C_p	specific heat at constant pressure (J/kg K)
C_v	specific heat at constant volume (J/kg K)
D	Dubinin-Astakhov constant (K^{-1})
D1	diameter of inner pass tube (m)
D2	internal diameter of absorber tube (m)
D3	external diameter of absorber tube (m)
D_o	surface diffusion coefficient (m^2/s)
E_a	activation energy of surface diffusion (J/mol)
E_o	characteristic adsorption energy for a reference vapour (J/mole)
ESCOP	Effective Solar Coefficient of Performance
h	specific enthalpy (J/kg)
h	heat transfer coefficient (W/m^2K)
H	heat of desorption or adsorption per unit mass of methanol (J/kg)
I_T	incident solar radiation (W/m^2)
k	thermal conductivity (W/m K)
k	adsorbent constant
L	latent heat (J/kg)
L_c	collector length (m)
M, m	mass (kg)
m_m	methanol uptake (kg)
n	Dubinin-Astakhov constant
N_g	number of glass cover
n_{tube}	number of absorber tubes
P	system pressure (Pa)
Q	heat amount (J)
R	gas constant (J/mole K)
r	radius (m)
R1	radius of inner pass tube (m)
R2	internal radius of absorber tube (m)
R3	external radius of absorber tube (m)
r_p	average radius of adsorbent particles (m)
SCOP	Solar Coefficient of Performance
SCP	Specific Cooling Power (W/kg)

T	temperature (^oC or K)
t	time (s) / thickness (m)
TIM	Transparent Insulation Material
U	overall heat transfer coefficient ($W/m^2.K$)
V	micropore volume filed with the adsorbed phase (m^3/m^3)
V_o	limiting micropore volume (m^3/ m^3)
V_w	wind velocity (m/s)
W_c	collector width (m)
x	concentration ratio of adsorbate inside adsorbent (kg/kg)
x_o	maximum limit of mass adsorbed (kg/kg)

Greek Symbols

Δ	difference / change
τ	transmittance
α	absorptivity
ε	emissivity
σ	Stefan Boltzmann constant ($W/m^2 K^4$)
β	affinity coefficient or collector tilt angle
ρ	density (kg/m^3)

Subscripts

1,2,3,4	processes terminal locations
ac	activated carbon
a	adsorption
amb	ambient
b	back
c	condenser
d	desorption
e	evaporator
eq	equivalent
g	generation / glass
i	insulation

ice	ice
is	collector side insulation
L	collector overall
m	methanol
max	maximum
min	minimum
pw	absorber plate wall
s	side
sa	starting adsorption
sat	saturated
sd	starting desorption
sol	solidification
t	top
w	water

ABSTRACT

Full Name : Naef Abduljalil Abdulrahman Qasem

Thesis Title : Thermodynamic analysis and modeling study of an intermittent adsorption refrigeration system

Major Field : Mechanical Engineering

Date of Degree : May, 2013

Solar adsorption refrigeration systems have been increasingly attracting some research interests since last decade because they are clean, cheap and simple for use in air conditioning, ice making, food preservation and vaccine storage specially for remote areas. The idea of these devices is the reversible physical adsorption of vapor on the surface of a porous solid. The system consists of three important components: solar collector with adsorbent bed, condenser and evaporator.

The main objectives of this work are to improve the performance of the solar intermittent refrigeration system that uses activated carbon and methanol as adsorbent and adsorbate pair. The improvement of the system's performance is achieved through investigating the effect of the main operative and constructive parameters of the system. EES and MATLAB computer programs are exploited to analyze the thermodynamic cycle of the system and to model the system under Dhahran climate conditions, respectively.

The results show that the increase in the condenser temperature needs high values of the desorption temperature while lowering values of the evaporator temperature needs low values in the adsorption temperature to improve the performance. The absorbers of collector should have thin wall and should be coated by high absorptivity and low emissivity material. About 14.1 kg/m^2 of activated carbon NORIT RX3-Extra per m^2 of

collector surface is a suitable optimum choice for adsorption ice maker devices. Furthermore, double glazing, tilt angle of the solar collector and starting the cycle at suitable time as well as suitable collector back insulation increase the performance. Moreover, the study proposes an activated carbon/methanol solar adsorption ice-maker that could produce from 5 kg up to 13 kg of ice per day per m^2 of collector area with improved solar coefficients of performance of 0.12 and 0.24 according to weather conditions in the hot and the cold days, respectively.

ملخص الرسالة

الاسم الكامل : نائف عبد الجليل عبد الرحمن قاسم

عنوان الرسالة : تحليل حراري و دراسة نموذجة لآلة التبريد المتقطع بالامتزاز المسخن شمسيا

التخصص : هندسة ميكانيكية

تاريخ الدرجة العلمية : مايو 2013م

في العقد الماضي زاد الاهتمام بدراسة التبريد بواسطة الامتزاز لما يعطيه من امتيازات كونه رخيص التشغيل ونظيف بيئيا بالإضافة الى امكانية استخدامه لأغراض التبريد والتكيف وحفظ الاطعمة واللقاحات الدوائية. فكرة هذه المنظومة قائمة على قدرة امتزاز المادة الصلبة المسامية – الممتزات – لبخار مائع التبريد – المزازه– عند درجة حرارة منخفضة وايضا طرد المزازة على شكل بخار عند التسخين. تتكون اجهزة الامتزاز من الممتزات المحتوية في مجمع شمسي غالبا ما يكون مسطح بالاضافة الى المكثف والمبخر– المبرد. في هذه الرسالة يتم التحليل الثيروموديناميكي – الحراري– لالة التبريد الممتز عن طريق دراسة اهم العوامل المؤثرة فيها مثل: درجة حرارة الممتز الكبرى ودرجة حرارة الامتزاز الصغرى بالإضافة الى حرارة وضغط كل من المكثف والمبخر. التحليل الحراري يعطينا انطباعا عن الأداء التمهيدي للمنظومة مثل كمية الثلج المتوقع انتاجها ومعامل الاداء وتتم هذه الدراسة باستخدام برنامج EES في حين أن الدراسة الفعلية للمنظومة تتم من خلال النموذجة بواسطة برنامج MATLAB على حسب ظروف مناخ الظهران لإظهار الاداء الفعلي وكمية الثلج المتوقعة خلال الايام الباردة والحارة من السنة. لهذا تهدف هذه الدراسة الى تحسين اداء منظومة الامتزاز الشمسي المتقطع (الذي لا يعمل بصورة مستمرة وينتج تبريدا طوال الليل والنهار) باستخدام الكربون المنشط والميثانول بواسطة دراسة وتحسين العوامل المؤثرة فيه: كنوع الكربون المنشط وسمك معدن الانابيب الماصة للأشعة الشمسية بالإضافة الى امتصاصية وانبعاثيه الطلاء الذي يغطي الماصات الشمسية الى جانب كل من كمية الكربون المنشط و الغلاف الزجاجي

المناسب وسماكة المادة العازلة التي تغطي قاعدة المجمع الشمسي وايضا زاوية ميلان المجمع الشمسي مع بداية التشغيل المناسبة. تهدف هذه الدراسة ايضا الى انتاج 5 كجم او اكثر من الثلج لكل متر مربع من المجمع الشمسي باليوم الواحد. نتائج التحليل الحراري تشير الى انه في حالة ارتفاع درجة حرارة المكثف يجب تسخين الكربون المنشط بدرجات حرارة عالية وايضا في حالة الذهاب الى درجة حرارة منخفضة داخل المبخر يجب ان تكون درجة حرارة الامتزاز منخفضة ايضا. اما نتائج دراسة النموذجة توضح ان حوالي 14.1 كجم من الكربون المنشط NORIT RX3-Extra لكل متر مربع من المجمع الشمسي يعطي نتائج افضل من الانواع الاخرى ويفضل ان يكون سمك الانابيب الماصة اصغر ما يمكن من اجل تحسين اداء المنظومة. كما اوضحت الدراسة الى ان الغلاف الزجاجي الذي يتكون من طبقتين مفصولتين من الزجاج افضل من اللوح الزجاجي الواحد او الانظمة الزجاجية السامحة للأشعة الشمسية والعازلة للحرارة المفقودة (TIM) بالإضافة الى ان سماكة المادة العازلة تزيد من الكفاءة لكن يجب ان لا تزيد المجمع الشمسي عبء اضافي كزيادة سماكته. المنظومة المحسنة بالخصائص السابقة مع تمييل المجمع الشمسي بزاوية مناسبة وبدء الدورة الحرارية عند الوقت المناسب يمكن ان ينتج كميات من الثلج تتراوح بين 5 كجم الى 13 كجم لكل متر مربع من المجمع الشمسي وبمعامل اداء شمسي يتراوح بين 0.12 و 0.24 للأيام الحارة والباردة على التوالي.

CHAPTER 1

INTRODUCTION

1.1 Introductory Background

Refrigeration and air conditioning demands are widely increasing because of the increase in population as well as the dramatically growth of industries. Many refrigeration technologies were developed during the last century. The vapor compression systems broadly dominate the human use for satisfying comfort conditions or food preservation. These traditional refrigeration systems consume a significant amount of electric power. In addition, such systems rely on refrigerants as chlorofluorocarbons CFCs and hydrochlorofluorocarbons HCFCs which increase the depletion of the Earth's ozone layer. Consequently, alternative refrigeration technologies became very much needed; especially the current sources of energy such oil may run dry in the near future. The electricity is not also covering all human living areas. For now, there are numerous places without electricity especially in countryside of some developing countries. So people living in such areas cannot preserve their food and store vaccine in their local clinics. Accordingly, solar adsorption refrigeration technology has attracted some research interests since 1990 because it is clean, cheap and simple for use in air conditioning, ice making, food preservation and vaccine storage. The idea of these devices is the reversible physical adsorption of vapor on the surface of a porous solid. An intermittent adsorptive

solar ice-maker is an attractive application that is composed from adsorbent bed as adsorptive reactor integrated into a solar collector for the desorption of the sorbent material during the day. During the night adsorption occurs by the adsorbent when the refrigerant comes back from the evaporator, in which the cooling effect is obtained and some ice may be produced.

This research aims to understand the thermodynamic processes of the intermittent adsorption cooling system and study the effect of the operative parameters on the performance of the system. Moreover, improving the performance of the system will be investigated through studying the effect of the constructive parameters and then proposing a solar adsorption ice-maker to produce 5 kg of ice or more per day per m^2 of collector area under Dhahran climatic conditions.

1.2 System and Processes Description

Intermittent adsorption systems usually have a single bed adsorption cycle that has been improved for some applications such as preservation of food and vaccine storage. The adsorption system consists of three main parts: solar collector with adsorbent bed where a porous solid material is placed, condenser and evaporator, Fig. 1.1. The operating cycle of the system has four processes as shown in the Clapeyron diagram in Fig. 2.2. The heating process (1-2) and the desorbing process (2-3) represent half the cycle while the cooling (3-4) and adsorption (4-1) processes represent the other half. During the heating period, the adsorbent bed receives heat from solar energy which raises the temperature of the pair of adsorbent and adsorbate as shown in Fig. 2.2 by line 1-2 (isosteric heating

process, at constant concentration of the adsorbate (x_{max}). When the adsorbent bed pressure reaches the pressure of the condenser, the adsorbate vapor diffuses from the collector and is collected and condensed in the condenser (line 2-3, desorption process at condenser pressure). So the concentration of the adsorbate in the reactor reaches the minimum value (x_{min}) at the end of this desorption process. This process is followed by cooling the generator (line 3-4, isosteric cooling process). Then, the liquid adsorbate flows from the condenser to the evaporator. After that, the adsorbent adsorbs the refrigerant that is coming from the evaporator (line 4-1, adsorption process at evaporator pressure). As a result, the liquid water in evaporator is converted into ice or become cold.

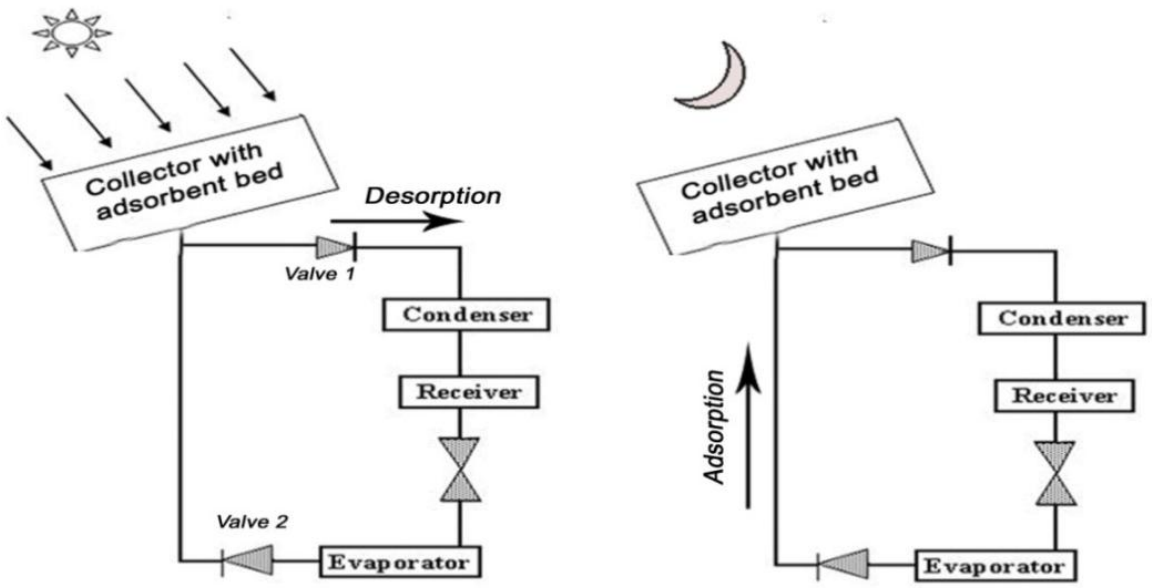

Figure 1.1 Schematic of the solar adsorption cooling system.

The heating and cooling processes are run at constant concentration of adsorbate while the concentration of refrigerant varies through adsorption and desorption processes.

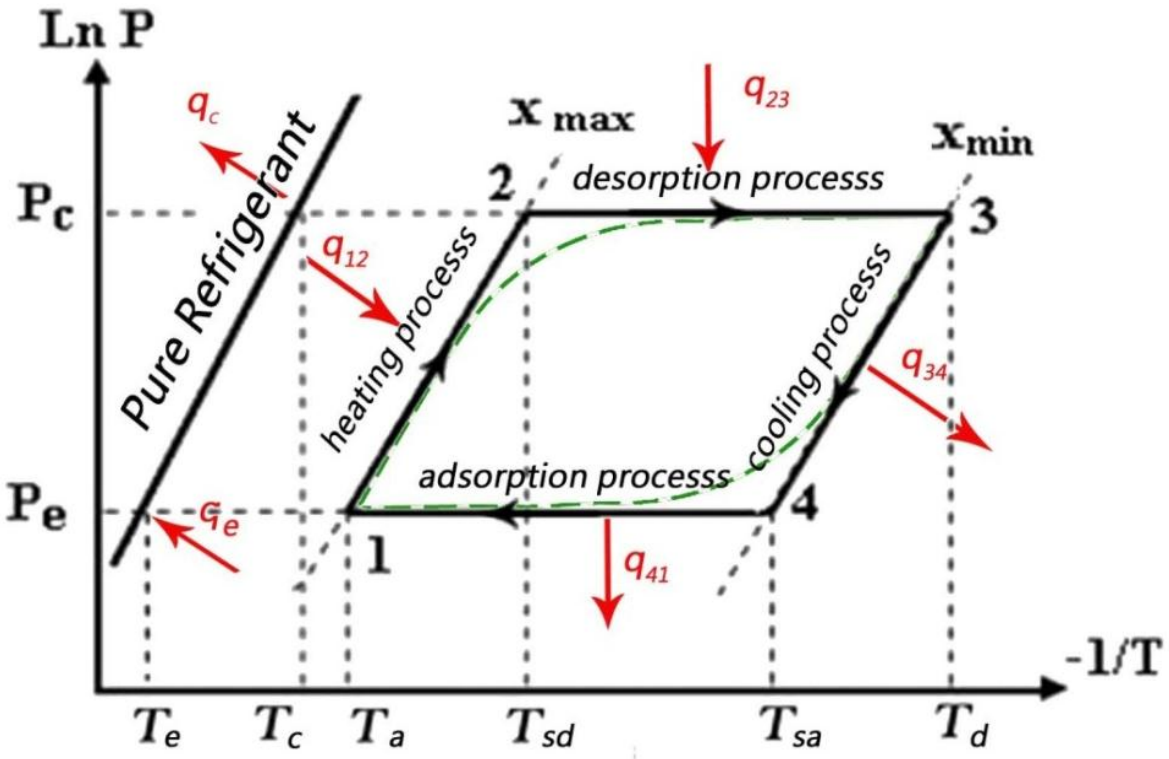

Figure 1.2 Schematic view of the adsorption process on Clapeyron diagram.

CHAPTER 2

LITERATURE REVIEW

2.1 Background

Although a refrigeration system has been founded since the middle of the eighteenth century by William Cullen, the practical refrigeration system was built as an ice-maker by Jacob Perkins in 1834 [1]. Since that time, there have been many refrigeration and heat pump systems that are categorized according to either the principle of work or the operating source of energy: vapor-compression, absorption refrigeration, adsorption refrigeration, thermoelectric refrigeration, vortex tube, paramagnetic refrigeration, sterling cycle, gas refrigeration cycle and vapor-jet refrigeration systems. However, there are five different technologies that are currently used for solar cooling systems: sorption (absorption/adsorption) refrigeration, photovoltaic vapor compression refrigeration, open-cycle refrigeration, and ejector cycle. Some of them are widely used because of their high coefficient of performance like the vapor compression **s**ystem for which we need electricity to run the compressor. On the other hand, some of the systems are not used for ice making because they cannot produce a temperature below zero degree. However, these systems are widely used for air conditioning and fresh food preservation. Examples of these systems are desiccant cycles, ejector cycle and some absorption and adsorption pairs.

Pridasawas [2] classified the cooling systems powered by solar energy into two types: solar thermal systems and PV systems (which are driven by electricity provided by PV cells). He also showed the cold temperature obtained by each system as shown in Fig. 2.1.

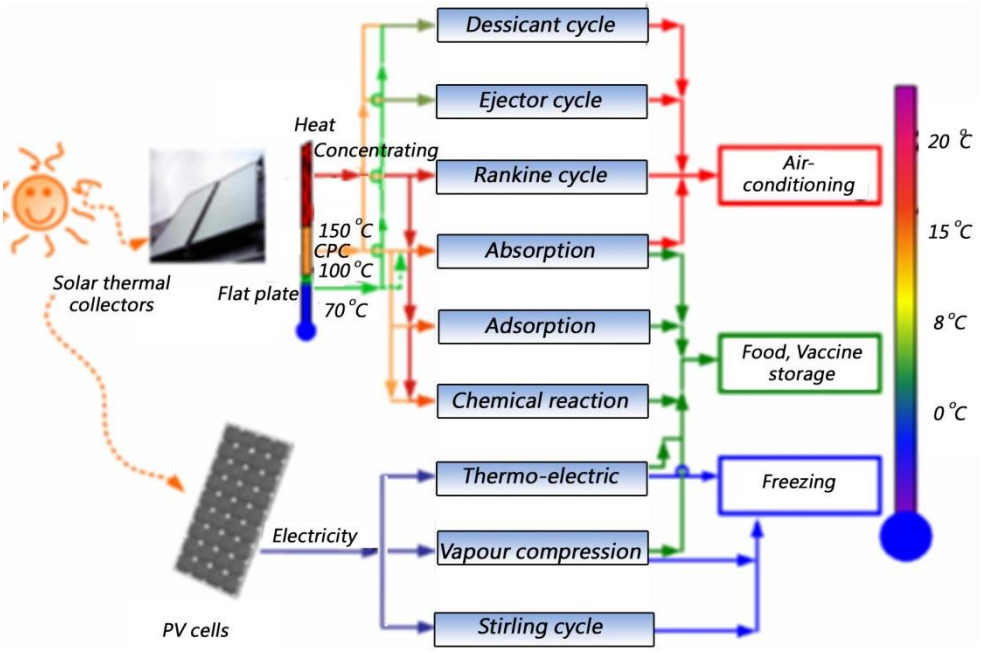

Figure 2.1 Solar cooling systems [2].

In this section, the adsorption cooling systems will be revised as studied in the literature.

2.2 Adsorption Working Pairs

The adsorption refrigeration systems depend critically on the working pairs. The common working pairs were investigated and compared by Critoph [3], San and Lin [4] and Wang et al. [5]. Askalany et al. [6] also revised several refrigerants that work with carbon adsorbent. Adsorption refrigeration materials are carefully reviewed by Alghoul et al. [7].

The study showed the important properties of the adsorbent and adsorbate pairs used in the adsorption refrigeration systems and also determined the pair and materials which are suitable when solar energy is used as the main energy source. The adsorbent/adsorbate pairs operate under typical operating pressure ranges of 0.01-0.35 and 3.0-13.5 bar, for the low and high-pressure adsorption coolers, respectively. The classification of the pairs according to the operative pressure is as follows:

Low pressure: silica gel/water, silica gel/methanol, zeolite/water and activated carbon/methanol.

High pressure: silica gel/sulfur dioxide, zeolite/fluorocarbon, activated carbon/ammonia and activated carbon/fluorocarbon.

The low pressure systems require a good manufacturing for avoiding leakage which significantly affects the performance. Whereas, the high pressure adsorption cooler systems require higher generation (desorption) temperature.

Activated carbon, zeolite, and silica gel are the essential common materials used as adsorbents whereas water, ammonia and methanol are the most important adsorbates. Thus, the most important working pairs exploited for adsorption cooling in previous researches are activated carbon/methanol, activated carbon/ ammonia, zeolite/water and silica gel/ water.

2.2.1 Activated Carbon/Methanol systems

Activated carbon is a substance of crystalline form having large internal pore structures with surfaces greater than 500 m^2/g. The word activation basically means creating pores in a nonporous material such as: coal, lignite, wood, nut shells and synthetic polymers by

means of chemical reactions, Askalany et al. [6]. There are many forms of activated carbon such powders, granulated, molecular sieves and carbon fibers, Srivastava and Eames [8].

Activated carbon with methanol as a working pair is broadly used in adsorption refrigeration due to the large adsorption quantity and low desorption heat, which is about 1800 - 2000 kJ/kg, Askalany et al. [6]. The adsorbent properties indicate that the activated carbon is a good choice for adsorption cooling because its high capacity for desorption and adsorption reaches 0.45 g/g, Wang et al. [9]. Moreover, the system of activated carbon methanol needs low grade heat source which is suitable to work by solar energy. On the other hand, methanol operates at sub atmospheric pressure; the low pressure systems require a good manufacturing for avoiding leakage which significantly affects the performance and can fail the system working. Another deficiency is that the methanol is not compatible with copper at temperatures greater than 120 ^{o}C , Alghoul [7], and also it decomposes at 150 $^{\circ}$C to formaldehyde (HCHO) or dimethyl ether (CH3OCH3) by the mechanism of dehydrogenation or dehydration, Eric [10]. The decomposition reaction of methanol with aluminum alloy is greater than the copper [10].

Vasta et al. [11] simulated an adsorptive ice-maker system. The different processes and phases of the thermodynamic cycle of the ice-maker components were studied. They used an active carbon/methanol as the working pair with a flat plate solar collector of 1.5 m^2 surface area that contained 13 concentric tubes filled with 37 kg of activated carbon and about 10.5 kg of methanol for simulation according to Messina, Italy, climatic conditions

($38^{o}12'$N, average useful solar radiation was about 520 W/m^2 for June and about 250 W/m^2 for December). For the most part of the year (from April to October), a daily ice production of 5 kg could be produced. This amount decreased to 4 kg in February and March. The coldest months in the year (January, November and December) had the amount of 2.0 - 3.5 kg. The net solar coefficient of performance (SCOP) had a minimum value of 0.045 in July, but the maximum one was about 0.11 in January, with an annual mean of 0.07.

Zhao et al. [12] used activated carbon/methanol to introduce a mechanical and experimental freeze proof solar adsorption cooling tube. The collector was constructed as outer tube, center tube and vacuum tube that were made of hard borosilicate glass. The radius of the outer tube was about 29 mm, and the radii of the vacuum tube were 23.5 mm and 18.5 mm. Furthermore, the radius of the center tube was 5 mm. The maximum temperature generated by the system was about 110 ^{o}C whereas the evaporator temperature reached -4 ^{o}C below zero. The device achieved 87-99 kJ of cooling capacity and about 0.11 of SCOP.

Hassan [13] assumed the effective thermal conductivity of the adsorbent bed and the system pressure to vary with time and space inside the reactor during desorption and adsorption processes in a theoretical simulation of a solar adsorption refrigeration system that used one m^2 flat collector with 20 pipes filled with activated carbon/methanol. The results showed that changing the effective thermal conductivity of reactor is very small (between 0.5-0.528 W/m.K) as well as the system pressure during adsorption and

desorption processes was almost constant. The maximum solar coefficient of performance reached was 0.2 according to Canada climate on 30th June.

An analysis of the thermodynamic cycle and the experimental performance of a solar adsorptive ice-maker was studied by Leite [14]. The system used methanol charcoal pair, 21 kg of activated carbon and 6 kg of methanol, and employed a solar energy technology to enhance the performance of the collector. The collector-adsorbent bed was made from nine multi tubular with an opaque black absorber surface and transparent insulation material (TIM) at top and bottom covers to minimize heat losses during desorption process. The solar radiation incident directly through the top face and indirectly reflected from the bottom face of the collector by means of semi-cylindrical reflectors. The simulation relied on meteorological data of Brazil during three times according to the predominant cloud cover degree. Three cycles had been examined with different conditions: First condition was a clear sky, second one with partially cloudy sky, and finally under entirely cloudy sky. The result emphasized that not only the incident solar radiation dominates the performance, there are many features that had also significant effects as degree of cloudy sky during the night. The maximum generating temperatures were 100.1, 87.3 and 92.7 ^{o}C enabled to produce 6.05, 2.10 and 0 kg of ice, respectively, and to condense 3.0, 2.0 and 2.3 kg of methanol per square meter of the collector for the three cycles of clear sky, partially cloudy and overcast nights, respectively. Leite compared his study with TIM cover and using water for condensation with Medini [15] who used a single glazing cover and selective surface for absorber. The TIM technique reduces the top heat losses from 5 W/m^{2}K to 1.34 W/m^{2}K.

The analysis of the cooling and adsorption processes was investigated by Ogueke and Anyanwu [16]. The purpose of the study was increasing the amount of adsorbate adsorbed by the adsorbent. Condenser pressure, evaporator pressure and the initial concentration of adsorbate in the adsorbent were the main parameters affecting the system performance during the cooling and adsorption processes. As the condenser pressure decreased, the adsorption process increased by increasing the time of adsorption. The second parameter was the evaporator pressure which affected directly the adsorption process with proportional relationship. The starting time of adsorption process is delayed as the vapor pressure decreases. On the other hand, the sufficient evaporation pressure to produce ice might not evaporate all adsorbate in the evaporator. Finally, the initial concentration of adsorbate in the adsorbent could play main roles in adsorption and desorption processes. The optimum value of initial concentration of activated carbon was 0.21 to obtain the best adsorbing of adsorbate and the maximum concentration was about 0.29. The produced ice increased from 0 kg of ice/kg of adsorbent to 0.4 kg, but the initial concentration value should not decrease than 0.21.

Li and Wang [17] studied theoretically and experimentally heat and mass transfer in an adsorbent bed for a flat plate solar adsorption ice-maker. 10 kg of Methanol and 42 kg of activated carbon were used in a rectangular adsorbent bed of 1.5 m^2 solar collector. For theoretical analysis, there were some assumptions such as considering adsorption bed is of uniform size particles with constant bed porosity and the methanol in the adsorption process acts as ideal gas. Moreover, the temperatures of charcoal and methanol vapor at

any portion are the same in the adsorption process. The experimental analysis was done by constructing a device in lab and simulating the solar radiation by means of quartz lamps. The result showed that the numerical results from theoretical study were in good accuracy with experimental study at SCOP of 0.125 and 0.132 for 30.24 and 29 MJ of incident solar radiation, respectively.

Chekirou et al. [18] studied theoretically the heat and mass transfer in tubular adsorbent filled with activated carbon AC-35 saturated with methanol. They focused on the main parameters affecting the solar performance coefficient and the cooling effects as condensation pressure, evaporation temperature, adsorption temperature, incident solar recitation and collector configuration. The results showed the SCOP increased with increasing the evaporation pressure and the insolation as well as with decreasing the condensation and adsorption temperatures. TIM cover and double glazing cover systems showed better SCOP and cooling power than single cover system. The SCOP was 0.13, 0.172 and 0.184 and the cooling effect was 168.192, 213.661 and 229.286 KJ/kg (AC) for single glazing, double glazing and TIM system, respectively.

On the other hand, the experimental work of Critoph and Tamainot-Telto [19] showed that the double glazing cover enhanced the performance more than TIM and single glazing covers. SCOP was 0.061, 0065 and 0.071 for single cover, TIM and double cover systems, respectively.

2.2.2 Activated Carbon/Ammonia Systems

Ammonia with activated carbon is also commonly used in adsorption refrigeration systems. Ammonia has a large latent heat of 1360 kJ/kg. Otherwise, ammonia works at high pressure (13 bar at 35^{o}C) so it needs high generation temperature, so flat plate collectors aren't adequate to optimize such systems, Anyanwu and Ogueke [20].

Tamainot-Telto et al. [21] investigated 26 types of activated carbon, under five constructed classifications, to work with ammonia as pair for adsorption cooling. The main results showed that the best types of activated carbon when using two beds of adsorbent were KOH-AC (monolithic) and SRD1352/2 (granular). The performance of KOH-AC and SRD1352/2 were evaluated as 66 and 36 MJ/m^3 for cooling effect and 0.45 and 0.48 for COP, respectively, at -4 ^{o}C evaporator temperature, 30 ^{o}C condenser temperature and 100 ^{o}C generation temperature.

Critoph and Metcalf [22] studied the specific cooling power intensification limits in carbon/ammonia adsorption refrigeration systems. They constructed a monolithic carbon/ammonia refrigeration system using a non-regenerative cycle with a COP of about 0.3 and 2 kW/kg of specific cooling power. The design was based on a 2 mm thick carbon layer with 0.2 mm stainless steel plates and 0.5 mm thick fluid channels. The driving and evaporation temperatures were 200 ^{o}C and 15 ^{o}C, respectively, where the minimum cycle time was 12 seconds.

Critoph [23] investigated a multiple bed regenerative adsorption cycle using the monolithic carbon/ammonia pair. The system consists of 32 modules. The performance of the system was found to reach a COP of 0.85 and 0.4 kW of a cooling power.

2.2.3 Zeolite/Water Systems

Zeolite material is a type of aluminasilicate crystal composed of alkali or alkali soil, Wang et al. [5]. About 40 types of zeolites exist in nature, but the important types for adsorption refrigeration are chabazite, sodium chabazite, cowlesite and faujasite. There are 150 types of zeolites that can be artificially synthesized named by one letter or a group of letters, such as type A, type X, type Y, type ZSM, etc. Zhang [24].

The zeolite/water pair can be utilized in adsorption refrigeration for air conditioning purposes and producing chilled water. The zeolite/water adsorption heat is higher than that in activated carbon/methanol or activated carbon/ammonia; it is about 3300–4200 kJ/kg. The zeolite/water is stable at high temperatures, so it can be used to recover heat above 200 ^{o}C, Wang et al. [9]. At middle temperature lower than 150 ^{o}C, the activated carbon/methanol is better on COP and SCP than zeolite/water.

Poyelle et al. [25] reported that the SCP of the zeolite/water adsorption system with heat and mass recovery cycle was about 97 W/kg at an evaporating temperature of 4 ^{o}C. For high temperature of evaporator, the SCP and the COP reached 135 W/kg and 0.68, respectively.

Jones [26] proposed a six-bed zeolite/water adsorption system with heat recovery that can get a cooling COP close to 1.5 (and hence the heating COP can reach 2.5) with water temperature from 4.4 to 37.8 ^{o}C.

Zhu et al. [27] developed a prototype of a zeolite 13X /water adsorption refrigeration system for producing chilled water to be used for preservation of fish in a fishing boat by utilizing waste heat from the engine.

2.2.4 Silica Gel/Water Systems

The silica gel is a type of amorphous synthetic silica. It is a rigid, continuous net of colloidal, connected to very small grains of hydrated SiO4, Yang [28]. Silica gel/water as a pair for adsorption cooling is considered as a low temperature working pair. Like activated carbon/ methanol, silica gel/water can be driven by about 75 ^{o}C heat source. The disadvantages of silica gel: it is expensive and is not available. Silica gel and activated carbon have almost linear pressure isotherms, but zeolite is not, Alghoul [7].

There are many practical silica gel/water adsorption systems, one of them is that showed on HIJC USA Inc. website [29] with the SCP and the COP of ADCM1-180 are approximately 629.5 kW and 0.59, respectively when the hot water used as generation source with temperature 90 ^{o}C and the cooling water temperature is 29.4 ^{o}C to provide a chilled water of 7 ^{o}C.

Demir et al. [30] focused their simulation on the heat and mass transfer in a cylindrical annulus adsorbent bed using silica gel/water pair. They solved governing equations

numerically by finite difference method for three values of porosity: 0.1, 0.2 and 0.3. The results showed that the temperature of the adsorbent bed sharply increased at the beginning of the adsorption process because of the adsorption generated heat. The adsorption temperature at the inner radius reached 370, 378 and 380 K for 0.1, 0.2 and 0.3 porosity values, respectively. The most important results explained that the increase in porosity reduces the thermal conductivity of the bed and heat transfer rate in the bed whereas the porosity increase rises the period of the adsorption process.

Kluppel and Gurgel [31] constructed two prototypes of solar adsorption cooling systems using a silica gel/water pair whereas the adsorbents were packed into the annular space between copper tubes. The results showed that SCOP of the system was 0.055 with evaporator temperatures below 4 ^{o}C. However, SCOP reached 0.077 for evaporator temperatures around 12 ^{o}C.

Alam et al. [32] used silica gel/water to investigate the parameters effect of the heat exchanger design. The research focused on adsorbent number of transfer unit, bed Biot number and the heat exchanger aspect ratio as well as the ratio of fluid channel radius to the adsorbent thickness.

2.2.5 Calcium Chloride/Ammonia Systems

The above working pairs are considered as physical adsorption systems, while calcium chloride/ammonia is used as a chemical adsorption system. The adsorption capacity of calcium chloride/ammonia is large: one mole calcium chloride can adsorb 8 moles ammonia and the combination is CaCl2.8NH3 which can adsorb four, six or eight moles

of ammonia relying upon the different desorption temperatures and pressures, Wang et al. [33]. Otherwise, the calcium chloride/ammonia adsorption system has a lot of problems such as decomposition, corrosion and expansion. The calcium chloride/ammonia adsorption system is preferred for use in fishing boats using the exhaust heat of the engine. Wang et al. [34] developed an ice-maker using calcium chloride ammonia adsorption for fishing boats. The system SCP and COP reached 731 W/kg and 0.38, respectively.

2.2.6 Other Working Pairs

A few researches in the literature were conducted with several other working pairs; the performance of activated carbon/ethanol and activated carbon fibers/ethanol were studied and tested by El-sharkawy et al. [35, 36] and Saha et al. [37, 38]. Other pairs based on adsorbent carbon is reviewed by Askalany et al. [6] including activated carbon/nitrogen, activated carbon/hydrogen, activated carbon/ diethyl ether, activated carbon/R134a, activated carbon/ R507A, activated carbon/n-butane, and activated carbon/CO2. The BaCl2/NH3 adsorption pair was investigated by Zhong et al. [39].

2.2.7 Previous Studies on Working Pairs Comparison

There are a number of studies in the literature on adsorption cooling working pairs comparison. The thermodynamic design procedure of solar adsorption cooling systems and the performance are analyzed by Anyanwu and Ogueke [20] for three adsorbent/adsorbate pairs: activated carbon/ methanol, activated carbon/ ammonia and zeolite/water. The generating temperature in the adsorbent bed in a solar flat plate collector was taken from 70 ^{o}C as a minimum to 140 ^{o}C as a maximum. They considered the evaporator temperature as constant. The results showed the best choice for food

preservation, deep freezing and ice making is the pair of activated carbon with ammonia with the maximum net solar coefficient of 0.19, but the generating temperature of activated carbon/ammonia is not optimized, it needs high generation temperature because of the ammonia systems work at high pressure. The zeolite-water pair used for air conditioning with 0.3 SCOP. Furthermore, the methanol charcoal had 0.16 as a maximum of SCOP. The COP depended mainly on condensation and adsorption temperatures and weakly on evaporator temperature.

According to working pair comparisons, for low-grade temperature sources as solar energy using flat collectors, the appropriate pairs for cooling purposes are activated carbon/methanol and zeolite/water, Alghoul [7]. However the zeolite/water pair is not utilized for freezing. More advantages of activated carbon/methanol than zeolite/water as per Critoph [3] are:

- Activated carbon is cheaper than zeolite.
- Activated carbon can be manufactured with wanted properties for a particular application.
- Methanol with suitable properties for refrigeration can be produce in developing countries.

Wang and Oliveira [40] showed some of the best adsorption cooling systems performances obtained by different models constructed during the past 20 years. Their results that are shown in Table 1 should not be compared to each other because they were examined under different working conditions. However, they can be used as indicators of what can be expected from these systems. Table 2.1 shows that the activated

carbon/methanol is appropriate for ice making, while silica gel/water and zeolite/water pairs are more suitable for producing chilled water and air conditioning.

Table 2.1 Performance of different adsorption cooling systems [40].

Application	Heat source temperature or insolation	Working pair	COP	SCP or ice production	Year
Ice making	20 MJ m^{-2} day^{-1}	AC-methanol	0.12	6 kg day^{-1} m^{-2}	1986
Ice making	105 °C	AC-NH_3	0.10	35 W kg^{-1}	1997
Ice making	18.1–19.2 MJ m^{-2} day^{-1}	AC-methanol	0.12–0.14	5.0–6.0 kg day^{-1} m^{-2}	2002
Ice making	17–20 MJ m^{-2} day^{-1}	AC-methanol	0.13–0.15	6.0–7.0 kg day^{-1} m^{-2}	2004
Ice making	15.4 MJ m^{-2} day^{-1}	Silica gel–water	0.16[a]	2.05 MJ day^{-1} m^{-2}	2004
Ice making	20 MJ m^{-2} day^{-1}	AC + blackened steel-methanol	0.16	9.4 kg day^{-1} m^{-2}[b]	2004
Ice making	< 120 °C	AC-methanol	0.18	27 W kg^{-1}	2005
Ice making	115 °C	AC + $CaCl_2$–NH_3	0.39	770 W kg^{-1}[c]	2006
Chilled water	55 °C	Silica gel–water	0.36	3.2 kW $Unit^{-1}$	2001
Chilled water	100 °C	AC-methanol	0.4	73.1 W kg^{-1}	2001
Chilled water	65 °C	Silica gel–water	0.28	12.0 kW $Unit^{-1}$	2004
Chilled water	75–95 °C	Silica gel–water	0.35–0.60	15.0 kW m^{-3}	2004
Chilled water	80–95 °C	Silica gel–water	0.3–0.6	20 W kg^{-1}[d]	2004
Chilled water	80 °C	Silica gel–water	0.33–0.5	91.7–171.8 W kg^{-1}	2005
Air conditioning	232 °C	AC-NH_3	0.42–1.19	NI[e]	1996
Air conditioning	204 °C	Zeolite–water	0.6–1.6	36–144 W kg^{-1}	1998
Air conditioning	230 °C	Zeolite–water	0.41	97 W kg^{-1}	1999
Air conditioning	310 °C	Zeolite–water	0.38	25.7 W kg^{-1}	2000
Air conditioning	100 °C	AC-NH_3	0.2	600 W kg^{-1}	2003
Air conditioning	230–300 °C	Zeolite–water	0.20–0.21	21.4–30 W kg^{-1}	2004

[a] Average value obtained during 30 days of continuous operation.
[b] Based on the area of the adsorber, which was different from the area of the reflector panels.
[c] The SCP is based on the mass of $CaCl_2$ inside one adsorbent bed and only in the duration of the adsorption phase.
[d] At generation temperature of 95 °C.
[e] Not informed.

2.2.8 Improving Adsorbent Heat Transfer

The adsorbent should have a high capability to adsorb and desorb vapor phase of a refrigerant. On the other hand, it has low heat transfer characteristics as thermal conductivity. For example, the effective thermal conductivity of the adsorbent bed of methanol/AC-35 is between 0.13 - 0.17 W/m.K, Guilleminot et al. [41]. So many researches have been conducted to increase the heat transfer in the reactor, e.g. the metallic foam additive method by adding materials with good thermal conductivity into the adsorbent (i.e. adding cuprum powder into activated carbon can improve its conductivity by 2–25%, Elton and Saying [42]).

Impregnation method is mainly used for activated carbon fiber, graphite fiber or expanded graphite. This method is done by dissolving the chemical material (as CaCl2) into water or other solvent and putting the physical adsorbent (as activated carbon) to the solution. Then, the solution is dried to remove the solvent [5]. Another impregnation process is by applying the chemical adsorbent as an impregnated salt and adding the physical adsorbent as a host matrix to build internal porous structure and improving thermal conductivity of adsorbent. Restuccia et al. [43] investigated improving the performance by adding some salts such as CaCl2, LiBr, LiCl, and MgCl2 into known adsorbents such as silica gel, activated carbon, and zeolite.

Consolidation of the adsorbent (as bricks) is another method to enhance the thermal conductivity of adsorbent [34]. Munyebvu et al. [44] produced monolithic activated carbon as discs between number of fins inside tubular adsorber to enhance thermal conductivity and heat conduction with metal elements. The thermo physical properties of monolithic, that is made by mixing bender material with activated carbon and then consolidating it by compressing and firing, were studied by Tamainot-telto and Critoph [45]. The adsorption capacity improved by 24% from 0.29 to 0.36 kg/kg and the density of carbon increased from 500 to 750 kg/m^3.The important improving was that increasing the thermal conductivity from 0.16 to 0.6 W/m.K. Mixing the different size of adsorbent granules together can also strengthen the heat transfer; the conductivity of the activated carbon increases by 35%, Guilleminot [46].

2.3 Adsorption Thermodynamic Cycles

2.3.1 Basic Single Bed Cycle (Intermittent Cycle)

As described in section 1.2, the intermittent adsorption systems have a single bed. The processes of this cycle are: heating, desorption, cooling and adsorption as shown in Figures 1.1 and 1.2. The only difference here rather than that in section 1.2 is the heating source can be by waste heating, hot water, solar energy, and so on.

2.3.2 Multi-Bed Cycle

The multi-bed cycle is produced to solve the intermittent cycle to be continuous. Using two adsorbent bed have been investigated by Liu et al.[47], Xia et al. [48] and Hassan et al. [49], while Uyan et al. [50] and Miyazaki et al. [51] went through three beds. Multi-stage multi-bed adsorbers got Sato et al. [52] four patents from US and Japan, the system schematic details are shown in Fig. 2.2.

Four beds also studied by Alam et al. [53]. Sato et al. [54] constructed an adsorption refrigerator with four beds; two adsorbers were different to the others (by adsorption capacity form) to improve the performance of the system and to make it more compact.

Critoph [55] invented a rotary thermal regenerative adsorption system in which adsorbent modules, adsorption refrigeration tube (ARTs), rotate about an axis in a hollow conduit as shown in Fig. 2.3. The results of a prototype reveal that the increasing of numbers of ARTs tends to rise COP and to decrease SCP.

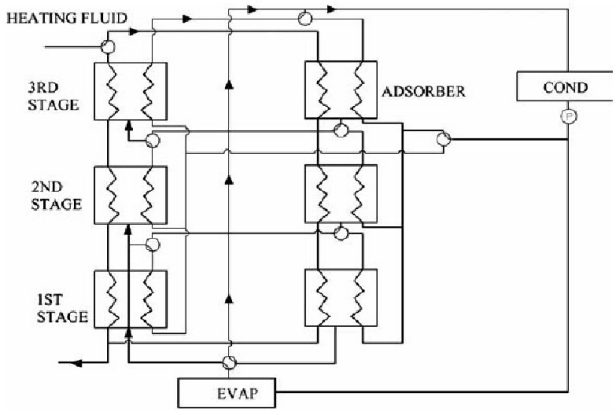

Figure 2.2 Multi-stage, Multi-bed adsorption refrigerator [52].

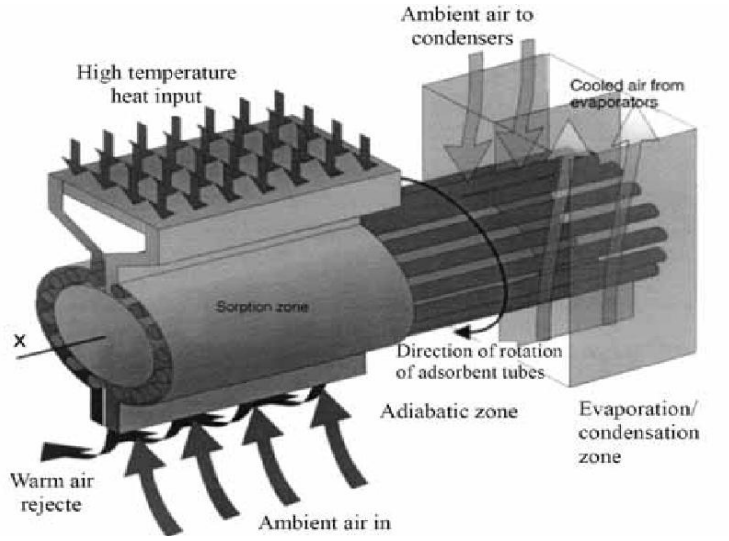

Figure 2.3 Rotary adsorbent generation device [55].

2.4.1 Heat Recovery Adsorption Cycle

Heat recovery cycle is effective strategy to increase the performance of the continuous systems. Two or more adsorbent beds are capable to get benefit from this technique. The adsorbent bed works with various phases This means one should be in the desorption phase and the other in the adsorption phase. Consequently, the heat released from

adsorption bed is used to heat the other bed which needs heating to desorb adsorbate. Closed cycle of water is utilized and switched for this purpose. Correspondingly, heat recovery can improve COP by 25% compared to basic adsorption cooling system, Wang [56].

2.3.3 Heat and Mass Recovery Adsorption Cycle

The mass recovery approach also can enhance the performance of the system by increasing the adsorption capacity. This approach is done by interconnecting the high pressure desorber by low pressure adsorber, therefore the hot bed desorbs more adsorbate, and the cold one adsorbs more. Actually, mass recovery process and heat recovery cycle can be simultaneously used as heat and mass recovery cycle for improving the system performance. Sumathy [57] reported that the mass recovery process can enhance adsorption cooling by 10% with remaining the COP without changing, while using heat recovery process that can contribute by 35% of energy required to operate the system.

2.3.4 Thermal Wave Cycle

Thermal wave cycle was initially proposed by Shelton [58]. The thermal wave cycle relays on two processes; two adsorbent beds are heated and cooled by heat exchangers via circulation an external medium (oil) as shown in Fig. 2.4. Assuming pumping to be clockwise and the bed 1 is hot (low concentration) and the other one is cold, then the external medium is heated firstly by the bed 1 and through passing external heat exchanger for heating bed 2. Bed 1 is cooled by another heat exchanger, so the refrigerant diffuses from bed 2 to condenser and the cold bed adsorbs adsorbate from evaporator. correspondingly, the bed 1 will have high concentration of refrigerant and the bed 2 have

minimum. In the second process the pump is reversed, bed 1 is heated and bed 2 is cooled in the same manner reaching first conditions and then the processes is repeating. The Shelton [58] results claimed that the heat taking from adsorption process can provide about 80% of adsorption process heat needs.

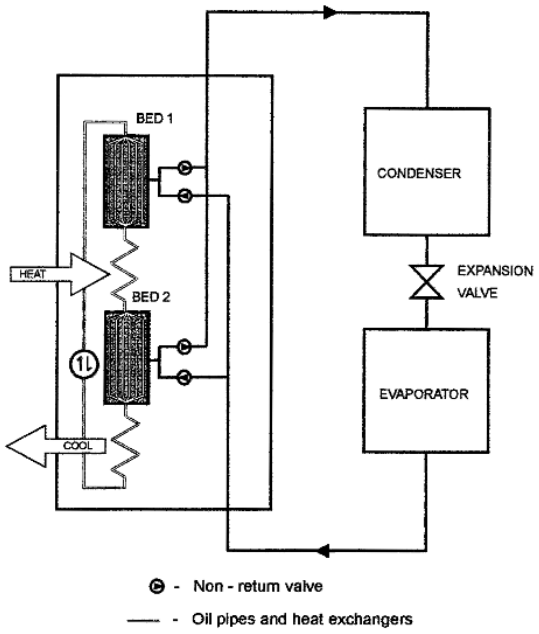

Figure 2.4 Thermal wave cycle [58].

Critoph [59] developed another cycle called convective thermal wave cycle, in which the refrigerant acts as external media to heat and cool the adsorbent directly for desorption and adsorption processes. As a result, the heat transfer is enhanced in this method. Lai [60] confirmed the results of Critoph [61] that said the COP obtained from the system use this cycle was 0.9 at the evaporator temperature 4^{o}C, the generation temperature 200 ^{o}C and the condenser temperature 40 ^{o}C. Oppositely, Tierney [62] accounted the pump power consumption and reduced it from the performance of the system. He found the COP and the SCP are decreased to about 0.27 and 1 W/kg, respectively.

2.3.5 Cascaded Cycle

The cascaded cycle was firstly suggested by Meunier [63]. In this cycle, different working pairs are represented with various temperatures. Hot temperature released from adsorption working pair is utilized to drive another sub-cycle as heat source for desorption process, and so on, as shown in Fig. 2.5. Zeolite/water bed as a main and silica gel/water as abed of sub-cycle, simulated by Liu and Leong [64], obtained 1.3 of COP.

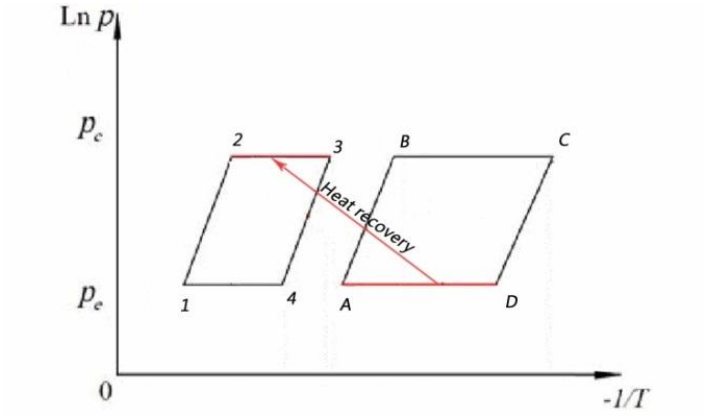

Figure 2.5 Cascaded cycle.

2.4 Solar Intermittent Adsorption Refrigeration Systems

As free, available and ecological energy source, solar energy is the most suitable to drive adsorption system that needs a low-grade power source as activated carbon methanol. The solar intermittent adsorption ice-maker consists of three main components: a solar collector with adsorbent bed, condenser and evaporator where ice or chilled water is produced. The thermal cycle of the system, as described in section 1.2, goes through four processes: two isosteric and two isobaric. The heating and desorbing are diurnal

processes. However the adsorption process which produces ice is considered nocturnal (even though, it usually starts before sunset) as shown in Fig. 1.1.

Figure 2.6 shows the almost full construction of ice maker as consisted from collector with adsorbent bed, condenser, evaporator, valves, reservoir and sensors, whereas there are some systems without the valves, reservoir and sensors.

There are some constructions, in literature review, were made for the sake of improving the solar adsorption ice making for methanol charcoal pair. The main specifications of the system components are the follows:

2.4.1 Collector

The collector is the main part of the system, so it should work efficiently with other components. For enhancing the performance of the system the collector should be:

- Heated efficiently during solar time (heating and desorption processes).
- Cooled efficiently during night (cooling and adsorption processes).
- Efficient heat transfer characteristics.

Generally the collector consists of some components as adsorbent bed, glaze cover, absorber metal and insulation material, the specifications of these components are the following:

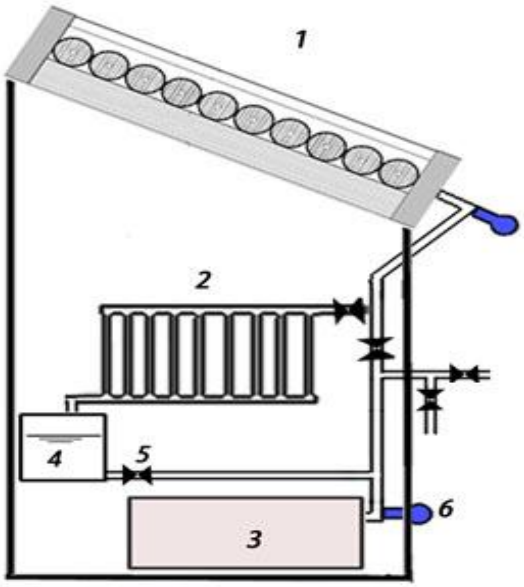

Figure 2.6 Solar adsorption cooling system.

1. Collector 2. Condenser 3.Evaporator 4.Graded bottle 5.Valves 6. Pressure gauges with temperature sensors.

***Adsorbent Bed*:**

- The adsorbent (as activated carbon) is the solid porous media which desorbs and adsorbs the vapour of adsorbate (as methanol). There are two types of adsorbent bed; one has rectangular geometry to hold adsorbent and the other is cylindrical geometry as shown in Fig. 2.7.

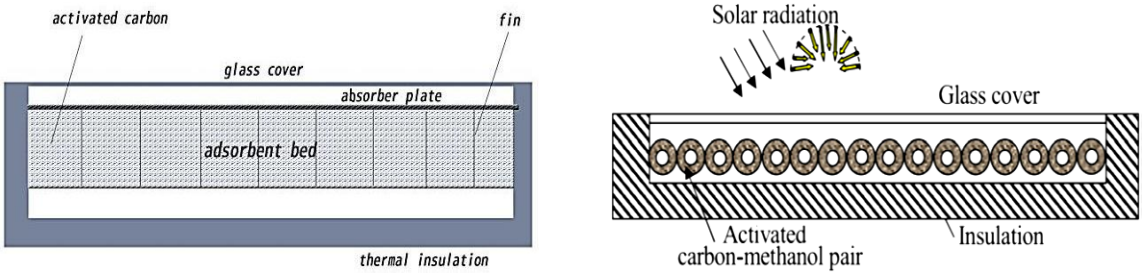

(a) Rectangular adsorbent bed (b) Tubular adsorbent bed

Figure 2.7 Geometry shapes of adsorbent bed.

- The two advantages of multi-tubular adsorbent are the simplicity of its construction and its capacity of standing pressure differences with thinner walls, consider the system operates under vacuum [65].
- The space for activated carbon in the adsorbent bed is taken between 3 to 5 cm in many publications. Thickness of 3.116, 3.71 and 3.8 cm are studied by Anyanwe and Ezekwe [66], Leite [65] and Hassan et al. [13], respectively, for tubular reactor whereas 4.5 cm width with 12.5 cm distance between fins for the rectangular geometry of the adsorbent studied by Li and Wang [17] as well as 3.5 cm thick with 5 cm distance between the fins is studied by Li et al. [67].
- To flux the vapor of methanol to or from the adsorbent, an axial metallic net tube is put in the axial center of each tube in the tubular reactor. For the rectangular reactor, the bottom palate should be perforated for the same purpose.
- Many types of activated carbon are used for filling the adsorbent bed, but the most recently attractive type was studied by literature is AC-35 (W_o = 0.425 l-methanol/kg-AC, D = 5.02* 10^{-7} and n = 2.15 where D, n are characteristic parameters).

Absorber Plate or Tube:

- The absorber should be made from metal with high thermal conductivity as copper if the generation temperature dose not reach 120 ^oC in case of methanol as mentioned before. That because of the copper material contributes in decomposition of methanol to formaldehyde and dimethyl ether at temperature greater than 120 ^oC, so, in this case the stainless steel is preferred [7].

- The thickness of absorber plate or tube is always thin between 1 to 3 mm. Li et al. [67] reduced the stainless steel plate thickness from 1.5 mm to 1 mm to increase heat transfer.
- The plate should be coated with material has high absorptivity and low emissivity as selective coating ($\alpha = 0.9$ and $\varepsilon = 0.1$) for absorbing a large amount of solar radiation. The performance of the system depends strongly on the absorptivity of the solar collector [68].
- The axial metal net tube should have an enough diameter for passing the adsorbed or desorbed refrigerant, 2-3 cm of diameter are used in the literature.
- The all tubes of adsorbent bed connected with steel header tube to connect with condenser and evaporator.
- The expansion of tubes is taken into consideration of designing. For example, for 1m long copper tubes, the expansion is 1.2 mm at 100 ^{o}C.

Glazing Cover:

- The purpose of glazing cover is to permit all solar radiation to pass to the adsorbent bed and to reduce heat losses from the absorber to the atmosphere.
- Single-glass cover, double-glass cover and TIM cover are used in solar adsorption collector. TIM cover (Fig. 2.8) followed by double-glaze increased the performance of the system significantly because the reduction of the top heat losses of the collector close to the half [65]. However, Critoph and Tamainot-Telto [19] showed that the double-glaze enhanced the performance more than TIM and single-glazing.

- The most researches used single glass with 3 - 3.5 mm thickness, 0.95 transmissivity, 0.05 absorptivity and 0.9 emissivity. TIM glaze thickness reaches 8 cm [14].
- The air gab between the glaze cover and the absorber should be considered to reduce heat transfer by radiation and conduction.

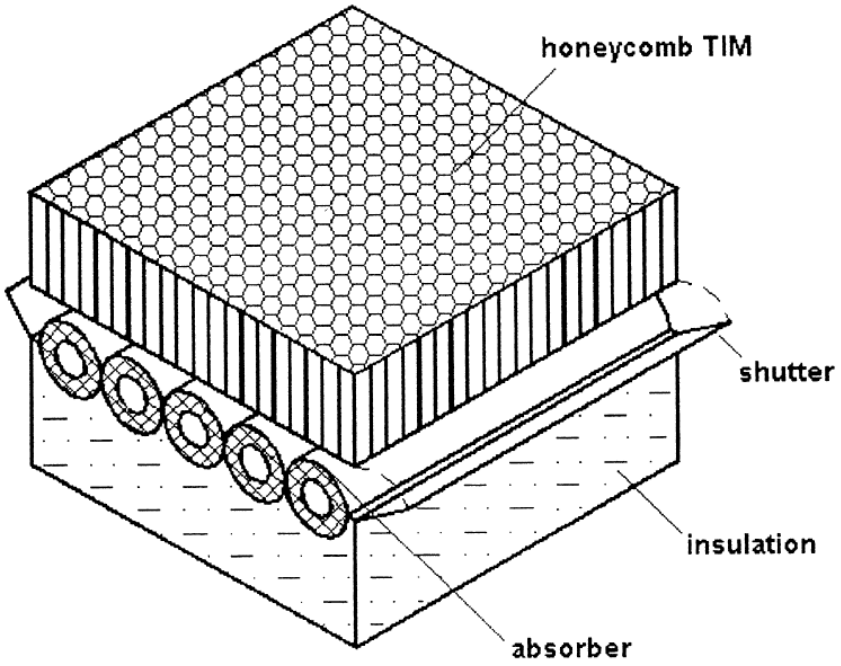

Figure 2.8 The solar adsorption collector with TIM cover [64].

Insulation:

- The good insulated collector during day hours remains the temperature of the reactor at high level by reducing the heat transfer to the ambient as minimum as possible.
- The insulation is placed at the bottom and the all sides of collector to avoid back and sides heat losses.

- The thickness of the insulation material is taken between 5-10 cm and the material should have a very low thermal conductivity as energylite (fiber glass 24 kg/m^3) which has thermal conductivity of 0.038 W/m.K at 150 ^{o}C [69]. The performance of the system depends strongly on its back insulation [68].

2.4.2 Condenser

The main purpose of the condenser is to dissipate heat from the vapor and condenses it back into a liquid during the process of desorption. To seek a better performance of the system, the condenser should have the following specifications:

- The orientation of the condenser is either in slope or vertical as has been presented in too many publications.
- The material of the condenser is to be made of high thermal conductivity materials such as copper. External aluminum fins are added (Fig. 2.9, (a) and (b)) to increase the area of cooling [67, 69].
- In the hot weather zones, cooling the condenser using the ambient air may not be very effective. Therefore, some researches pointed that the condenser is put in an open water tank as shown in Fig. 2.9, (c) and (d) [65, 66]. It should be noted that the condenser must be placed in shadow areas and avoid having it heated by the sun.

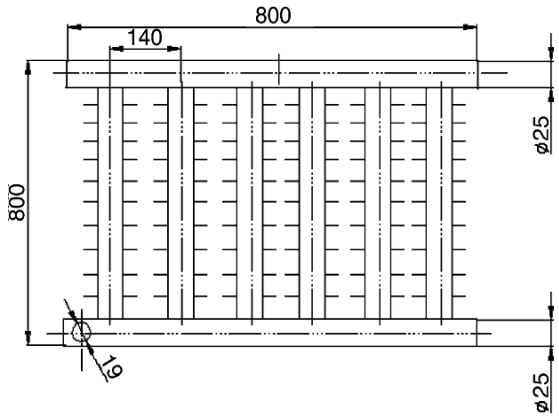

(a) Air condenser [67].

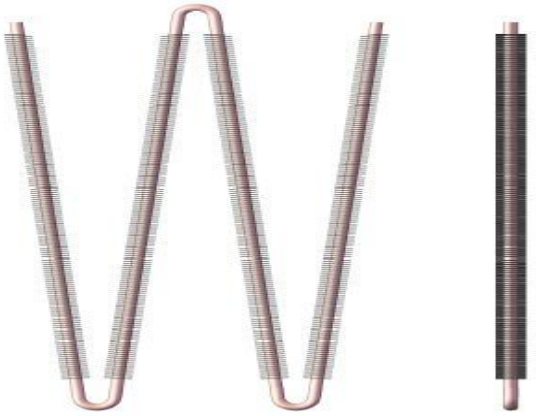

(b) Air condenser [69].

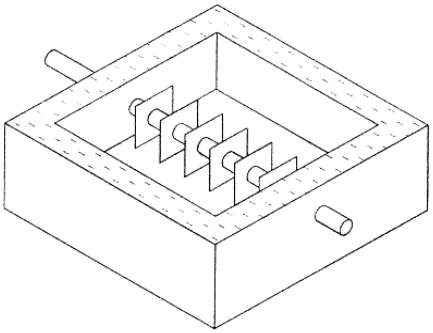

(c) Water condenser [65].

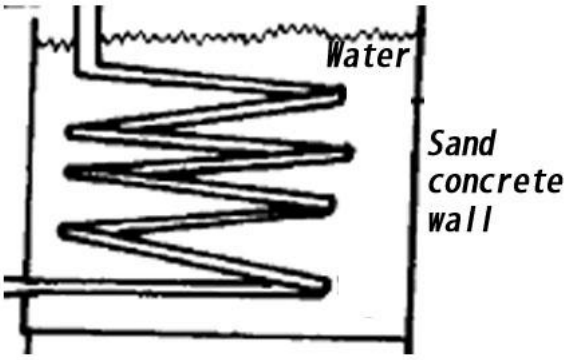

(d) Water evaporative condenser [66].

Figure 2.9 Air and water condensers.

2.4.3 Evaporator and Water Tank

The evaporator absorbs heat from the surrounding and removes it outside the cooled space by means of evaporating of the adsorbate. The evaporator should have the following specifications :

- The shape of evaporator should easily enable removing the formed ice in the water tank. Trapezoidal shape is a best example of an evaporator shape [67] or in tubular shape [14] as shown in Fig. 2.10.
- The capacity of evaporator should collect the maximum amount of refrigerant that injected to the system.
- The material of evaporator should have high thermal conductivity as copper.
- The evaporator is partly immersed in a water tank, which is made of stainless steel.
- Both the evaporator and water tank are placed in box covered with insulation. In the way that makes it very simple to remove the ice formed during adsorption cooling.
- The evaporator and water tank cabinet or box should made from high insulation material for example; 100 mm Energylite contained in 3 mm Perspex sheeting lined interior and exterior [69].
- Evaporator should be placed under shade to avoid having it heated during the day.

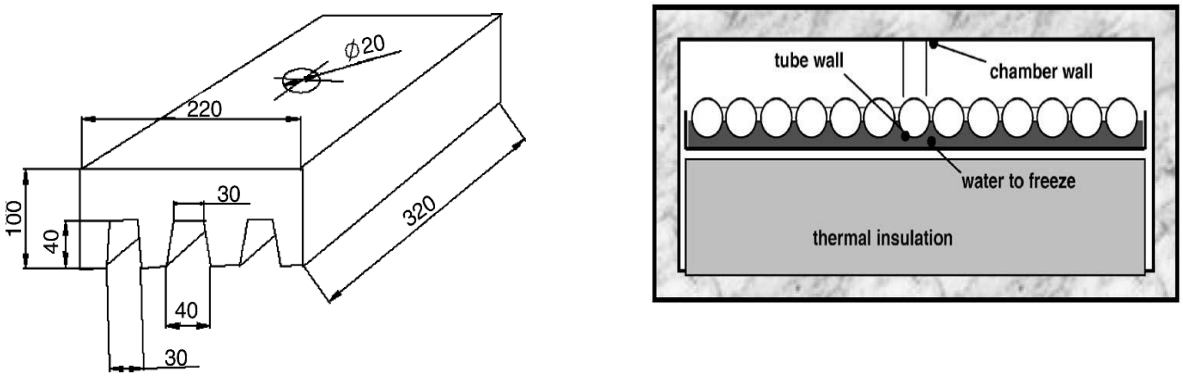

(a) Sketch of the trapezoidal evaporator (mm) [67].

(b) Tubular evaporator [17].

Figure 2.10 Trapezoidal and tubular configuration of the evaporator.

2.4.4 Reservoir, Valves and Sensors

Indeed, the methanol reservoir and system valves and sensor are required for reading measurements and adjusting flow path in search prototypes. That means for commercial purposes, the device can work efficiently without these parts. They are placed in the system as follows:

- Calibrated reservoir is put between the condenser and the evaporator to show the amount of condensed adsorbate after the desorption process.
- Some non-return valves are used in some systems for adjusting the flow path.
- Some pressure and temperature sensors are put in the adsorbent bed and also before and after the condenser and the evaporator to measure the temperatures and pressures of these components.

2.5 Objectives

Most of the literature review aimed at improving the performance of the continuous adsorption refrigeration systems. Otherwise, fewer researches have been focused on the solar intermittent adsorption cooling systems and the very low performance of such systems. The terminal objective of this study is to improve the performance of solar intermittent activated carbon/methanol adsorption refrigeration systems through thermodynamic analysis and modeling study of the system.

The specific objectives to address the above main objective are:

1. To obtain the optimum operative and constructive parameters of the system.
    - The operative parameters are:
        - Condensation temperature and pressure.
        - Evaporative temperature and pressure.
        - Adsorption temperature.
        - Desorption temperature.
    - And the constructive parameters are:
        - Activated carbon type.
        - Adsorbent bed thickness.
        - Glassing cover type and number.
        - Absorbing plate and absorbing coating.
2. To propose a solar intermittent activated carbon/methanol adsorption ice-maker for producing 5 kg or more of ice per meter square of solar collector per day under Dhahran climatic conditions in clear sky days.

CHAPTER 3

THERMODYNAMIC ANALYSIS AND MODELLING

The basic adsorption refrigeration cycle can be presented by two methods: ideal cycle (solid lines) and actual cycle (dashed lines), as shown in Fig. 3.1. The ideal cycle consists of two isosteric and two isobaric processes. The primary evaluation of the COP and the cooling effect are analyzed by ideal cycle. For more accurate results, the actual cycle is employed to represent the analyses of the system and study the effect of constructive parameters. The system dead volume and heat transfer characteristic for each component are needed for the determination of the paths of actual cycle.

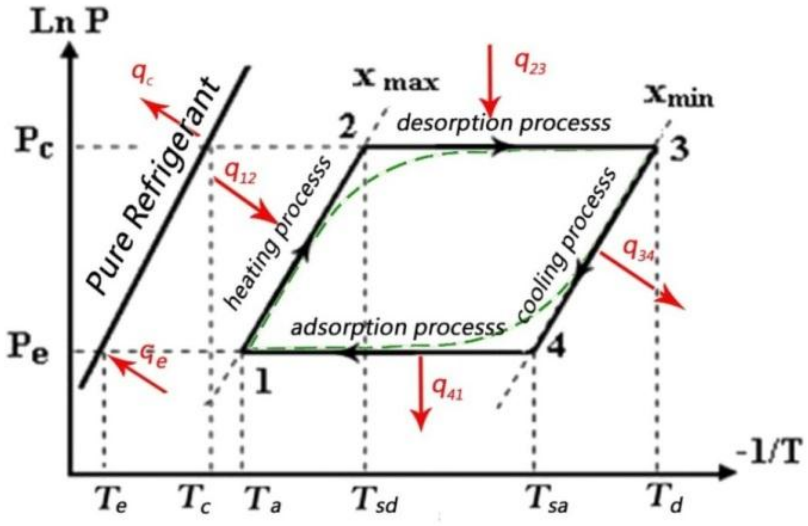

Figure 3.1 P-T-x diagram of ideal and actual adsorption refrigeration cycle.

In this chapter, the thermodynamic analysis and heat and mass transfer analysis will be formulated.

3.1 Thermodynamic Analysis

3.1.1 Sorption Concentration Rate

The rate of adsorption in physical adsorption is usually determined by Langmuire equation, Freundlich equation or Dubinin-Astakhov equation in which the adsorption equilibrium is described through three parameters, adsorbate concentration (x), adsorbent temperature (T) and system pressure (P) [70].

$$x = f(T, P) \tag{1}$$

The more accurate equation for physical micropores rate of sorption is introduced by Dubinin-Radushkevich equation that basically established for carbonaceous [71].

$$V = V_o \exp\left[-\left(\frac{\varepsilon}{\beta E_o}\right)^2\right] \tag{2}$$

where, the Polanyi adsorption potential ε is given by:

$$\varepsilon = RT\ ln\left({P_{sat}}/{P}\right) \tag{3}$$

Thus, Eq. (2) will be

$$\mathrm{V} = \mathrm{V_o} \exp\left[-\left(\frac{\mathrm{R}}{\beta \mathrm{E_o}}\right)^2 \left(\mathrm{T}\ \ln\left({\mathrm{P_{sat}}}/{\mathrm{P}}\right)\right)^2\right] \tag{4}$$

where:

V is the micropore volume filed with the adsorbed phase (m^3/m^3).

Vo is the limiting micropore volume (m^3/ m^3).

T is the system temperature (K).

β is an affinity coefficient or similarity coefficient, and expresses the ratio of the characteristic free energies of adsorption for the test and reference vapours (benzene gas is used as reference vapour for carbonaceous materials) [71].

E_o is the characteristic adsorption energy for a reference vapour on one specific adsorbent (J/mole). E_o is different from an adsorbent to another according to the micropore structure of the adsorbent.

R is the gas constant (J/mole .K).

P_{sat} is the system pressure according to adsorbent temperature.

P is the pressure of the adsorbed phase within the micropores; it equals to condenser pressure and evaporator pressure during desorption and adsorption processes, respectively.

Accordingly, multiplying by the density ρ(T) both sides of Dubinin-Radushkevich equation, the mass adsorbed *x* (T, P) becomes

$$x(\mathrm{T},\mathrm{P}) = \mathrm{V_o}\,\rho(\mathrm{T})\exp\left[-\left(\frac{\mathrm{R}}{\beta \mathrm{E_o}}\right)^2\left(\mathrm{T}\ln\left({}^{\mathrm{P_{sat}}}/_{\mathrm{P}}\right)\right)^2\right] \qquad (5)$$

$\mathrm{V_o}\,\rho(\mathrm{T})$ can be expressed as x_o, the maximum limit mass adsorbed.

An extension of the equation is introduced by Dubinin-Astakhov to allow a better fit to some adsorbent characteristics, which employs a variable index n instead of 2.

$$x(\mathrm{T},\mathrm{P}) = x_o \exp\left[-\mathrm{D}\left(\mathrm{T}\ln\left(\mathrm{P_{sat}}/\mathrm{P}\right)\right)^{\mathrm{n}}\right] \quad (6)$$

where D represents the value of $\left(\frac{\mathrm{R}}{\beta \mathrm{E_o}}\right)^{\mathrm{n}}$, which is determined by the characteristics of both adsorbent and adsorbate; it is independent of temperature.

Another expression of Dubinin-Astakhov equation is driven by using the relationship between saturation temperature and pressure

$$\ln(\mathrm{P_{sat}}) = \mathrm{a} - \frac{\mathrm{b}}{\mathrm{T_{sat}}} \quad (7)$$

where a and b are constants. By instituting in Eq. (6), the x will be

$$x = x_o \exp\left[-\mathrm{D}\left(\mathrm{T}\ln\left(\frac{\exp(\mathrm{a}-\frac{\mathrm{b}}{\mathrm{T_{ad}}})}{\exp(\mathrm{a}-\frac{\mathrm{b}}{\mathrm{T_{c,e}}})}\right)\right)^{\mathrm{n}}\right] \quad (8)$$

The $\mathrm{T_{ad}}$ is the adsorbent temperature replaced by T for simplifying, and $\mathrm{T_{c,e}}$ is the condenser or evaporator temperature denoted as $\mathrm{T_{sat}}$, the new expression is given by:

$$x(\mathrm{T},\mathrm{T_{sat}}) = x_o \exp\left[-\mathrm{D}\left(\mathrm{T}\ln\left(\frac{\mathrm{b}}{\mathrm{T_{sat}}} - \frac{\mathrm{b}}{\mathrm{T}}\right)\right)^{\mathrm{n}}\right] \quad (9)$$

Thus

$$x(\mathrm{T},\mathrm{T_{sat}}) = x_o \exp\left[-\mathrm{k}\left(\frac{\mathrm{T}}{\mathrm{T_{sat}}} - 1\right)^{\mathrm{n}}\right] \quad (10)$$

where k is constant equals to ($\mathrm{D*b^n}$).

3.1.2 Isosteric Heating Process

In this process, the concentration of methanol in the adsorbent bed remains constant at maximum value (x_{max}) as shown by line 1-2, in Fig. 3.1. The heat absorbed from solar energy is utilized to heat up both activated carbon and methanol. Then, the isosteric heat addition is expressed as:

$$\boldsymbol{Q_{12}} = \int_{T_a}^{T_{sd}} \left(M_{ac} C_{p(ac)} + M_{ac}\, x_{max}\, C_{vm} + M_{metal} C_{metal} \right) dT \qquad (11)$$

where:

x_{max} is the maximum concentration of methanol, it is a function of the minimum adsorption temperature and the evaporator pressure, f (T_a, P_e).

M_{ac} is the mass of adsorbent (activated carbon) (kg).

M_{metal} is the mass of absorber metal (kg).

$C_{p(ac)}$ is the specific heat of activated carbon (J/kg.K).

C_{vm} is he specific heat of methanol at constant volume (J/kg.K).

C_{metal} is he specific heat of the metal of absorber (J/kg.K).

T_a is the minimum adsorption temperature.

T_{sd} is the starting desorption temperature.

While T/T_{sat} is constant along an isostere, T_{sd} can be estimated by:

$$\frac{T_a}{T_e} = \frac{T_{sd}}{T_c} \qquad (12)$$

where T_e and T_c are the evaporator and condenser temperature respectively.

3.1.3 Isobaric Desorption Process

The desorption process is represented by the line (2-3) in Fig. 3.1 in which heat is supplied by solar energy. This heat is used to raise the temperature of activated carbon and to desorb the adsorbate from reactor to condenser. Therefore, the concentration of methanol in the activated carbon decreases to minimum value (x_{min}). The heat provided during this process can be written by:

$$\boldsymbol{Q_{23}} = \int_{T_{sd}}^{T_d} \left(M_{ac} C_{p(ac)} + M_{ac}\, x\; C_{pm} + M_{metal} C_{metal}\right) dT + \int_{x_{min}}^{x_{max}} M_{ac}\, \Delta H\; dx \quad (13)$$

where:

x is a function of the adsorbent temperature and pressure, as mentioned in Eq. (6).

x_{min} is the minimum concentration of methanol, it is a function of the maximum desorption temperature and the condenser pressure, $f(T_d, P_c)$.

T_d is the maximum desorption temperature .

C_{pm} is he specific heat of methanol at constant pressure (J/kg.K).

ΔH is the heat of desorption per unit mass of methanol (J/kg-methanol). ΔH is usually taken as constant for proper working pairs, i.e. $\Delta H = 1400$ kJ/kg-methanol for activated carbon/methanol pair [72]. It can be also estimated for any point on desorption or adsorption path from the slope of line (1-2) or line (3-4) in the Fig. 3.1 [70] as the following:

$$\Delta H = R \left[\frac{\partial(\ln P)}{\partial(1/T)}\right]_x \quad (14)$$

where R is the specific gas constant of methanol (259.5 J/kg.K).

Moreover, as long as $\frac{T}{T_{sat}}$ is constant along the isostere, so the adsorption heat is written as a function of latent heat of methanol [70]:

$$\Delta H = L_e \frac{T}{T_{sat}} \quad (15)$$

L_e is the latent heat of methanol vaporization at the adsorbent pressure (J/kg-methanol). ΔH is larger than the L_e due to the Van der Waals bonding between the adsorbate and adsorbent [73].

The desorption heat together with the isosteric heat are called generation or regeneration energy and expressed as:

$$\boldsymbol{Q_g = Q_{12} + Q_{23}} \quad (16)$$

3.1.4 Isosteric Cooling Process

The adsorbent bed in this process is cooled down by means of atmospheric air. Therefore, the system pressure drops from condenser pressure to evaporator pressure due to decreasing of adsorbent temperature. Like heating process, the concentration of methanol remains constant but at the minimum value (x_{min}) as shown by line 3-4. The sensible heat rejected from this process can be calculated by:

$$\boldsymbol{Q_{34}} = \int_{T_{sa}}^{T_d} \left(M_{ac} C_{p(ac)} + M_{ac}\, x_{min}\, C_{vm} + M_{metal} C_{metal}\right) dT \quad (17)$$

where T_{sa} is the temperature of point 4 at starting adsorption. It can be estimated from Eq. (18).

$$\frac{T_{sa}}{T_e} = \frac{T_d}{T_c} \tag{18}$$

3.1.5 Isobaric Adsorption Process

This process (line 4-1) is responsible on the vaporization of methanol from evaporator to be adsorbed by activated carbon. The heat is generated due to adsorbent cooling and adsorption heat at constant evaporator pressure. Eq. (19) is used to evaluate the isobaric adsorption heat.

$$\boldsymbol{Q_{41}} = \int_{T_a}^{T_{sa}} \left(M_{ac} C_{p(ac)} + M_{ac}\, x\; C_{pm} + M_{metal} C_{metal}\right) dT + \int_{x_{min}}^{x_{max}} M_{ac}\, \Delta H\, dx \tag{19}$$

where x is a function of the adsorbent temperature and the condenser pressure, as explained in Eq. (6).

ΔH here is heat of adsorption. It may not have the same value as in desorption process because the latent heat here will be at the evaporator pressure rather than that at the condenser pressure.

3.1.6 Evaporation and Condensation Heats

The evaporation heat acts firstly to reduce the temperature of the condensed methanol from the condenser temperature to the evaporator temperature, and then to cause cooling effect in the evaporator which used to produce ice or chilled water.

$$\boldsymbol{Q_e} = \Delta x * M_{ac} * (h_{gas,\ evap} - h_{liquid,\ cond}) \tag{20}$$

where:

Q_e is the evaporation heat.

$h_{gas,\ evap}$ is the specific enthalpy of the refrigerant gas leaving the evaporator (J/kg).

$h_{gas,\ cond}$ the specific enthalpy of the condensed liquid (J/kg).

Δx is the difference between the maximum concentration (x_{max}) and the minimum concentration (x_{min}).

The cooling effect occurs during adsorption process (4-1). On the other hand, condensation of methanol takes place throughout the desorption process (2-3). The condensation heat can be expressed as

$$\boldsymbol{Q_c} = M_{ac}\,\Delta x\,L_c \qquad (21)$$

where L_c is the latent heat of condensation at condenser temperature.

If ice is obtained in the water tank inside the evaporator during adsorption process, then the heat required to cool water from its initial temperature to 0 °C and then to produce ice that includes latent heat of water solidification at subzero centigrade temperature is given by:

$$Q_{cooling} = M_{ice}\,(L_{ice} + C_{pw}(T_{iw} - 0) + C_{p\_ice}(0 - T_{ice})) \qquad (22)$$

Where;

M_{ice} is the mass of produced ice,

L_{ice} is the latent heat of water solidification or fusion of ice at subzero temperature,

T_{ice} is the ice temperature (^oC).

T_{iw} is the initial water temperature usually equals an ambient temperature (^oC).

C_{p_ice} is the specific thermal capacity of the ice (J/kg.K).

3.1.7 Performance of the System

The performance of the system is described by the coefficient of performance of the cycle (COP) without including solar collector performance, the overall solar coefficient of performance (SCOP) that considers the diurnal incident solar energy as the input source or the effective solar coefficient of performance (ESCOP).

$$\mathrm{COP} = \frac{\mathrm{Q}_e}{\mathrm{Q}_g} \tag{23}$$

$$\mathrm{SCOP} = \frac{\mathrm{Q}_e}{\int_{t=sunrise}^{t=sunset} A_c\, I_T(t)\, dt} \tag{24}$$

$$\mathrm{ESCOP} = \frac{\mathrm{Q_e}}{\int_{\mathrm{t=sunrise}}^{\mathrm{t=end\ of\ generation\ process}} \mathrm{A_c}\, I_T(\mathrm{t})\mathrm{dt}} \tag{25}$$

where $I_T(t)$ is the incident solar radiation energy rate per unit area and t is the time. A_c represents the collector area. Q_e and Q_g are the cooling effect and collector generation heat, respectively. The specific cooling power SCP (W/kg) is also used only when chilled water is produced. It is defined as the ratio between the heat of refrigeration per unit mass of adsorbent for all cycle time:

$$SCP = \frac{Q_e}{M_{ac}\, t_c} \tag{26}$$

where M_{ac} is the mass of activated carbon (kg) and t_c is the whole cycle time.

3.2 Heat and Mass Transfer Modeling

3.2.1 Physical Description of the System

The model explains the estimation of heat and mass transfer in the three main components of activated carbon/methanol intermittent solar adsorption cooling system. These components are collector with adsorbent bed (reactor or generator), condenser and evaporator.

The adsorbent bed consists of a number of metallic tubes placed side by side as shown in Fig. 3.2. The activated carbon is put in an annular space between to axial tubes; the external tube is postulated to absorb the solar radiation energy, therefore it is coated by selective coating to increase the absorptivity of the surface, and the inner tube (metallic net tube) is perforated to permit flow of methanol vapor to or from the activated carbon from the evaporator or to the condenser. Using tubular reactor has advantages rather than rectangular bed by the simplicity of construction and capability of standing the pressure difference.

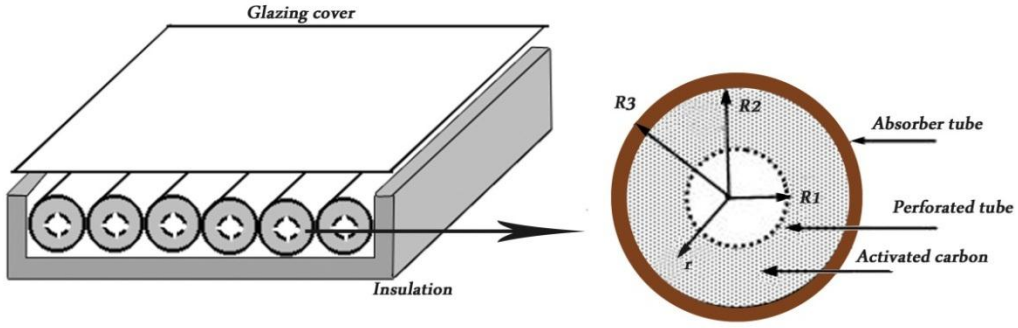

Figure 3.2 Schematic of solar collector and adsorbent bed.

For minimizing energy losses from generator, the rear and lateral insulation are coupled with collector. In addition, glazing cover is placed above the generator by leaving some space between adsorbent bed and glazing cover to reduce convection and radiation heat transfer. The glazing cover may be single glass cover, doubled glass or transparent insulation material TIM, as shown in Fig. 3.3.

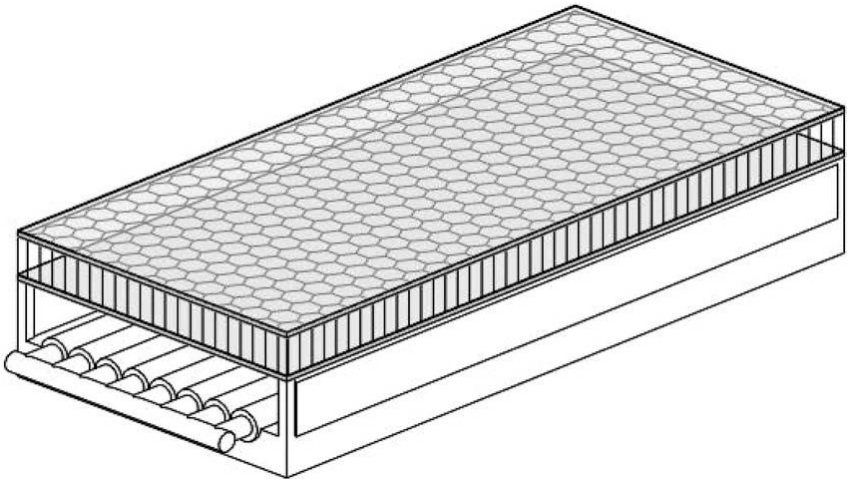

Figure 3.3 TIM cover in adsorption solar collector [74].

Condenser is usually made from metallic tubes, with coupling sometimes some fins to increase area of heat transfer to air. However, the high temperature of atmosphere in Dhahran affects badly on performance of the condenser and the whole system. Therefore, submerging the condenser in static water placed on an open tank helps to minimize condense temperature due to evaporation and radiation effects in low humidity environments.

Evaporator should be made from high thermal conductivity material in shape of connected tubes or trapezoidal (Fig. 3.4) for removing the ice easily with sufficient heat transfer area.

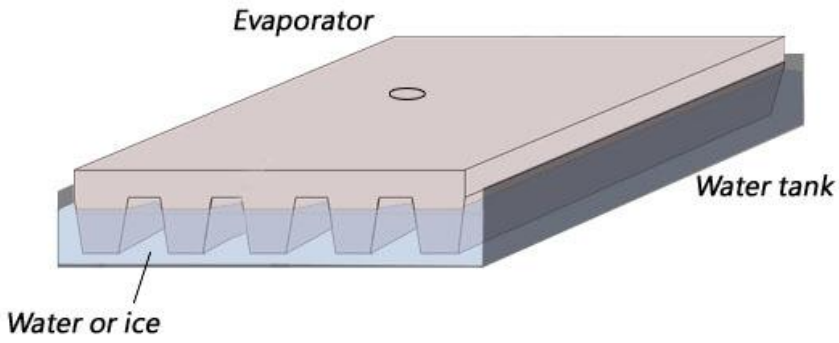

Figure 3.4 Schematic of trapezoidal evaporator.

3.2.2 Modeling Assumptions

In order to simulate and analyze the heat and mass transfer processes in the adsorbent bed, the following assumptions are utilized:

- The bed porosity is constant and the adsorbent consists of uniform size particles.
- The vapor methanol behaves as ideal gas.
- The desorption and adsorption occur in the vapor phase of methanol.
- The temperature of methanol and charcoal at the same point is the same.
- The variation of temperature occurs in radial direction only.
- The convection effects within the porous bed are negligible.
- The wall of absorber tubes is homogeneous and thin, therefore the thermophysical properties and temperature will be the same for each point.
- The specific heat of the desorbed or adsorbed methanol is considered as that of the bulk liquid methanol.

3.2.3 Collector Overall Heat Transfer Coefficient

As absorber wall absorbs a lot of energy during solar hours, it also releases some energy to the ambient even with existing of glazing cover and back and side insulation. In the night hours during cooling and adsorption process, back insulation should be removed or opened from collector to cool the adsorbent bed by atmospheric air.

The overall heat transfer coefficient U_L is expressed by

$$U_L = U_{top} + U_b + U_s \tag{27}$$

where U_{top}, U_b and U_s are the heat losses coefficients of the top, bottom and sides of the absorber, respectively.

Duffie and Beckman [75] showed an imperial equation developed by Klein (1979) for simplifying both hand and computer calculations of the top losses coefficient. This equation is fit to calculate U_{top} with small error equals ± 0.3 W/m^{2}K for the absorber temperature between ambient temperature and 200 ^{o}C:

$$U_{top} = \left[\frac{N_g}{\frac{c}{T_{pw}}\left(\frac{T_{pw}-T_{amb}}{N_g+f}\right)^e} + \frac{1}{h_w}\right]^{-1} + \left[\frac{\sigma(T_{pw}+T_{amb})(T_{pw}^2+T_{amb}^2)}{(\varepsilon_{pw}+0.00591N_g h_w)^{-1}+\frac{2N_g+f-1+0.133\varepsilon_{pw}}{\varepsilon_g}-N_g}\right] \tag{28}$$

where:

$N_g =$ number of glass covers

$f = (1 + 0.089h_w - 0.1166h_w\varepsilon_{pw})(1 + 0.07866N_g)$

$c = 520(1 - 0.00005\beta^2)\ \ for\ 0^o < \beta < 70^o$

$e = 0.430\left(1 - 100/T_{pw}\right)$

$\beta = collecor\ tile\ angle\ (degree).$

$\varepsilon_{pw} = emittance\ of\ the\ wall\ of\ the\ absorber\ tube$

$\varepsilon_g = emittance\ of\ the\ glass$

$T_{pw} = mean\ absorber\ tube\ temperature\ (Kelvin)$

$T_a = ambient\ temperature\ (Kelvin)$

$\sigma = Stefan - Boltzman\ cosistant\ (5.6704\ \times 10^{-8}\ W/m^2K^4)$

$h_w = wind\ heat\ transfer\ cofficient\ (W/m^2\mathrm{K})$

For transparent insulation material TIM, Rommel and Wanger [76] developed an imperial equation for calculating the top heat losses coefficient as a function of temperature difference between the absorber tube and the ambient. Moreover, Leite et al. [74] confirmed the agreement of this equation with his experimental results. That equation is given by:

$$U_{top(TIM)} = 1.14 + 0.011(T_{pw} - T_{amb}) \tag{29}$$

The back losses coefficient U_b depends on insulation material and its thickness and can be evaluated by:

$$U_b = \frac{k_i}{t_i} \tag{30}$$

where k_i and t_i are thermal conductivity and thickness of the insulation, respectively.

When the bottom insulation is opened during cooling and adsorbing processes, the back heat transfer coefficient is simplified by a function of wind velocity according to position and configuration of the collector and wind direction.

Finally, the edge (side) losses coefficient is almost neglected because of its small value. It can be estimated by heat flow around the perimeter of the collector and it should be referenced to the collector area [75].

$$U_{side} = \frac{\frac{k_i}{t_{is}} \times 2(L_c + W_c) t_c}{A_c} \quad (31)$$

where t_{is}, t_c, L_c, W_c *and* A_c are the side insulation thickness, collector thickness, collector length, collector width and the collector area, respectively.

3.2.4 Absorber Plate

The absorber wall is thin and homogeneous, so it has uniform temperature for all points. The absorber wall temperature T_{pw} can be predicted by the calculation of the heat balance at the external wall of the tube ($r = R3$, Fig. 3.2) as follows:

$$m_{pw}\, C_{pw}\, \frac{\partial T_{pw}}{\partial t} = (\tau_g\, \alpha_{pw}) I_T(t)\, D3\, L_t - U_L \frac{\pi}{2}\, D3\, L_t (T_{pw} - T_{amb}) - h\pi\, D2\, L_t (T_{pw} - T_{r=R_2}) \quad (32)$$

where m_{pw} and C_{pw} are mass and specific heat capacity of the absorber metallic tube, respectively. The both glass transmissivity (τ_g) and wall plate absorptivity (α_{pw}) contribute strongly on energy absorption. The absorber thickness is determined by the difference between external and internal radii of the tube (*R3-R2*). L_t represents the tube length, and h is the heat transfer coefficient between the absorber and the adsorbent which its value was estimated about 16.5-17 W/m^2K in the literature. I_T is the intensity of incident solar radiation on the collector (W/m^2); it is evaluated from incident solar radiation on horizontal plane by using Duffie and Beckman model [75] as a function of latitude angle, declination angle, collector slope angle, surface azimuth angle, ground reflectance (usually 0.2 for glass cover), and hour angle. Duffie and Beckman model

[75] is also used to estimate ($\tau_g \alpha_{pw}$) as a function of incident solar angle for both single and double glazing systems whereas τ_g of TIM is evaluated according to Leite model [65].

The horizontal incident solar radiation, ambient temperature and wind velocity are recorded by Research Institute, KFUPM for Dhahran climate conditions.

3.2.5 Adsorbent Bed

According to the mentioned assumptions in section 3.2.2, the adsorbent bed heat transfer is only in the radial direction between inner tube (*r=R1*) and internal surface of external tube (*r=R2)*. It can be expressed as following:

$$\rho_{ac}\,[C_{p(ac)} + xC_{pm}]\frac{\partial T}{\partial t} = k_{eff}\left[\frac{\partial^2 T}{\partial r^2} + \frac{1}{r}\frac{\partial T}{\partial r}\right] + \rho_{ac}\,\Delta H\,\frac{\partial x}{\partial t} \qquad (33)$$

where k_{eff} is effective thermal conductivity of the bed. *(r)* represents the local radius of the adsorbent bed varies between radius of the inner tube *R1* and that in the internal surface of the outer absorber tube *R2*.

$\frac{\partial x}{\partial t}$ denotes to rate of sorption that its value could be driven from the derivation of the sorption equilibrium state equation Eq. (6) (Dubinin-Astakhov equation), if the resistance to mass diffusion inside the micropores of activated carbon is neglected as:

$$\frac{\partial x}{\partial t} = nx\,D\,T^n\left(ln\left(\frac{P_{sat}(T)}{P}\right)\right)^{n-1}\left[\frac{\partial \ln P}{\partial t} - \frac{\Delta H}{RT^2}\frac{\partial T}{\partial t}\right] \qquad (34)$$

Otherwise, for accurate results, the resistance to mass diffusion is considered, so the kinetics of sorption $\frac{\partial x}{\partial t}$ is governed by a linear driving force (LDF) [17, 77, 78, 79]:

$$\frac{\partial x}{\partial t} = \left[\frac{15\, D_o}{r_p^2} \exp\left(\frac{-E_a}{R\, T}\right) \right] (x_{eq} - x) \qquad (35)$$

where the term between brackets is called mass transfer coefficient, D_o surface diffusion coefficient (m^2/s), r_p average radius of adsorbent particles (m), E_a the activation energy of surface diffusion (J/mol), x_{eq} the equilibrium concentration at the corresponding pressure and temperature that is estimated from Dubinin-Astakhov equation Eq. (6) and x represents the actual concentration. For activated carbon/methanol pair, the parametric reference values of Eq. (35) are: $\frac{15\, D_o}{r_p^2} = 7.35 * 10^{-3}$ (s^{-1}) and $\frac{E_a}{R} = 978\ (K)$ [77].

3.2.6 Condenser and Evaporator

The condenser is important component for dissipating methanol vapor energy that gained from generation process and then condensing it. The condenser equation depends mainly on ambient air or static water temperature where it is put in, it can be written as:

$$M_c\, C_{pc} \frac{\partial T_c}{\partial t} = -L_c\, M_{ac} \frac{\partial x}{\partial t} - h_c A_c (T_c - T_{amb}) \qquad (36)$$

where Mc is the metallic mass of the condenser, C_{pc} specific thermal capacity of metallic material of the condenser, h_c the heat transfer coefficient, A_c the heat transfer condenser area, T_{amb} is either the atmospheric temperature for air condenser or water temperature for evaporator condenser. The water temperature in case of evaporative condenser could be estimated by radiation and evaporation heat transfer to air from water surface.

Morever, the simplified equation to evaluate the condenser temperature for evaporative condenser that its tank made of sandcrete is expressed as following [80]:

$$T_c = 159.6 + 0.4575T_{amb} \tag{37}$$

The evaporator transient equation is:

$$\left[M_e\, C_{pe} + (M_m - x\, M_{ac})C_{pm}\right]\frac{\partial T_e}{\partial t} =$$

$$h_{e-w}A_{e-w}(T_w - T_e) + U_{e-amb}A_{e-amb}(T_{amb} - T_e) - L_e M_{ac}\,\frac{\partial x}{\partial t} \tag{38}$$

where M_e is the metallic mass of the evaporator, M_m the total amount of methanol that should be injected to the system, C_{pe} the specific heat capacity of the evaporator material, $h_{e\text{-}w}$ the heat transfer coefficient between evaporator and water; it is repleaced by $h_{e-w,ice}$ and h_{e-ice} during and after forming ice respectively, $A_{e\text{-}w}$ the heat transfer area that conducts the evaporator with water, $U_{e\text{-}amb}$ the heat transfer coefficient between the evaporator and the atmosphere and $A_{e\text{-}amb}$ the heat transfer area of the evaporator that facing the ambient.

The ice should be produced if T_w reaches below zero. The following equations used to calculate freezing water temperature and ice mass M_{ice} as well:

when $T_w > 0\ ^oC$:

$$M_w\, C_{pw}\frac{\partial T_w}{\partial t} = h_{e-w}A_{e-w}(T_e - T_w) + U_{w-amb}A_{w-amb}(T_{amb} - T_w) \tag{39}$$

when $T_w = 0\ ^oC$:

$$L_{sol}\frac{\partial M_{ice}}{\partial t} = h_{e-w,ice}A_{e-w}(T_e - T_w) + U_{w-amb}A_{w-amb}(T_{amb} - T_w) \quad (40)$$

when $T_w < 0\ ^oC$:

$$M_w\, C_{p(ice)}\frac{\partial T_w}{\partial t} = h_{e-ice}A_{e-w}(T_e - T_w) + U_{ice-amb}A_{w-amb}(T_{amb} - T_w) \quad (41)$$

where M_{ice} is the formed ice mass, $C_{p(ice)}$ the specific heat capacity of the ice, $A_{w\text{-}amb}$ the heat transfer area corresponding to heat exchange between tank water and ambient, $U_{w\text{-}amb}$ the heat transfer coefficient between water and atmosphere, $U_{ice\text{-}amb}$ the overall heat transfer between ice and atmosphere, $h_{e\text{-}w,ice}$ the heat transfer coefficient between the evaporator and mixing of formed ice and water, $h_{e\text{-}ice}$ the heat transfer coefficient between the evaporator and ice and L_{sol} the latent heat of solidification.

3.2.7 Boundary and Initial Conditions

The variation of climate conditions plays a basic role for the operation of the solar adsorption refrigeration system. Therefore, the performance of the system varies day by day according to insolation and ambient temperature changing. The initial conditions of the system for a new day are updated from the end of the previous day conditions.

Initial conditions can be given by:

for $t=0$, $T = T_{pw} = T_{iw} = T_{amb}$ (for starting first day), $x = x_{max}$, $P = P_e$

for starting desorption; $T_c = T_{amb}$

for starting adsorption; $m_{ice} = 0\ kg$

Boundary conditions:

The boundary condition is utilized to estimate Eq. (33) as following:

$$\left.\frac{\partial T}{\partial r}\right|_{r=R1} = 0 \tag{42}$$

$$-k_{eff}\left.\frac{\partial T}{\partial r}\right|_{r=R2} = h\left(T_{pw} - T|_{r=R2}\right) \tag{43}$$

The first B.C supposes that the adiabatic heat transfer between adsorbent and diffused vapor of methanol due to the very small value of thermal conductivity of methanol vapour 0.016 *W/m K.*

3.3 Research and Solution Methodology

The approach to achieve the thesis objectives consists of four main phases; namely: (1) updating the literature review, (2) thermodynamic analysis, (3) system modeling, (4) improving performance and proposing a solar adsorption ice-maker to produce 5 kg/day or more of ice per m^2 of collector area. The details of these phases are briefly described in the following sections.

3.3.1 Overall Literature Review

During this phase literature review was updated to include all the previous research work about solar adsorption refrigeration systems. An update of the literature related to intermittent activated carbon/methanol adsorption refrigeration systems is been conducting during the progress of the study. The literature review is providing guidelines that will help in achieving the objectives of this study.

3.3.2 Thermodynamic Analysis

EES computer program is used for thermodynamic analysis of the system and investigating the effect of operative parameters. The analysis relies on inserting some parameters into the program as minimum adsorption temperature, maximum desorption temperature, condenser and evaporator temperatures, amount and characteristics of activated carbon. The ideal performance of the system and the effect of the main operative parameters on the COP and amount of ice that can be produced will be investigated. The important parameters are the adsorption, desorption, condenser, evaporator and initial water temperatures as well as the evaporator and condenser pressures.

3.3.3 System Modeling

MATLAB computer program is utilized for modeling under Dhahran climatic conditions to optimize the important constructive parameters of the collector. The flat plate tubular reactor that is filled by activated carbon is utilized in the modeling, Fig. 3.2.

The following are the steps to model the system:

1. Using the weather data of Dhahran; these data include:
    - Average hourly incident solar radiation.
    - Average hourly atmospheric temperature.
    - Average hourly wind speed.
2. Determination of the characteristics and properties of the main materials of the system as activated carbon, glazing, insulation material, metal tubes and methanol from literature.
3. Modeling the system by using MATLAB program using the heat and mass transfer of each component of the system. The explicit finite difference scheme is used for simulation.
4. Calculating the actual SCOP and predicted amounts of produced ice and plotting the dynamic temperatures and pressures during 24 hours as: adsorbent bed temperature and pressure, condenser temperature and pressure and evaporator temperature and pressure as well as the concentration of methanol in the reactor.
5. Investigating the effect of the main operative parameters on the performance of the system such as the type and amount of activated carbon, absorptivity and emissivity of the absorber, glazing type and the back insulation thickness.

3.3.4 Improving the Performance

The optimal performance of the system (as SCOP and amount of produced ice) according to the best results of the thermodynamic analysis and the modeling study will be obtained. Accordingly, a solar adsorption ice-maker will be proposed to produce more than 5 kg of ice per m^2 of solar collector each day.

CHAPTER 4

RESULTS AND DISCUSSION

As mentioned before, this study focuses on two phases: thermodynamic analysis of the system without considering the volumetric parameters and the actual modeling of the system under Dharan climate conditions. Therefore, this chapter concerns with the results of these two phases.

4.1 Thermodynamic Analysis Results

The effects of the operative parameters on the COP and the amount of produced ice have been investigated through an EES program that is built for analyzing the cycle of the system thermodynamically. The results have focused on the main parameters as the desorption temperature and the minimum adsorption temperature. Furthermore, the evaporator temperature and the condenser temperature have been taken into consideration.

For validation of the EES code, the present results are compared with those of Wang et al. [81] using the same adsorbent bed parameters and operating conditions as shown in Table 4.1. The performance results of the present study (as COP and produced ice) are in close agreement with those of Wang et al. [81] and therefore the code is validated.

In order to investigate operative prarameters performance, 18 kg of activated carbon AC-35 have been used (which is very convenient for adsorption cooling purposes) and the limited adsorption capacity of AC-35 is taken as 0.425 liter of methanol per kg of activated carbon [18]. For evaporator and water tank containers, 7.5 kg and 4 kg of stainless steel are considered for holding about 5.9 kg and 7 kg of methanol and water, respectively; other specifications are shown with each figure below.

Table 4.1 Validation of the present results with those of Wang et al. [81].

Parameters	**M_{ac}=28 kg, m_{metal} =5 kg, x_o=0.284, k=10.21, n=1.39**							
Conditions	T_{iw}=15 °C T_c=25 °C T_e=-10 °C T_a=23.7 °C T_d=93.6 °C		T_{iw}=25 °C T_c=35 °C T_e=-10 °C T_a=31 °C T_d=100 °C		T_{iw}=10 °C T_c=20 °C T_e=-10 °C T_a=19.6 °C T_d=86.6 °C		T_{iw}=10 °C T_c=15 °C T_e=-10 °C T_a=19.5 °C T_d=84.9 °C	
Study	Wang et al.,2000	Present	Wang et al.,2000	Present	Wang et al.,2000	Present	Wang et al.,2000	Present
COP	0.44	0.45	0.32	0.324	0.48	0.495	0.51	0.52
M_{ice} kg/ ($2m^2$)	6.3	6.29	3.05	2.96	7.9	7.86	8.7	8.67

Figures 4.1 (a) and (b) give the effect of the adsorption temperature T_d on the COP and the ice production (M_{ice}), respectively, for various selected condenser temperatures while fixing the other parameters: Ta (adsorption temperature) = 30 °C, T_e (evaporator temperature) = -3 °C and (initial water temperature) T_{iw}= 30 °C. Fig. 4.1.a shows dramatic increase in COP with the desorption temperature from 60 to 95 °C for any given condenser temperature greater than 25 °C. The COP remains almost steady for large values of T_d (T_d > 95 °C) with Tc ≥ 35 °C and shows an almost linear slight decrease for Tc ≤ 35 °C. This linear small decrease in the COP is interpreted to the fact that most of

the methanol had desorbed below 100 ^{o}C, so the increase in heat input decreases the COP.

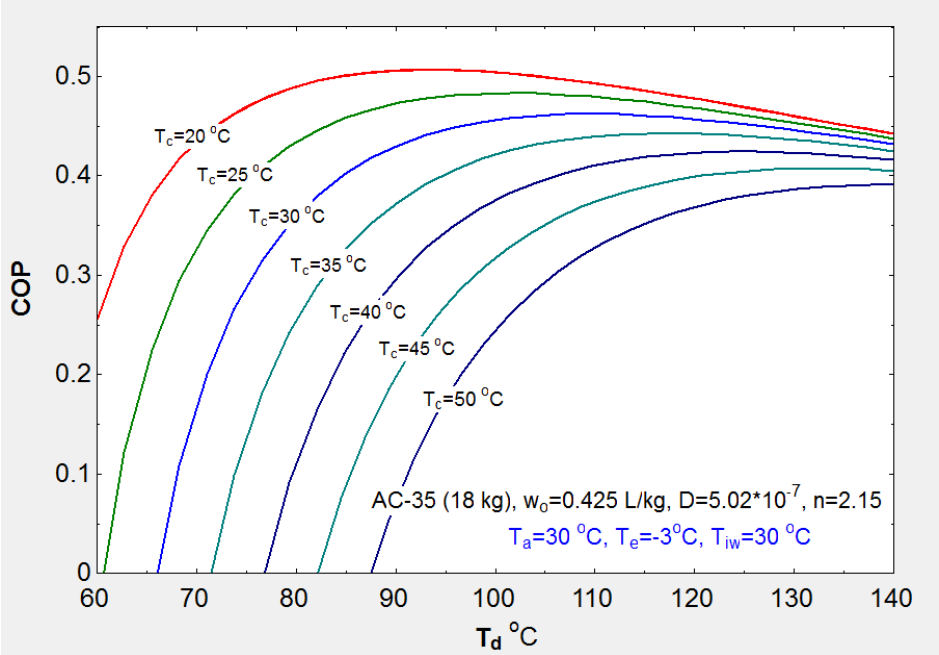

a. Effect of the desorption and condenser temperatures on the COP.

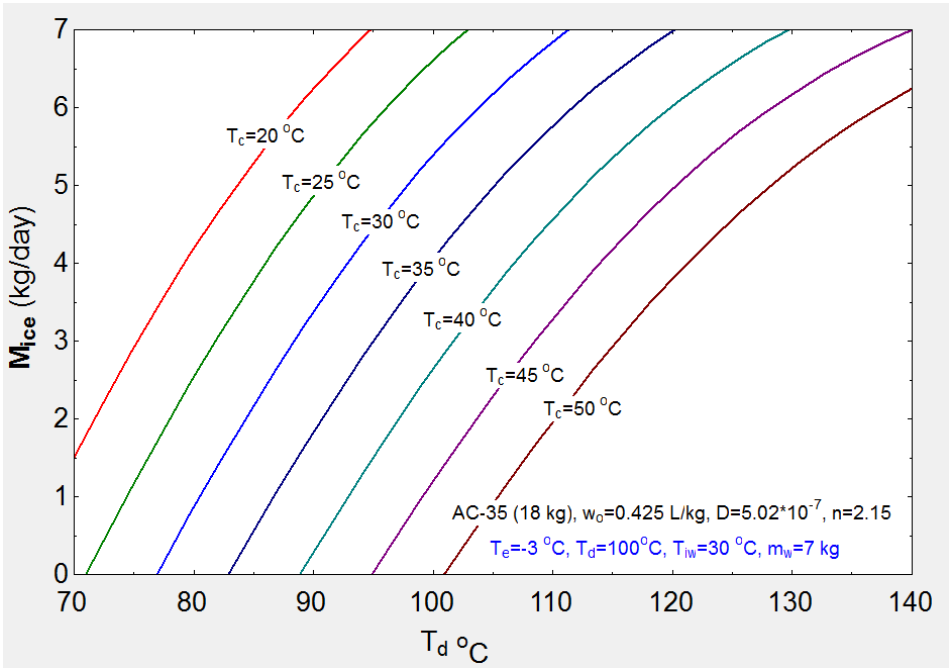

b. Effect of desorption and condenser temperatures on the amount of produced ice.

Figure 4.1 Effect of the desorption and condenser temperatures on the performance.

Moreover, increasing the condenser temperature obviously reduces the COP, that is because of the delaying of the desorption process which starts when the reactor pressure equals to the condenser pressure. The amount of produced ice is shown in Fig. 4.1.b versus the desorption temperature T_d. For a given T_c, the trend shows sharp increase in M_{ice} with increasing value of T_d then at a certain T_d, according to the condenser temperature, M_{ice} increases slightly.

Figure 4.2 presents the effects of both adsorbent and evaporator temperature on the performance due to simultaneous operating and direct influencing on each other as the case of the desorption temperature with the condenser temperature. The adsorption temperature and evaporator temperature have opposite effect on the performance as compared to the desorption temperature and condenser temperature, respectively, as shown in Fig. 4.2. The COP is shown in Fig. 4.2.a versus the adsorption temperature T_a with changing T_e from 0 ^oC to -10 ^oC . The trend shows slight decreases in the COP with increasing values of T_a (as $T_a \leq 35$ ^oC). The COP decreases sharply for $T_a < 35$ ^oC, that is because of shortening the adsorption process time. The evaporator temperature is also one of the important parameters that dominate the performance of the system. That is because of the adsorption process operates when the reactor pressure drops to be the same value as the evaporator pressure. Fig. 4.2.a also shows increase of the COP by increasing the evaporator temperature T_e. Furthermore, the amount of produced ice decreases in almost linear trend with increasing of T_a as shown in Fig. 4.2.b. The higher values of evaporator temperature with lower values of adsorption temperature enhance the performance of the system.

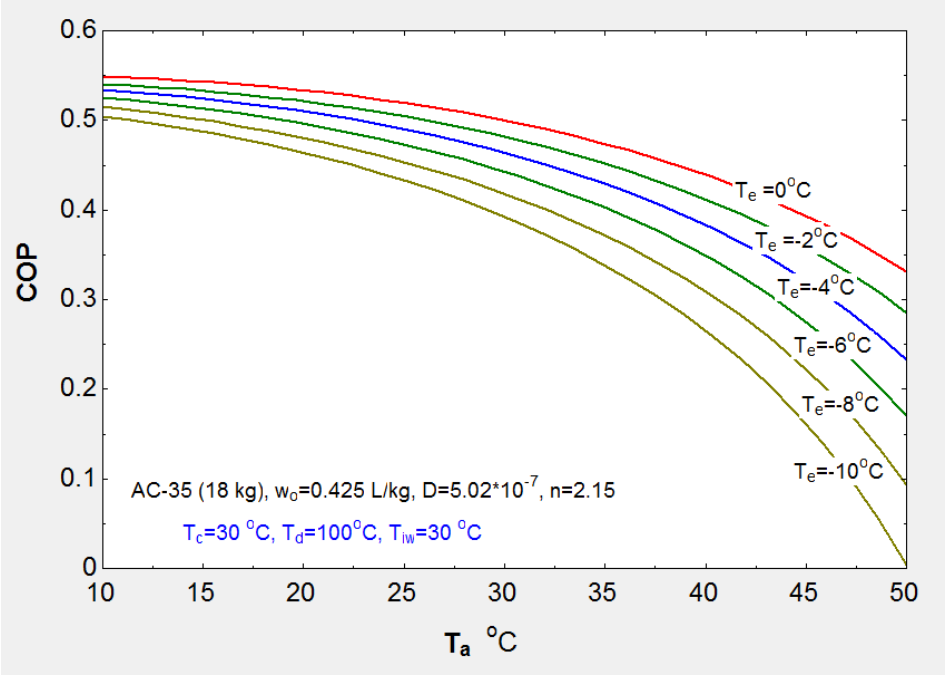

a. Effect of the adsorption and evaporator temperatures on the COP.

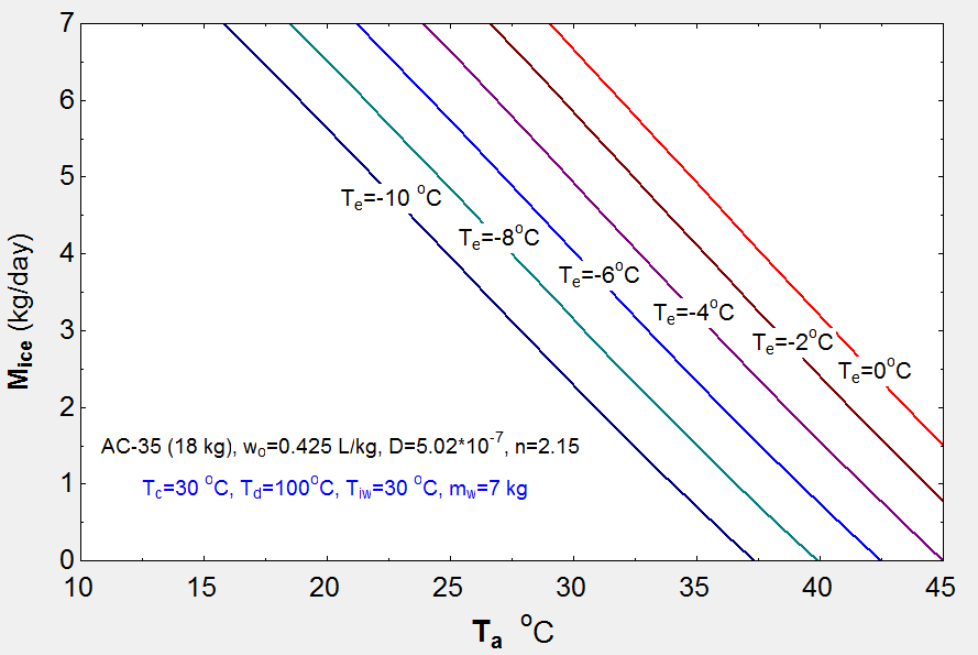

b. Effect of the adsorption and evaporator temperatures on the prdicted amount of produced ice.

Figure 4.2 Effect of the adsorption and evaporation temperatures on the performance.

Condenser and evaporator pressures as functions of their saturated temperatures have impact effects on the performance by affecting on the amount of methanol desorbed (m_m

(d)) and adsorbed (m_m (a)) respectively. Fig. 4.3 shows the increases of condenser pressure delay the desorption process, and thus the amount of methanol desorbed minimizes. Unlike condenser pressure, the increases of evaporator pressure accelerate the adsorption process, so the best result of cooling effect can be obtained at higher values of evaporator pressure as shown in Fig. 4.4.

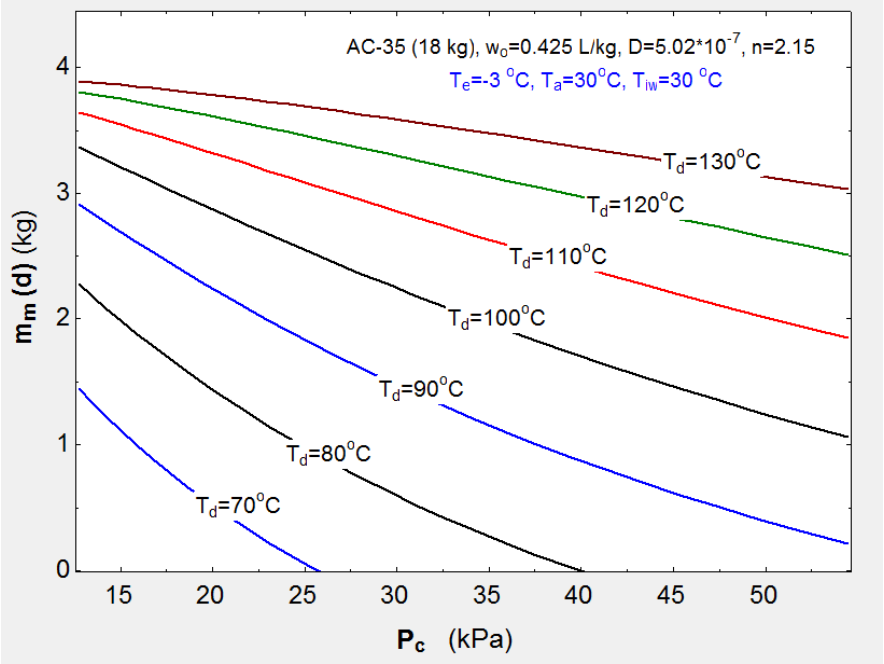

Figure 4.3 Effect of the condenser pressure on the methanol desorbed.

Sensible heat, that is required to cool water (from its intial temperature T_{iw} to 0 °c) inside a water tank in the evaporator, has a considerable effect on the amount of ice produced especially when the T_{iw} is high as shown in Fig. 4.5.

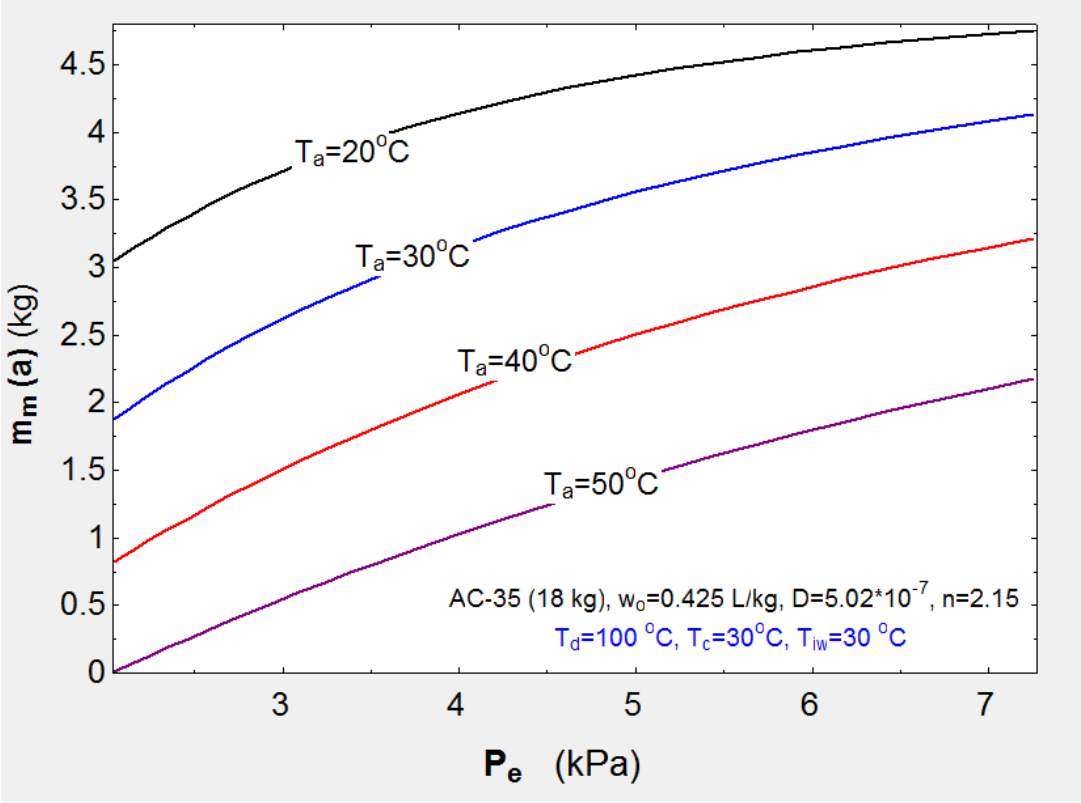

Figure 4.4 Effect of the evaporator pressure on the methanol adsorbed.

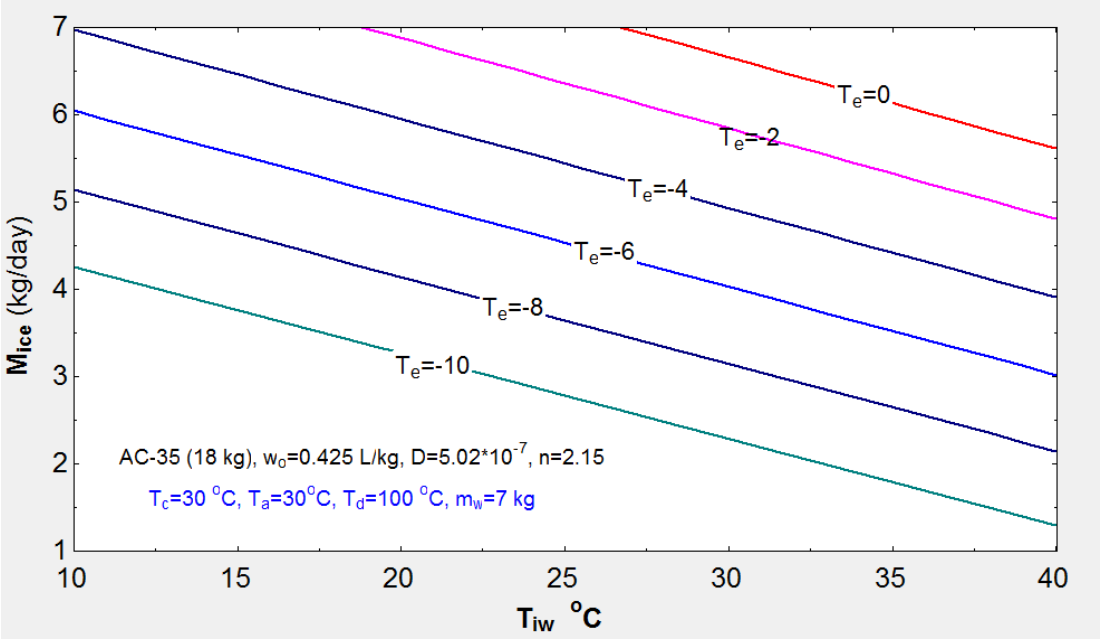

Figure 4.5 Effect of intial water temperature on amount of produced ice.

From previous Figures 4.1 - 4.5, the optimal results of COP (as 0.37 - 0.5) can be obtained for $T_c \leq 35\ ^oC$ (when $T_d \geq 90\ ^oC$). However, the amount of ice produced could be greater than 5 kg out of 7 kg of water (for $T_d \geq 105\ ^oC$ and $Tc \leq 35\ ^oC$, or $T_d \geq 97\ ^oC$ for $Tc \leq 30\ ^oC$) by neglecting the heat losses from evaporator. The amount of ice will be improved when the amount of water is lesser than 7 kg (i.e., 5 kg of ice is produced for $T_d = 91\ ^oC$ and $Tc = 30\ ^oC$ as $m_w = 5$ kg). On the other hand, the optimal results are achieved for freezing purposes if the evaporator temperature is close to zero ($0\ ^oC \geq T_e \geq -4\ ^oC$) for $T_a < 30\ ^oC$. Consequently, the optimum of condenser and evaporator pressures are lower than 25 kPa and greater than 3 kPa, respectively. Finally, 5 kg of ice can be produced, if the evaporator temperature is larger than $-4\ ^oC$ for intial water temperature below 30^oC.

4.2 Modeling Results

Section 3.2 explains the equations which are used in modeling by utilizing MATLAB program. However, the missed equation in that section is that pertinent to the wind heat transfer coefficient on the collector due to the difficulty of formulating it as a result of position and configuration of collector itself and the wind direction. So the next section discusses this issue before estimating the modeling performance results.

4.2.1 Wind Heat Transfer Coefficient of Top and Back Faces of Solar Collector

Wind velocity (V_w) contributes to cold glaze cover of solar collector during all adsorption cooling cycle time as well as to cold the back wall of adsorbent bed during cooling and adsorption processes. Whereas Watmuff et al. [82] had proposed the following imperical equation (Eq. (44)) to evaluate wind heat transfer coefficient as a function of free stream wind velocity at top of the collector (glass-ambient) for $V_w \leq 5$ (m/s), many researchers used this equation for unlimited wind speed, e.g. Anyanwe et al. [80] and Checkriou et at. [18].

$$h_w = 2.8 + 3\,V_w \qquad (44)$$

where h_w is the wind heat transfer coefficient from glass of collector to atmosphere (W/m^2 K) and V_w is the free stream wind velocity (m/s).

Therefore, one square meter collector tilted 26.3^o (Dhahran latitude), in which the direction faces the azimuth (south), is simulated by use of Gambit and Fluent computer programs to validate Eq. (44) and also to determine more accurate convection heat

transfer coefficient equations for the top and bottom of the solar collector (when the back insulation is removed).The collector is assumed to be above the ground by 1.3 m.

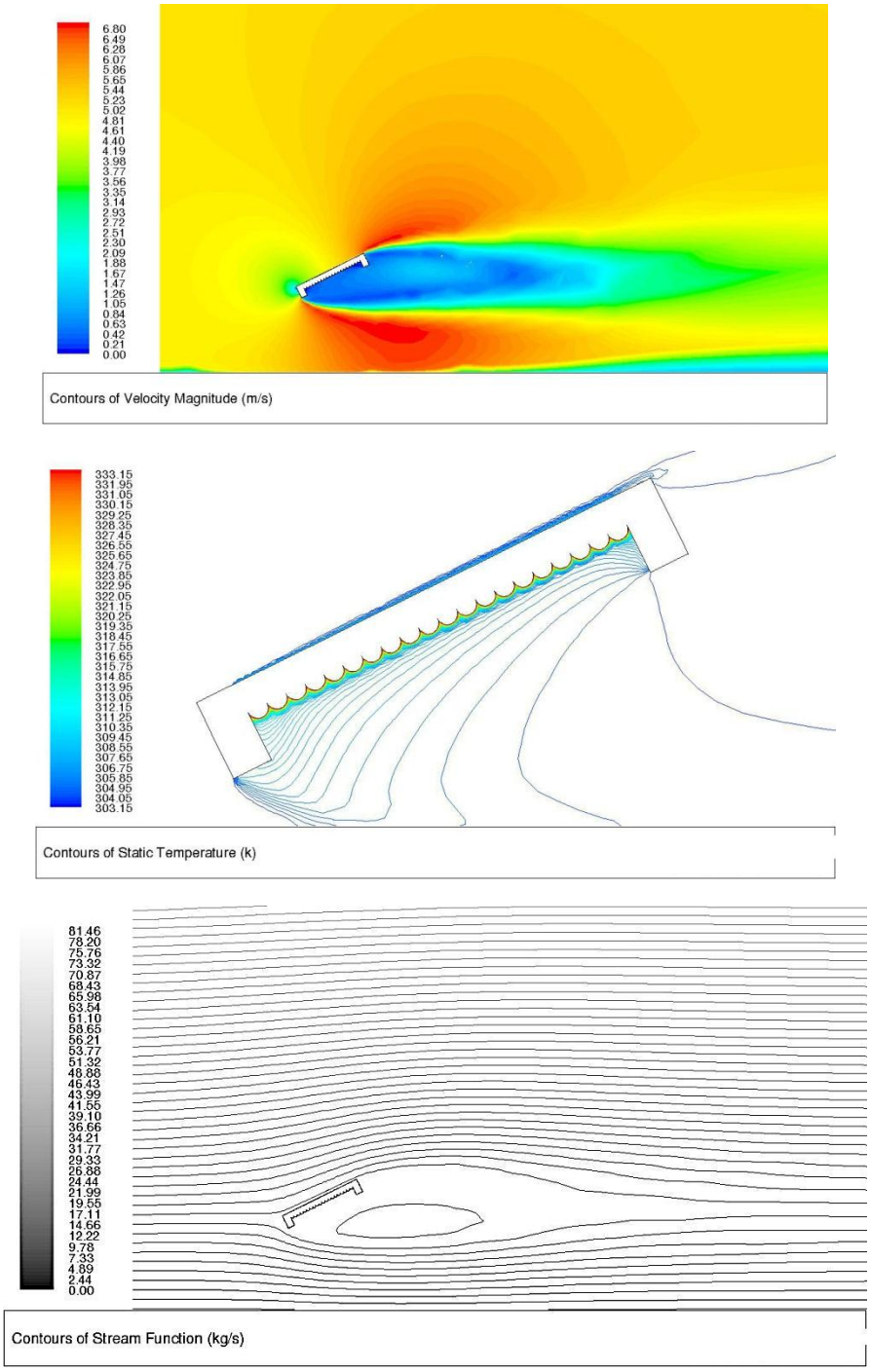

Figure 4.6 Velocity, temperature and stream function contours for almost southerly winds.

Figure 4.6 shows the contours of velocity, temperature and streamlines function as example for southerly wind (with V_w= 5 m/s, T_{pw}= 60 ^oC and T_{amb} = 30 ^oC). The contours show that the vortices appear at the right side (north) of the collector.

The top and bottom heat transfer coefficients are evaluated versus the free stream velocity as shown in Fig. 4.7. Changing of glass cover, absorber plate wall and ambient temperatures are taken into consideration. However, the obtained results show that the heat transfer coefficient varies only with wind velocity.

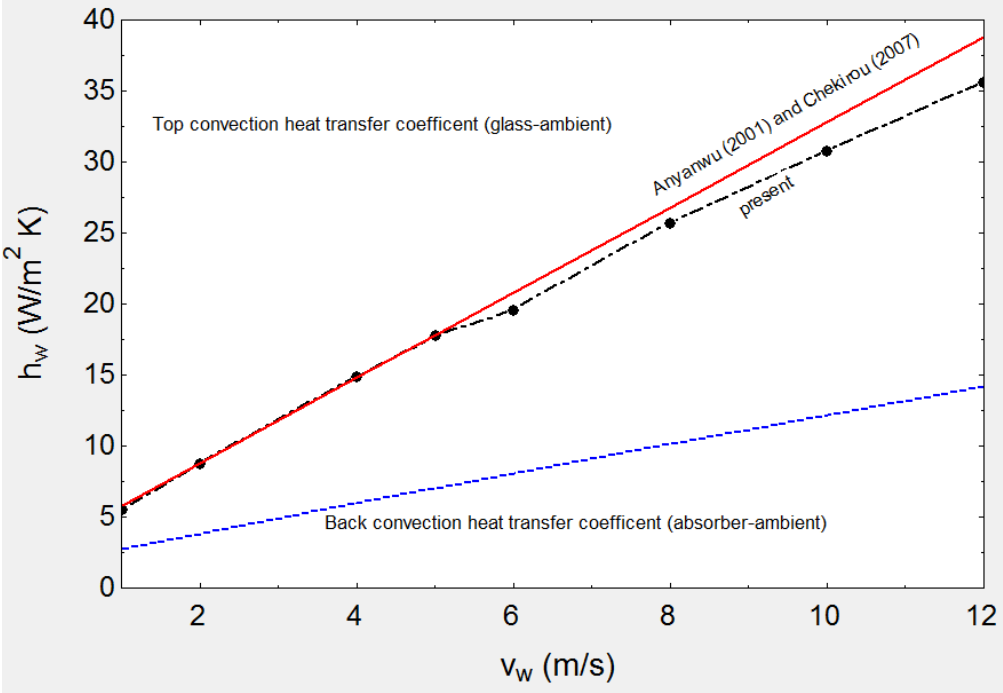

Figure 4.7 Effect of southerly wind velocity on the top and back wind heat transfer coefficient of the collector.

Fig. 4.7 shows that the convection heat transfer coefficient values validate Eq. (44) only when $V_w \leq 5$ m/s as had been indicated by Watmuff et al. [82]. For $12 \geq V_w \geq 5$ m/s, the results show that Eq. (44) can be used with a maximum error of 8.8 %.

New correlation polynomial equations are fitted from curves of accurate values in Fig. 4.7 with maximum error equals 2.9 % (to obtain wind heat transfer coefficient as a function of free stream wind velocity) instead of Eq.(44) are:

$$\left.\begin{aligned} h_{w(top)} &= 2.2433 + 3.405\,V_w - 0.058333{V_w}^2 && for V_w \le 5 \\ h_{w(top)} &= 3.2501 + 2.93543V_w - 0.0191138\,{V_w}^2 && for V_w > 5 \end{aligned}\right] \quad (45)$$

$$h_{w(back)} = 1.74316 + 1.0451\,V_w \quad (46)$$

However, Dhahran climatic conditions usually show northerly, north westerly or north easterly winds during most days of the year. This means that the direction of the wind is almost opposite to that studied in Equations 44, 45 and 46.

Figure 4.8 shows the contours of velocity, temperature and streamlines function for northerly wind as example when V_w = 6 m/s, T_{pw} = 60 ^oC and T_{amb} = 30 ^oC. The vortices obviously appear in the left side (south) of the collector. The change of wind direction (with remaining the same other conditions as in southerly wind case) causes a significant change on the convection heat transfer coefficient as shown in Fig. 4.9. Thus, the new correlation polynomial equations that are fitted from Fig. 4.9 for top and back convection heat transfer coefficients as functions of wind (almost northerly wind, as Dhahran case) with maximum error equals 1% are:

$$h_{w(top)} = 2.98467 + 1.82814\,V_w \quad (47)$$

$$h_{w(back)} = 1.54 + 1.63214\,V_w - 0.015\,{V_w}^2 \quad (48)$$

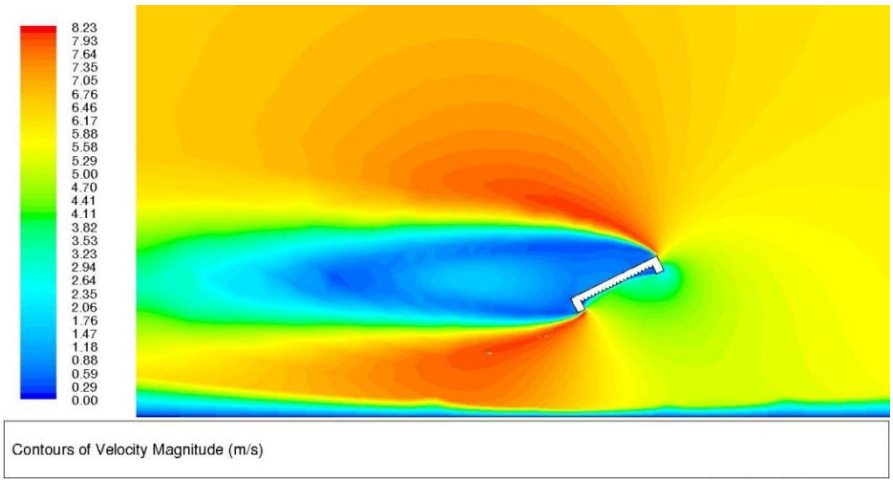

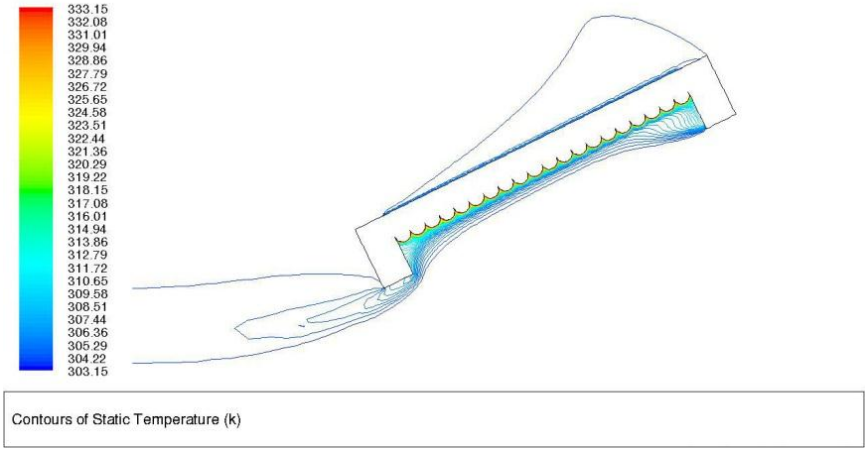

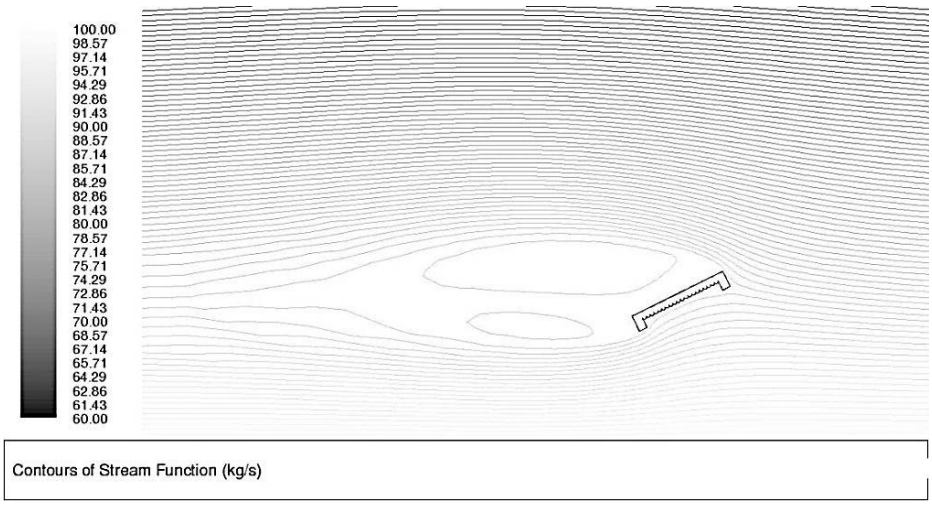

Figure 4.8 Velocity, temperature and stream function contours for almost northerly wind

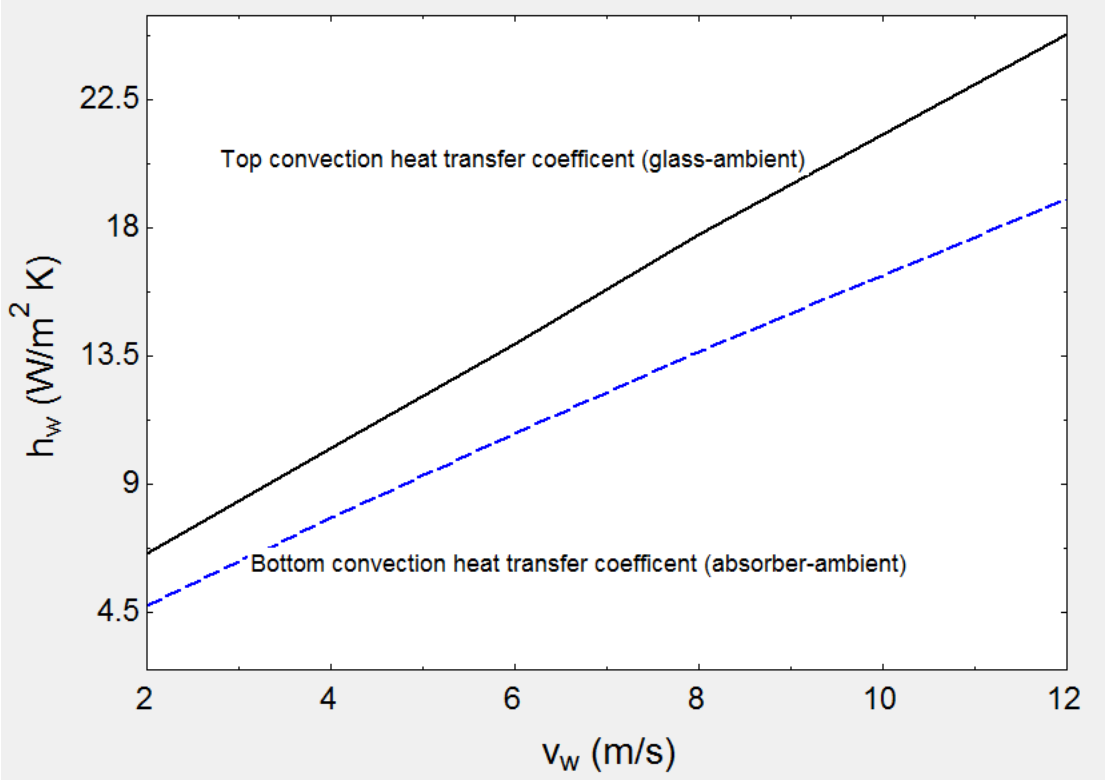

Figure 4.9 Effect of northerly wind velocity on the top and back wind heat transfer coefficient of the collector.

4.2.2 Overall Top Heat Transfer Coefficient (U_{top})

Heat losses from adsorbent bed to atmosphere are always calculated from a summation of convection and radiation heat transfers from adsorbent absorber plate to glass and then from glass to ambient. For single glaze cover, the overall top heat transfer coefficient is given by:

$$U_{top} = \left(\frac{1}{h_{c,pw-g}+h_{r,pw-g}} + \frac{1}{h_w+h_{r,g-amb}}\right)^{-1} \quad (49)$$

where:

$h_{c,pw-g}$ is convection heat transfer coefficient from absorber wall to glass (W/m^2 K).

$h_{r,pw-g}$ is radiation heat transfer coefficient from absorber wall to glass (W/m^2 K).

$h_{r,g-amb}$ is radiation heat transfer coefficient from glass to ambient (W/m^2 K).

The heat transfer from absorber plate to ambient is obviously affected by the emissivity of the plate. For example, if the plate is coated by selective material (ε_{pw} = 0.1, in this case the collector is called selective collector), the heat losses values will decrease to about half of that in nonselective collector (ε_{pw} = 0.9) as shown in Tables 4.2 and 4.3 (for T_{pw} = 50 ^{o}C, T_{amb} = 25^{o}C and V_w varies from 1 to 12 m/s).

Table 4.2 Heat losses from selective collector (ε_{pw}= 0.1, T_{pw}= 50 ^{o}C, T_{amb}= 25^{o}C).

Wind velocity V_w (m/s)	Total top Heat losses q (W/m^2)	Convection (absorber-glass) $q_{c,pw-g}$ (W/m^2)	Radiation (absorber-glass) $q_{r,pw-g}$ (W/m^2)	Convection (glass-ambient) q_w (W/m^2)	Radiation (glass-ambient) $q_{r,g-amb}$ (W/m^2)
1	67.53	58.87	8.657	29.52	38.01
2	70.43	61.51	8.924	36.49	33.95
3	72.81	63.67	9.139	42.14	30.67
4	74.78	65.46	9.316	46.82	27.96
5	76.45	66.98	9.464	50.75	25.69
6	77.87	68.28	9.59	54.11	23.77
7	79.11	69.41	9.699	57	22.11
8	80.19	70.39	9.793	59.52	20.66
9	81.14	71.26	9.876	61.74	19.4
10	81.98	72.03	9.95	63.71	18.28
11	82.74	72.72	10.01	65.46	17.28
12	83.42	73.34	10.07	67.03	16.39

Tables 4.2 and 4.3 show the total top heat losses and their components such as convection and radiation heat transfers between plate wall and glazing cover and then from glazing cover to ambient for the plate emissivity equals 0.1 and 0.9, respectively.

For selective coating collector, the values of radiation heat transfer from plate to glass decrease almost 90 % when compared with the case of nonselective collector. Consequently, the total heat losses reduce to about a half.

Table 4.3 Heat losses from nonselective collector (ε_{pw} = 0.9, T_{pw}= 50 °C, T_{amb}= 25°C)

Wind velocity V_w (m/s)	Total Top Heat losses q (W/m^2)	Convection (absorber-glass) $q_{c,pw-g}$ (W/m^2)	Radiation (absorber-glass) $q_{r,pw-g}$ (W/m^2)	Convection (glass-ambient) q_w (W/m^2)	Radiation (glass-ambient) $q_{r,g-amb}$ (W/m^2)
1	119	40.76	78.25	51.35	67.66
2	126.9	44.17	82.7	65.04	61.83
3	133.5	47.1	86.45	76.63	56.91
4	139.3	49.64	89.65	86.58	52.72
5	144.3	51.88	92.42	95.2	49.09
6	148.7	53.85	94.83	102.8	45.93
7	152.6	55.6	96.96	109.4	43.14
8	156	57.16	98.84	115.3	40.68
9	159.1	58.57	100.5	120.6	38.48
10	161.9	59.85	102	125.4	36.5
11	164.4	61.01	103.4	129.7	34.72
12	166.7	62.07	104.6	133.6	33.1

Eq. (50) will be more complicated when the number of gazing covers is greater than two covers. Therefore, Eq. (28) is easier for both hand and computer calculations.

Both Equations (28) and (50) include all parameters that are needed to estimate the top heat transfer coefficient such as: absorber, glass and ambient temperatures, absorptivity and emissivity of the absorber wall, transmissivity and emissivity of glazing cover, collector tilt angle, etc. The only parameter that had never been involved in Eq. (28) is the space between absorber and glazing cover.

That is because Eq. (28) assumes all spaces between absorber and glazing cover could satisfy the heat transfer mechanism without changing values of the top heat transfer coefficient, while in reality the space should be greater than 10 mm to avoid conduction and radiation heat losses as shown in Figures 4.10 and 4.11 for single and double gazing cover collectors, respectively. Both Figures 4.10 and 4.11 show the effect of space

(between absorber plate and glazing cover) on the overall top heat transfer coefficient as solid lines, while the dashed lines present the corresponding constant values of U_{top} that are obtained by using Klein equation.

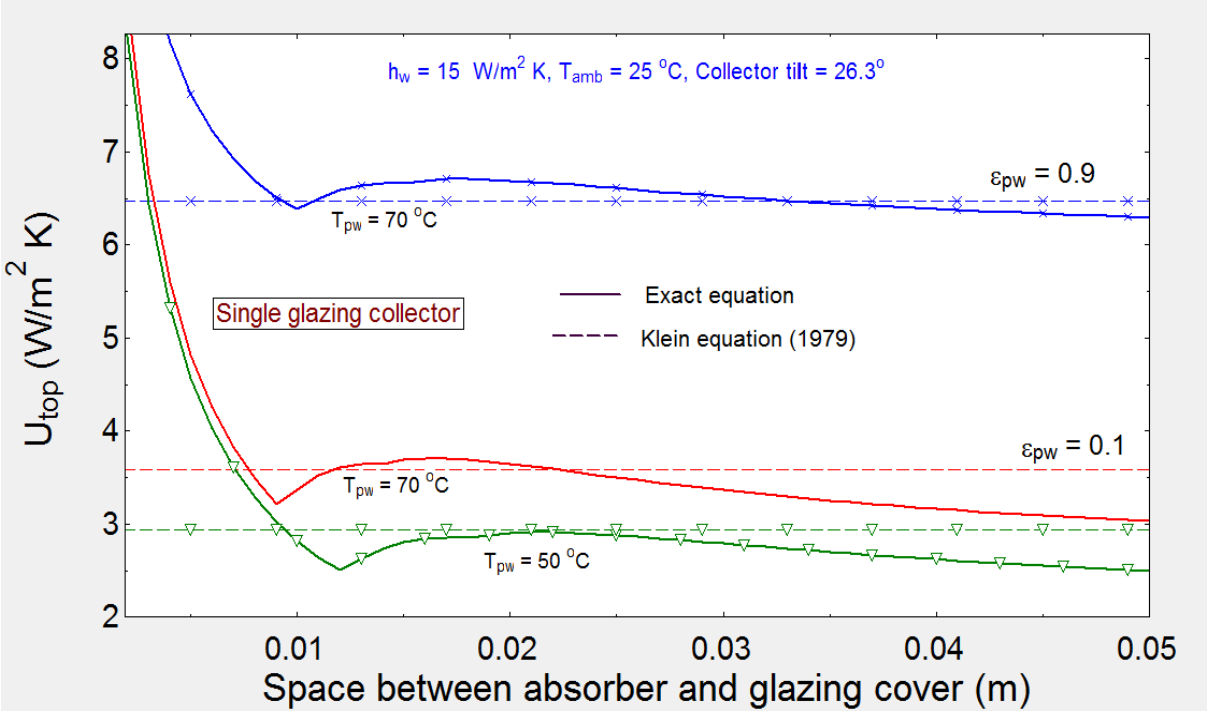

Figure 4.10 Effect of space between absorber and single glazing cover on top heat transfer coefficient for some selected values of T_{pw} and ε_{pw}.

As these figures show, for given absorber wall temperature and emissivity, U_{top} decreases from high values (caused by conduction and radiation heat transfers for spaces < 10 mm) to a certain low value for space between 10 and 15 mm and then U_{top} fluctuates slightly.

In double glazing collector, space between covers equals to space between absorber and first cover. The values of space on the horizontal axis of Fig. 4.11 are only between the absorber wall and the first cover, therefore the total space between metal absorber and the second cover has double value of that shown in Fig. 4.11.

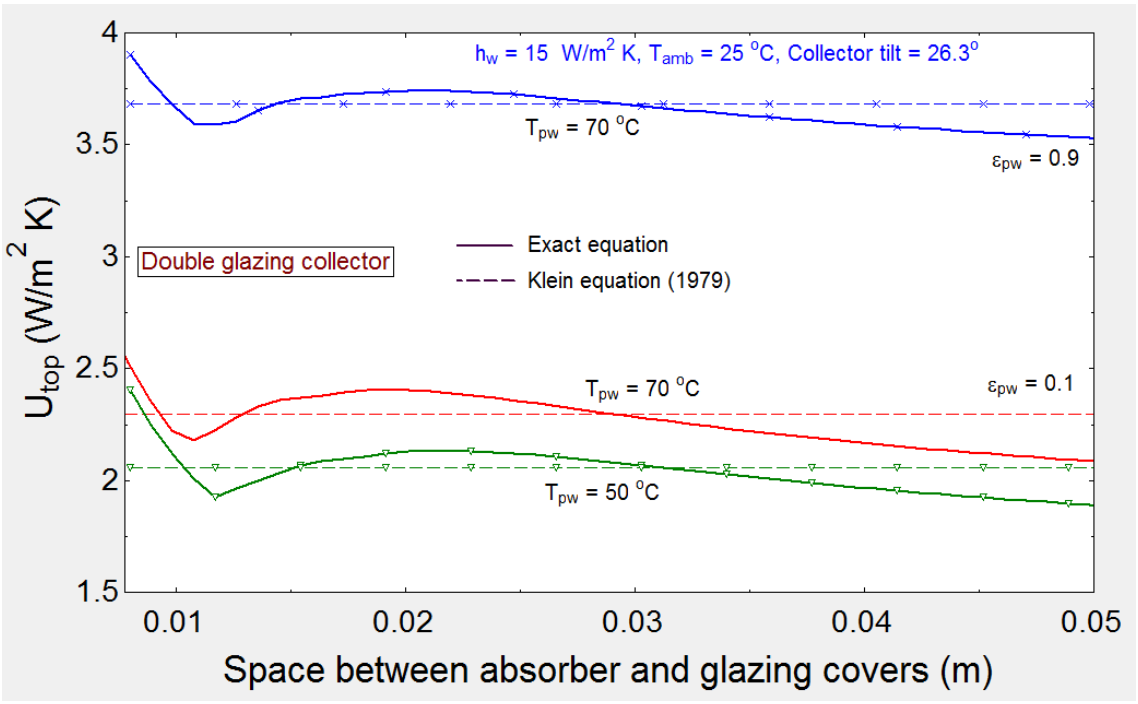

Figure 4.11 Effect of space between absoeber and double glazing cover on top heat transfer coefficient for some selected values of T_{pw} and ε_{pw}.

From Figures 4.10 and 4.11, one can evaluate the error percentage when the Klein equation (Eq. (28)) is used instead of exact equation for single glazing cover with selective (ε_{pw} = 0.1) and nonselective (ε_{pw} = 0.9) collectors, respectively. The best use of Klein equation for single glazing cover (for ε_{pw} = 0.1) is by taking the space about 22 mm in which the erorr is close to zero for various absorber temperatures. However, the error is smaller than 4% for space greater than 10 mm in nonselective collector.

For selective double glazing cover, the error values are less than 5% for space range (10 – 35 mm). Otherwise, that error reduces to lesser than 2% for nonselective double glassing collector.

In general, Eq. (28) can be used for calculating the U_{top} with small error (for 10 mm $\leq$ space $\leq$ 40 mm). Use of selective double glazing cover collectors can reduce the top heat

losses by about 25% than nonselective double glazing and by about 65% than the nonselective single glazing cover collectors.

4.2.3 Actual Thermal Behavior of the System

4.2.3.1 Validation of the Code

Under Dhahran climate conditions on 10 - 11 May 2011, the single glass cover system is simulated to compare the performance results with the experimental investigation performance by Midini et al. [15] in Tunisia as shown in Table 4.4. Activated carbon (AC-35) has been used in the two studies. The present results are obtained for a system consisting of 0.8 m^2 single glass cover collector (with 10 stainless steel tubes, 1.93 cm adsorbent thickness and 8 cm outer absorber diameter), air condenser (copper aluminum finned tubes: A_c = 1 m^2) and stainless steel trapezoidal evaporator (7.5 kg) as well as stainless steel water tank (4.2 kg).

Table 4.4 presents the important parameters of the two studies to be compared such as solar coefficient of performance (SCOP), amount of methanol desorbed and condensed ($m_m(d)$) , amount of produced ice (M_{ice}), maximum desorption temperature (T_d), minimum adsorption temperature (T_a), minimum evaporator temperature (T_e), maximum condenser temperature during desorption process (T_c), average atmosphere temperature during all cycle time (T_{amb}) and total incident solar radiation on the collector (I_T).

At the same solar radiation (I_T), collector area (A_c) and amount of activated carbon (M_{ac}) with experimental prototype study, first simulation (present (a), Table 4.4) shows T_d is higher than that of Medini prototype by about 23 ^oC because the 35 ^oC of the ambient

temperature in Dhahran is much higher than the 16 ^{o}C of Tunisia at the same time of the year. Consequently, the smaller difference between absorber and ambient temperature reflects to minimize heat losses from collector. Another reason is the larger condenser temperature ($T_{c\ (max)}$ = 42.5 ^{o}C) that delays the desorption process. For the same reasons, the methanol desorbed amount (m_m(d)) is less (2.06 kg) instead of 2.5 kg. Some of this condensed amount cannot be absorbed during the night due to the large adsorption temperature (T_a = 34 ^{o}C) which impacts negatively on the system performance (as M_{ice} = 1 kg and SCOP= 0.1).

Table 4.4 Comparsion between present simulation results with Medini [15] exprirmental results.

Study	T_d (^{o}C)	T_a (^{o}C)	T_c (max) (^{o}C)	T_e (min) (^{o}C)	T_{amb} (mean) (^{o}C)	I_T (MJ)	A_c (m^2)	M_{ac} (kg)	m_m(d) (kg)	M_{ice} (kg)	SCOP
Medini (1991), Tunisia	90	13	30	-2	16	20	0.8	15	2.5	4.2	0.15
Present (a), Dhahran	113.5	34	42.5	-1	35	20	0.8	15	2.06	1	0.10
Present (b)	91	15	30	-1.7	16	20	0.8	15	2.6	4.5	0.153

For the same I_T, T_{amb} and T_c as the experimental values, in the present simulation results (present (b), Table 4.4) show the excellent agreement with the experimental performance results (as SCOP, M_{ice} and m_m(d)) and approximately similar obtained parameters (as T_e, T_d and T_a). Correspondingly, the modeling code is validated.

4.2.3.2 Performance under Hot and Cold Climate Conditions.

The flat plate solar collector with tubular adsorbent bed shown in Fig. 4.12 is studied in this investigation. About 20 kg of AC-35 is placed inside the 13 stainless steel tubes (each one has outer diameter equals 7.3 cm and 2 cm for inner pass tube); the corresponding methanol mass is xo*Mac = 0.33*20 = 6.6 kg. The tubes are coated by

selective coating (with maximum absorptivity (α_{pw}) and transmissivity (ε_{pw}) equal 0.9 and 0.05 respectively); single glazing (of the water white or also known as low iron glass type) cover is also used. Copper aluminum finned tubes (A_c = 1m^2) form the air cooled condenser, and trapezoidal stainless steel evaporator is used as shown in Fig. 3.4. Mass of evaporator metal is 7.4 kg and mass of water tank is 4.5 kg for holding 13 kg of water as a maximum (7 kg of water is studied in this section). Finally, fiber glass insulation is used on the sides (5 cm thick) and rear (10 cm thick) of the collector and also in the box that surrounds the evaporator (10 cm thick).

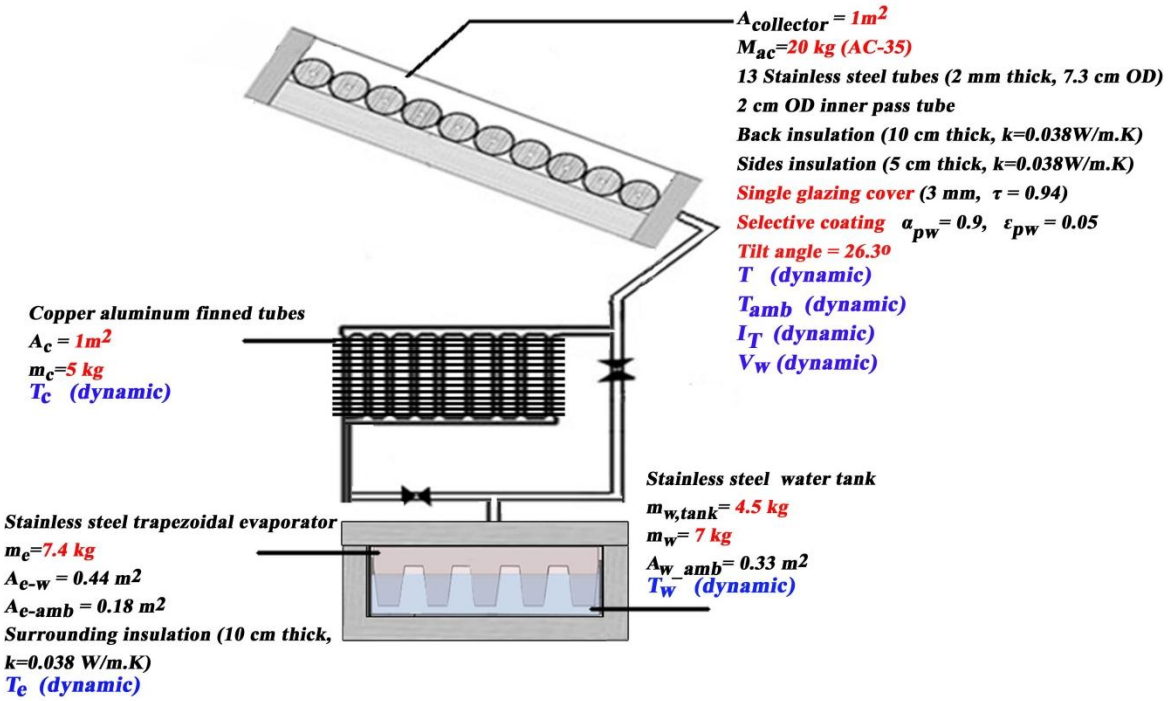

Figure 4.12 System configuration details

Under Dhahran hot climate conditions from 14th to 20th of June 2011, the system behavior and performance are estimated as shown in Figures 4.13, 4.14 and 4.16 and Table. 4.5. Fig. 4.13 shows the recorded ambient temperature and the incident solar radiation on collector (Tilt = 26.3^{o}) that is calculated from the measured incident solar radiation on horizontal surface. The maximum incident solar radiation on the collector is between 850 and 950 W/m^2 and the ambient temperature changes from about 30 ^{o}C as a minimum to about 45 ^{o}C as a maximum.

Figure 4.14 presents the thermal behavior of the system as: collector absorber temperature (T_{pw}), adsorbent bed temperature (T), condenser temperature (T_c) and evaporator temperature (T_e). The maximum generation temperature (T_d) varies between 102 ^{o}C on 14th June to 112.4 ^{o}C on 20th June by using air condenser (T_c is greater than T_{amb} by some degrees, up to 5 ^{o}C). Due to high ambient temperature during the night, the adsorption temperature (end cycle temperature) is high, which influences negatively the evaporator temperature; T_e reaches -0.3 ^{o}C only at the end of adsorption process on 19th June, so there is little ice produced ($M_{ice} \leq 0.05$ kg) as shown in Fig. 4.16. Fig. 4.15 shows the variation of methanol uptake m_m and system pressure (P) in details during one day.

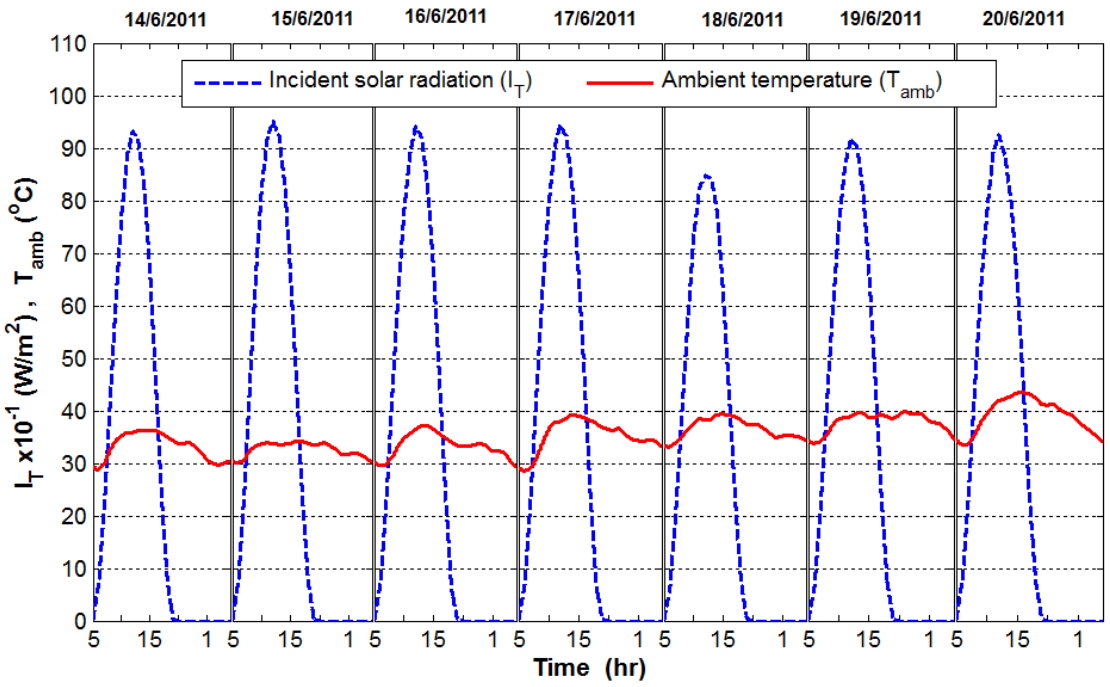

Figure 4.13 Solar radiation on collector (I_T) and ambient temperature (T_{amb}) recorded during June 14-20, 2011.

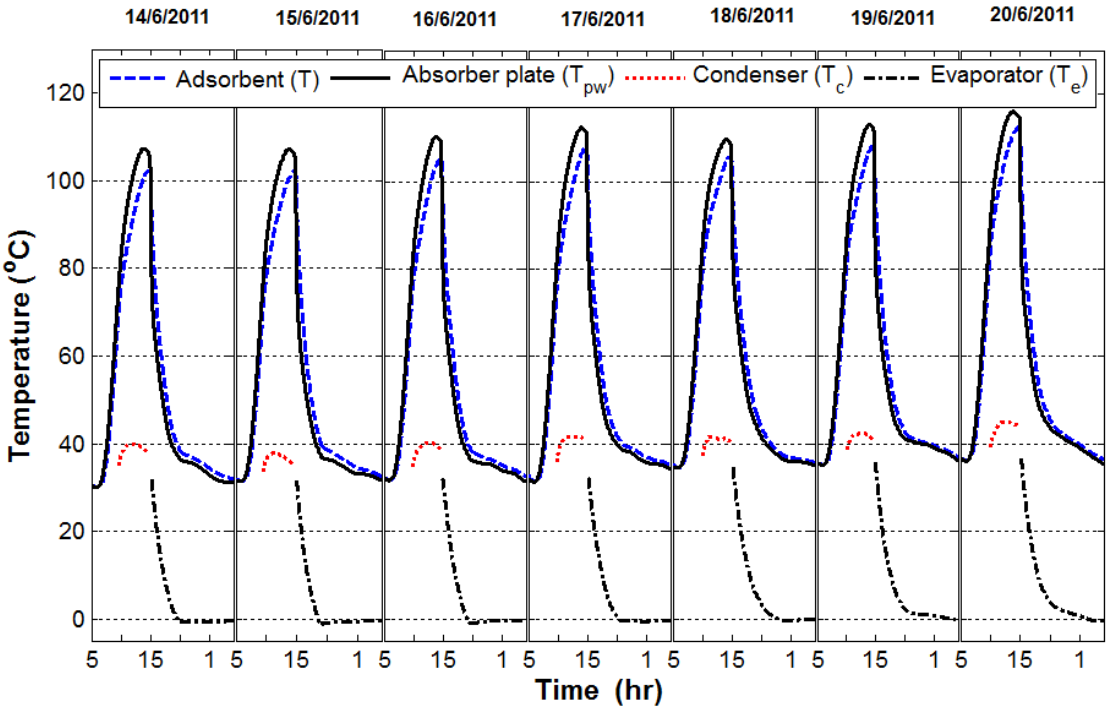

Figure 4.14 Collector absorber (T_{pw}), adsorbent bed (T), condenser (T_c) and evaporator (T_e) temperatures calculated for the period 14-20 June 2011.

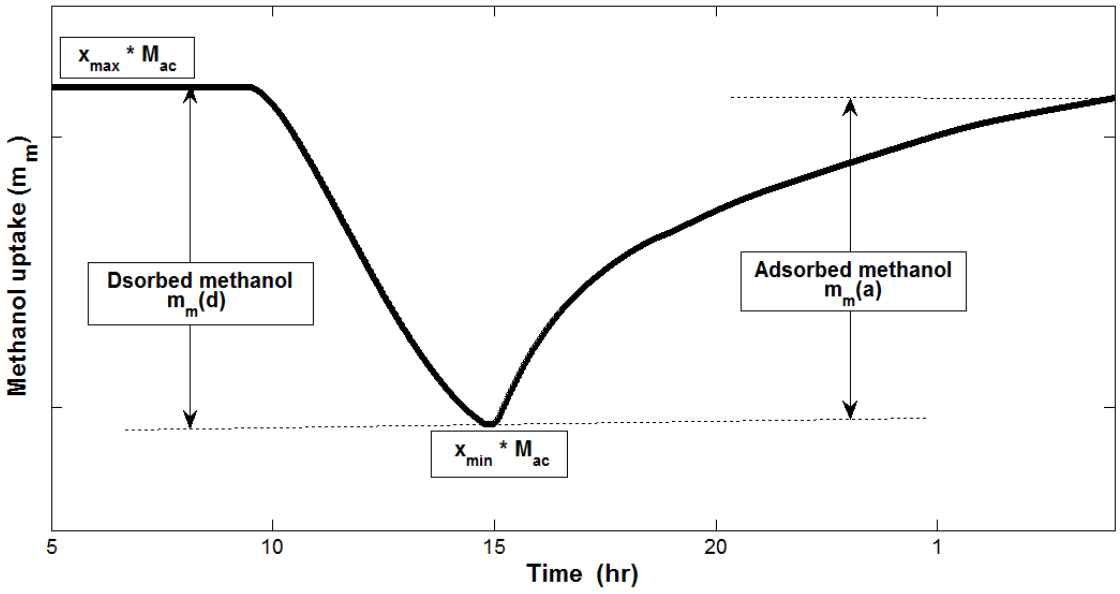

a- Methanol uptake (m_m) for one day.

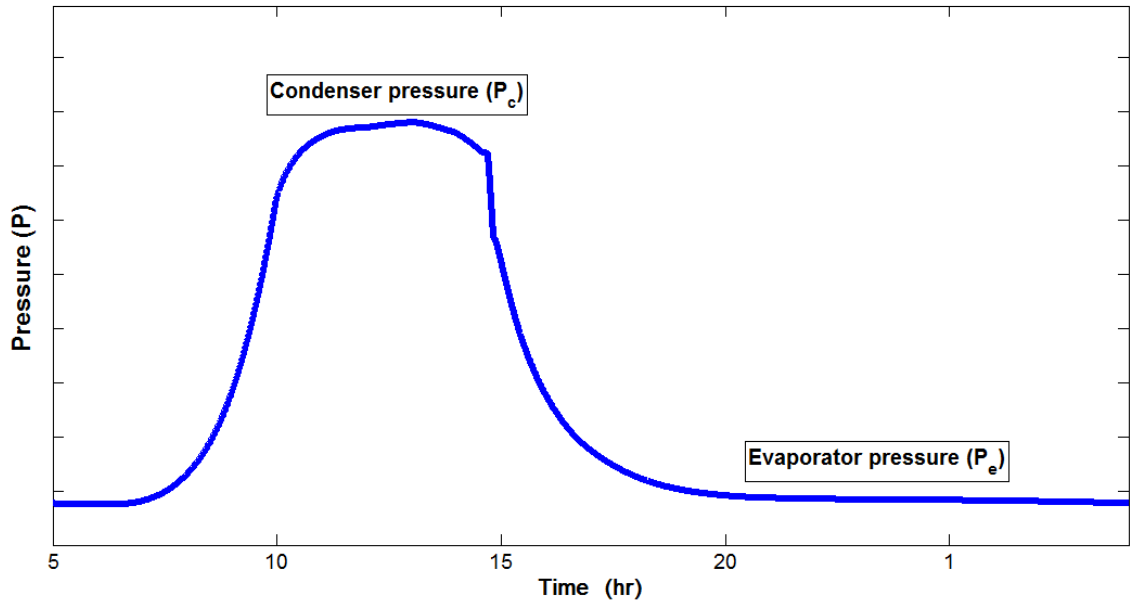

b- System pressure (P) for one day.

Figure 4.15 Schematic diagram for variations of methanol uptake and system pressure for one day.

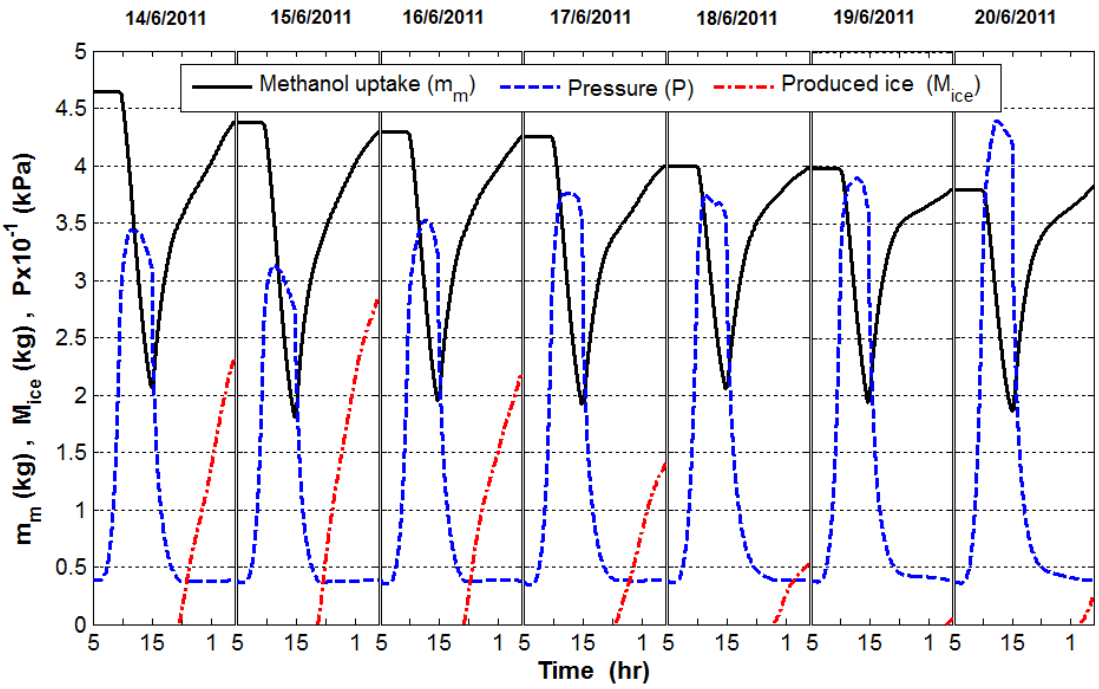

Figure 4.16 Methanol uptake(m_m), adsorbent bed pressure (P) and amount of produced ice (M_{ice}) calculated for the period 14-20 June 2011.

Figure 4.15 explains the schematic diagram in details for both methanol uptake (m_m) and pressure (P) variations during one day. Maximum amount of ice (2.85 kg) and better performance (COP = 0.36, SCOP = 0.101, ESCOP = 0.122 and SCP = 1.54 W/kg) are obtained on 15th June (as shown in Fig. 4.16 and Table 4.5) due to two main reasons: first one is the lower condenser pressure which enables the adsorbent bed to desorb more methanol (2.57 kg); the second reason is the lower adsorption temperature that helps activated carbon to absorb more methanol from the evaporator (2.49 kg) during the night. The worst performance (M_{ice} = 0.05 kg, COP = 0.28, SCOP = 0.077, ESCOP = 0.096 and SCP = 1.12 W/kg) is on 19th June due to high adsorption temperature (T=37.2 ^{o}C).

For Dhahran cold days in winter, the atmospheric temperature is considered low (as low as 11-21 ^{o}C) and the insolation on a horizontal surface is also low compared to that in summer (winter maximum insolation is between 590 and 690 W/m^2 on 17-23 December

2011). However, the tilted collector (26.3^{o}) can receive more radiation than that on horizontal surface and reaches about 750 and 920 W/m^{2} as a maximum for the same period as shown in Fig 4.17. For such a good insolation radiation and low ambient temperature, the performance is better.

Table 4.5 System performance for June 2011.

Date	14/6	15/6	16/6	17/6	18/6	19/6	20/6
COP	0.33	0.36	0.34	0.3	0.31	0.28	0.3
SCOP	**0.097**	**0.101**	**0.096**	**0.085**	**0.084**	**0.077**	**0.080**
ESCOP	0.115	0.122	0.117	0.100	0.102	0.096	0.095
SCP (W/kg)	1.42	1.54	1.42	1.27	1.16	1.12	1.18
M_{ice} (kg)	**2.31**	**2.85**	**2.19**	**1.39**	**0.52**	**0.05**	**0.26**
m_m(d) (kg)	2.58	2.57	2.34	2.33	1.94	2.04	1.93
m_m(a) (kg)	2.31	2.49	2.31	2.07	1.92	1.85	1.96
P_e (kPa)	3.79	3.78	3.80	3.83	3.87	3.89	3.86
P_c (kPa)	33.02	29.79	33.42	36.30	36.32	37.80	41.97

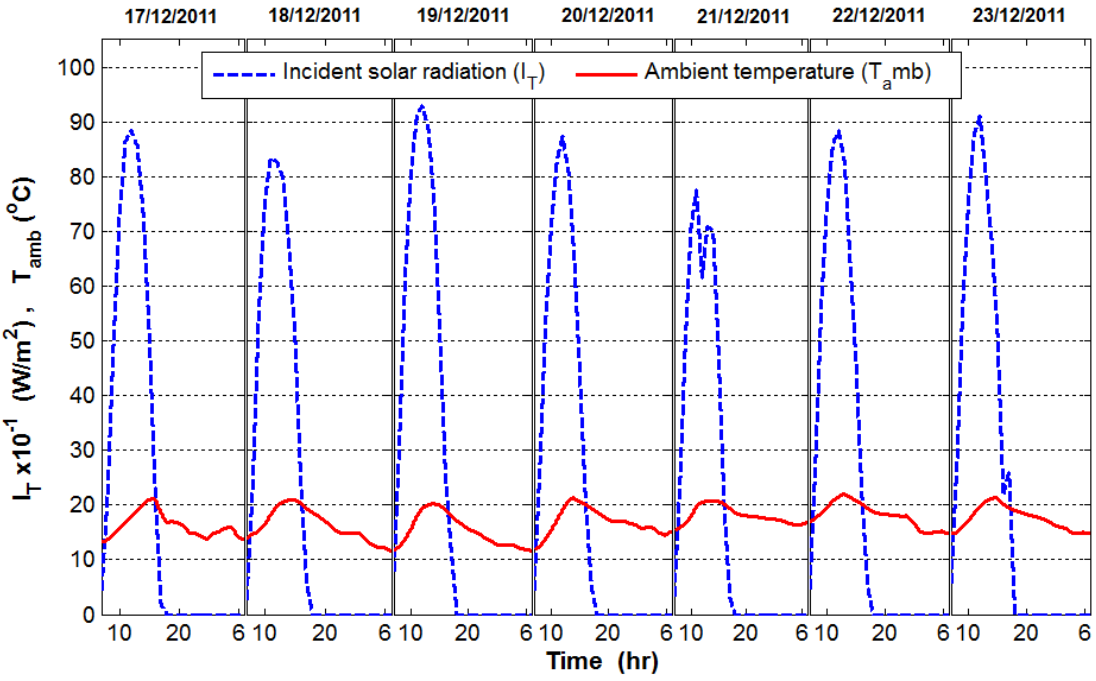

Figure 4.17 Solar radiation on collector (I_T) and ambient temperature (T_{amb}) recorded during December 17-23, 2011.

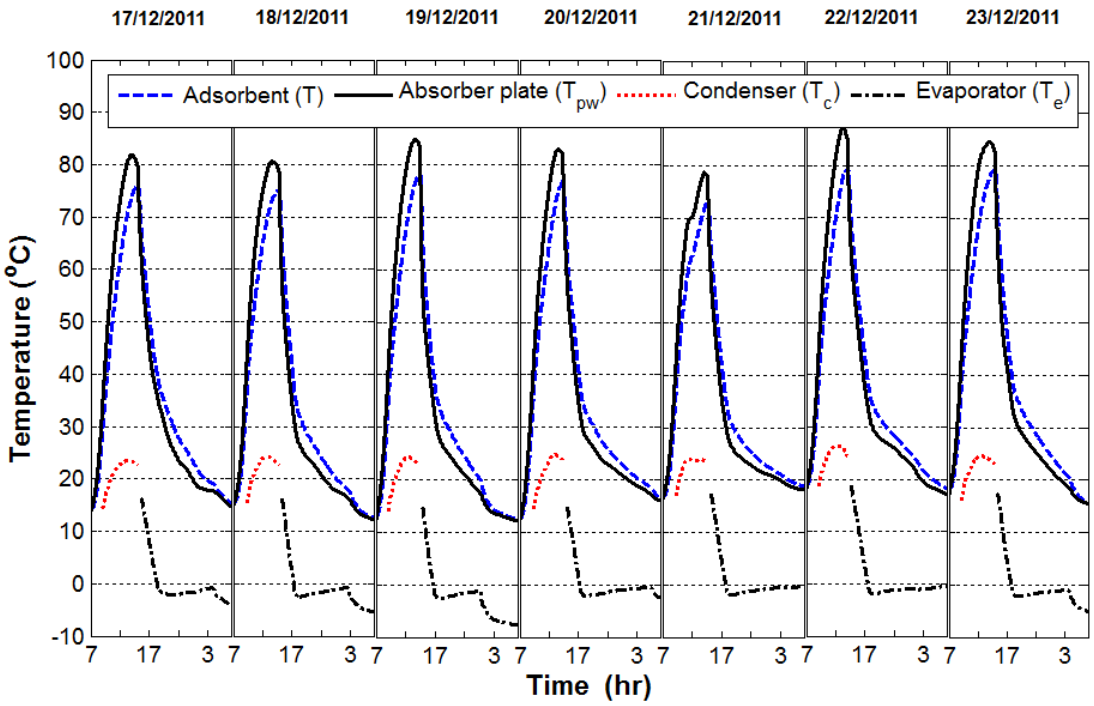

Figure 4.18 Collector absorber (T_{pw}), adsorbent bed(T), condenser (T_c) and evaporator (T_e) temperatures calculated for the period 17-23 December 2011.

Fig. 4.18 shows that the maximum generation temperature varies between 72 ^{o}C and 79 ^{o}C. This temperature drop in the maximum generation temperature from summer to winter is not only because of the lower insolation, but also because the lower ambient temperature that increases the difference between ambient and adsorbent

adsorbent temperature, so heat losses from the collector increase. Otherwise, those generation temperatures are adequate to desorb more amount of methanol (about 3 kg) at low condeser pressures (as about 14-17 kPa) as shown in Fig. 4.19.

The evaporotor temperature goes below zero for the all week days (17-23 December), and the minimum is (-7.68 ^{o}C) on 19th December for adsorption temperature below 13 ^{o}C as shown in Fig. 4.18. For these good conditions, the amount of produced ice is greater than 5 kg and SCOP is more than 0.15 for all week days as shown in Fig. 4.19 and Table 4.6.

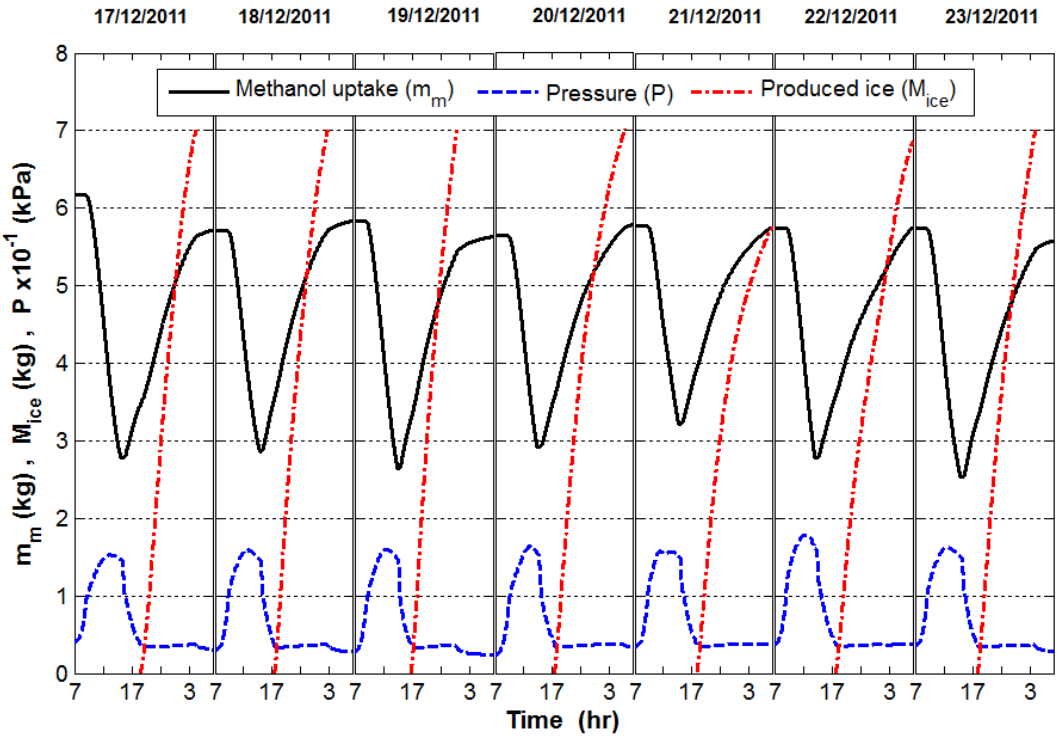

Figure 4.19 Methanol uptake (m_m), absorbent bed pressure (P) and amount of produced ice (M_{ice}) calculated for the period 17-23 December 2011.

For the first sight, it may appear that the best performance is on 18th December (COP = 0.45, SCOP = 0.169, ESCOP = 0.19, SCP =1.92 W/kg, and M_{ice} = 7 kg). However, the best performance is actually on 19th December with T_e = -7.85 ^oC, even though the COP, SCOP ESCOP are less than those on 18th December due to larger heat input on 19th December ($T_{(max)}$=77.12 ^oC compared to 74.5^oC on 18th December). In other words, if the amount of water is increased to 10 kg instead of 7 kg inside the water tank, the amount of produced ice reaches 7.52 kg with $T_{e\ (mean)}$ = -1.23 ^oC, COP = 0.48, SCOP = 0.18, ESCOP = 0.203 and SCP =2.06 W/m^2 on 18th December while 8.45 kg of ice can be produced with $T_{e\ (mean)}$ = -1.32 ^oC, COP = 0.46, SCOP = 0.17, ESCOP = 0.20 and SCP = 2.2 W/m^2 on 19th December. Consequently, the amount of produced ice and the

evaporator temperature can be considered the two parameters that reasonably evaluate the performance of an adsorption ice-maker.

Table 4.6 System performance for December 2011.

Date	17/12	18/12	19/12	20/12	21/12	22/12	23/12
COP	0.40	0.45	0.41	0.43	0.40	0.44	0.43
SCOP	**0.163**	**0.169**	**0.151**	**0.165**	**0.159**	**0.165**	**0.160**
ESCOP	0.178	0.190	0.177	0.194	0.182	0.200	0.180
SCP (W/kg)	1.89	1.92	1.93	1.85	1.64	1.91	1.95
M_{ice} (kg)	**7**	**7**	**7**	**7**	**5.75**	**6.86**	**7**
m_m(d) (kg)	3.38	2.85	2.34	2.71	2.56	2.96	3.2
m_m(a) (kg)	2.93	2.97	3.19	2.85	2.54	2.95	3.04
P_e (kPa)	3.50	3.39	3.10	3.63	3.71	3.67	3.45
P_c (kPa)	13.78	14.49	14.12	14.26	14.86	16.34	14.85

The previous results are obtained under Dhahran climate conditions in hot and cold days, therefore, the conclusion is that the performance of the system during any day in a whole year is in between the values corresponding to winter and summer, as given in Table 4.7.

Table 4.7 System summer and winter performance predected for 2011.

M_{ice} (kg)	**COP**	**SCOP**	**ESCOP**	**SCP** (W/kg)	**T_e** (^oC)
0 – 7	0.28 – 0.45	**0.08 – 0.17**	0.1 – 0.2	1.1 – 2	0 – (-7.7)

4.2.3.3 Activated Carbon Type

Dubinin-Astakhov equation (Eq. (5)) shows that the sorption ability of an activated carbon depends on some physical parameters as: limited adsorption capacity (x_o), Dubinin-Astakhov constants (D and n) and other operative parameters as T and P. Among many types of activated carbon produced by some global companies, the best

known eight types of activated carbon are selected in this investigation. Some of them were successfully examined with methanol as AC-35 by Medini [15], Anyanwu and Ezekwe [66], Leite et al. [14, 74], and WS-480 and 207EA by Zhao et al. [83]. The thermal and sorption characteristics of some others were recently examined experimentally (as x_o, *D, n, density (*ρ*), specific heat capacity (C)*) with only some limited thermodynamic analysis as: Maxsorb III by El-sharkawy et al. [84]; Carbo Tech A35/1, G32-H, NORIT R1-Extra and NORIT RX3-Extra by Henninger et al. [85]. Therefore, this is the first time to model Maxsorb III, Carbo Tech A35/1, G32-H, NORIT R1-Extra and NORIT RX3-Extra with methanol under actual climate conditions. Table 4.8 shows the main properties of these activated carbon types. These eight types are examined in this section under Dhahran actual conditions on the worst and best days of 19th June and 19th December, respectively, to determine the best type that can be selected as the adsorbent for the adsorption ice-maker.

Table 4.8 Characteristics of activated carbon types.

Activated Carbon	x_o (kg/kg)	**D** (K^{-1})	**n**	**ρ** (kg/m^3)	**C** (kJ/kg K)
AC-35	0.33	$5.02 *10^{-7}$	2.15	430	0.92
WS-840	0.269	$9.08 *10^{-6}$	1.781	420	0.93
207EA	0.28	$8.45 *10^{-7}$	2.08	460	0.92
Maxsorb III	1.24	$4.022 *10^{-6}$	2.0	281	0.93
Carbo Tech A35/1	0.58	$1.37 *10^{-5}$	1.76	330	0.95
G32-H	0.38	$1.94 *10^{-8}$	2.59	370	0.95
NORIT R1-Extra	0.41	$2.19*10^{-7}$	2.27	420	0.95
NORIT RX3-Extra	0.425	$9.6 *10^{-7}$	2.06	370	0.95

For the same collector configuration as described in previous section with constant volume inside the annular space between the tubes (V = 0.0465 m^3), the performance for different activated carbon types is investigated as shown in Tables 4.9 and 4.10. Table 4.9

shows the main constructive and operative parameters of the system as: amount of activated carbon that fills the annular space (M_{ac}), the corresponding amount of methanol for each type (M_m), maximum desorption temperature (T_d), minimum adsorption temperature (T_a), mean condenser temperature (T_c), mean condenser pressure (P_c), mean evaporator pressure during and after water solidification process or minimum evaporator pressure if solidification process is not obtained (P_e), amount of desorbed methanol during the desorption process ($m_m(d)$) and amount of amount of adsorbed methanol during adsorption process ($m_m(a)$). On the other hand, the evaporator temperature (T_e) and amount of ice produced (M_{ice}) are given into the other table (Table 4.10) with the performance coefficients (COP, SCOP, ESCOP, SCP) to show the performance of the system.

Table 4.9 Main constructive and operative parameters of the activated carbon types on 19th June and 19th December 2011.

Activated carbon	M_{ac} (kg)	M_m (kg)	Date	T_d (°C)	T_a (°C)	T_c (mean) (°C)	P_c (mean) (kPa)	P_e (mean) (kPa)	m_m (d) (kg)	m_m (a) (kg)
AC-35	20	6.6	19/6	**108.0**	37.2	41.81	37.78	3.89	**2.04**	**1.85**
			19/12	**77.35**	12.49	21.86	14.18	3.15	**3.27**	**2.98**
WS-840	20	5.4	19/6	**114.16**	37.01	41.34	36.96	4.33	**1.79**	**1.70**
			19/12	**81. 81**	12.5	21.67	14.03	3.27	**3.22**	**2.94**
207EA	21.4	6	19/6	**109.38**	37.12	41.67	37.50	3.95	**1.95**	**1.79**
			19/12	**78.8**	12.49	21.69	14.06	3.25	**3.19**	**2.94**
Maxsorb III	13	16.2	19/6	**102.77**	37.48	42.49	39	4.3	**2.96**	**2.67**
			19/12	**61.19**	13.93	23.68	15.67	3.38	**4.92**	**3.49**
Carbo Tech A35/1	15.35	8.9	19/6	**110.27**	37.16	41.81	37.77	4.06	**2.22**	**2.05**
			19/12	**72.73**	12.64	22.73	14.86	3	**4.01**	**3.26**
G32-H	17.2	6.5	19/6	**105.57**	37.04	42	38.11	3.9	**2.29**	**1.77**
			19/12	**78.73**	12.37	21.42	13.89	3.23	**3.12**	**2.9**
NORIT R1-Extra	19.5	8	19/6	**104.84**	37.36	42.09	38.26	3.88	**2.21**	**1.95**
			19/12	**74.23**	12.56	22.2	14.45	3.06	**3.42**	**3.05**
NORIT RX3-Extra	17.2	7.3	19/6	**107.51**	37.29	41.92	37.95	3.88	**2.14**	**1.9**
			19/12	**76.52**	12.49	22.09	14.36	3.04	**3.4**	**3.04**

Table 4.9 shows the overall maximum amount of activated carbon is 21.4 kg for 207EA and the overall minimum amount of methanol (5.4 kg) for W-840 whereas Maxsorb III has the overall minimum amount of activated carbon with the overall maximum amount of methanol as 13 kg and 16.2 kg, respectively. Because of this large capacity of Maxsorb III for methanol and lower mass of adsorbent, Maxsorb III has the overall lowest maximum desorption temperatures as: 102.77 ^{o}C and 61.19 ^{o}C for the hot and the cold day, respectively, and it also has the best desorbed and adsorbed methanol amounts during both the hot and the cold days as shown in Table 4.9. Otherwise, the overall highest maximum desorption temperatures in the hot and the cold days are 114.16 ^{o}C and 78.8 ^{o}C, respectively, and are obtained by WS-840 that has the overall lowest methanol capacity. Other parameters in Table 4.9 (as T_a, T_c, P_e, P_c) have values close to each other for all the activated carbon types. Therefore, the desorbed and adsorbed amounts of methanol and the desorption temperature are considered as the main behavior parameters of the activated carbon, but they are not the only parameters that control the performance as confirmed in Table 4.10. For the hot day, T_e does not go below 0^{o}C for WS-840, 207EA, Maxsorb III and Carbo Tech A35/1 types while the other types can produce a little amount of ice with some advantages for NORIT RX3-Extra, NORIT R1-Extra and AC-35, respectively.

The cold days show good conditions that enable all types to solidify all amount of water (7 kg). However, the evaporator temperatures show the best performance for Carbo Tech A35/1 type with T_e = -9.6 ^{o}C followed by NORIT RX3-Extra and NORIT R1-Extra types with T_e = -8.44 ^{o}C and T_e = -8.4 ^{o}C, respectively. Maxsorb III has the best COP, SCOP, ESCOP and SCP followed by Carbo Tech A35/1 and then NORIT RX3-Extra.

Table 4.10 The performance of the activated carbon types on 19th June and 19th December 2011.

Activated carbon	Date	$T_{e\ (min)}$ (oC)	M_{ice} (kg)	SCP (W/kg)	COP	SCOP	ESCOP
AC-35	19/6	**-0.3**	**0. 04**	1.11	0.28	**0.077**	0.096
	19/12	**-7.27**	**7**	1.93	0.41	**0.150**	0.177
WS-840	19/6	**1.49**	**0**	1.06	0.29	**0.071**	0.090
	19/12	**-6.32**	**7**	1.91	0.41	**0.149**	0.173
207EA	19/6	**0.03**	**0**	1.02	0.28	**0.075**	0.093
	19/12	**-6.32**	**7**	1.78	0.40	**0.148**	0.174
Maxsorb III	19/6	**1.38**	**0**	2.37	0.37	**0.107**	0.130
	19/12	**-7**	**7**	3.22	0.39	**0.164**	0.200
Carbo Tech A35/1	19/6	**0.47**	**0**	1.63	0.33	**0.086**	0.106
	19/12	**-9.6**	**7**	2.68	0.41	**0.160**	0.190
G32-H	19/6	**-0.22**	**0.01**	1.24	0.26	**0.074**	0.092
	19/12	**-5.86**	**7**	2.2	0.41	**0.148**	0.175
NORIT R1-Extra	19/6	**-0.35**	**0.07**	1.18	0.28	**0.079**	0.099
	19/12	**-8.4**	**7**	2.0	0.4	**0.150**	0.180
NORIT RX3-Extra	19/6	**-0.34**	**0.08**	1.33	0.29	**0.079**	0.099
	19/12	**-8.44**	**7**	2.28	0.41	**0.153**	0.180

However, the cooling effect that goes to water is lower for Maxsorb III. To illustrate that, as we know, the cooling effect is divided into components: the main component goes to cool the water, a second component this heat is lost to atmosphere and other components cool the evaporator and water tank metals as well as the methanol inside the evaporator. For example, according to weather conditions, the amount of methanol inside Maxsorb III in the morning of 19th December is 10.7 kg out of 16.2 kg as shown in Fig 4.20. That means there is about 5.5 kg of methanol remained inside the evaporator from previous day and then that increases to about 10.4 kg after desorption process; the increases in such amount decrease the amount of cooling heat that cools and freezes the water. Consequently, the coefficients of performance appear higher while the amount of produced ice is lower (as the hot day) or the evaporator temperature is higher if the produced ice amounts are the same (as the cold day). On the other hand, about 2.5 and

0.9 kg of methanol remained in the evaporator from previous day for Carbo Tech A35/1 and NORIT RX3-Extra, respectively.

The conclusion is that the best type that can be used for cold days is Carbo Tech A35/1 followed by NORIT RX3-Extra while NORIT RX3-Extra and NORIT R1-Extra have the best performance in hot days. Thus, the optimum performance results that can be obtained during all year days is by use of NORIT RX3-Extra.

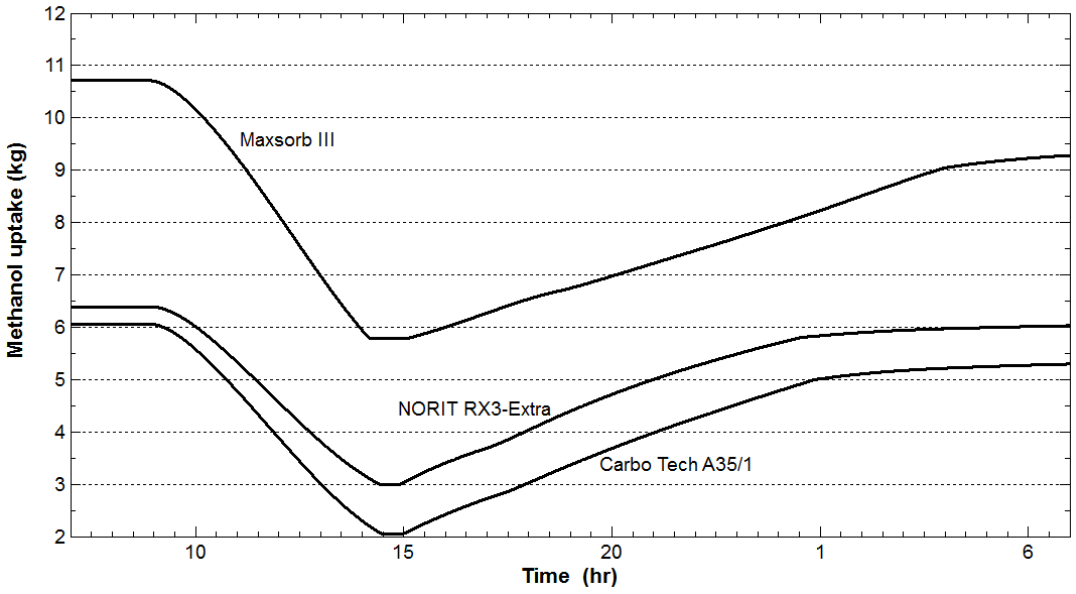

Figure 4.20 Methanol uptake (m_m) for three types of activated carbon for 19th December.

4.2.3.4 Absorber Plate and Absorber Coating

The suitable material for the tubes of the absorber is stainless steel due to the issues that can be caused by use other metals such as methanol decomposition with copper and aluminum. Furthermore, thin stainless steel tubes can handle the pressure in which the system operates under vacuum. Oppositely, the stainless steel surface has a low absorptivity to solar radiation. Therefore, the tubes should by covered or coated by high

absorptivity and low emissivity material such as chrome-black selective layer type AS+ (produced by Energie Solarine SA, Switzerland) with high absorptivity α_{pw} = 0.95 and low emissivity ε_{pw} = 0.07. In this section, the effects of metal tubes thickness and absorptivity and emissivity of coating on the system behavior and performance are investigated, consecutively, on the typical hot day of 19th June.

Tables 4.11 and 4.12 show the parameters and performance behavior by changing the absorber thickness from 1 mm to 4 mm at the same collector configurations that were described before.

Table 4.11 The effect of absorber tube thickness on the system operating parameters.

t_{metal} (mm)	M_{ac} (kg)	M_m (kg)	T_d (^oC)	T_a (^oC)	T_c (mean) (^oC)	P_c (mean) (kPa)	P_e (mean) (kPa)	m_m (d) (kg)	m_m (a) (kg)
1	**17.75**	**7.54**	**108.88**	37.52	41.94	38.0	3.88	**2.30**	**2.0**
1.5	**17.50**	**7.44**	**108.20**	37.42	41.94	38.0	3.88	**2.23**	**1.95**
2	**17.26**	**7.37**	**107.51**	37.28	41.93	37.98	3.88	**2.17**	**1.90**
2.5	**17.02**	**7.24**	**106.08**	37.15	41.91	37.94	3.90	**2.11**	**1.87**
3	**16.8**	**7.14**	**106.02**	37.23	41.88	37.90	3.97	**2.06**	**1.84**
3.5	**16.6**	**7.04**	**105.22**	37.28	41.85	37.78	4.06	**2.01**	**1.81**
4	**16.3**	**6.95**	**104.33**	37.32	41.82	37.79	4.16	**1.98**	**1.77**

It is clear that, increasing the thickness (from 1 to 4 mm) reflects negatively on all main parameters since the desorption temperature decreases from about 109 ^oC to about 104 ^oC. Moreover, the desorbed and adsorbed amount of methanol decreases slightly from about 2.3 and 2 kg to about 2 and 1.8 kg, respectively, due to that decreases in the desorption temperatures and also the decreases in the amount of activated carbon from about 17.8 kg to about 16.3 kg as well. Correspondingly, the amount of produced ice decreases from about 0.3 kg to 0 kg with the evaporator temperature varying between -

0.44 and 0.88 °C, respectively. COP, SCOP, ESCOP and SCP also decrease (due to that change in the metal thickness) from about 0.34, 0.083, 0.0107 and 1.36 to about 0.23, 0.074, 0.09 and 1.31, respectively, as shown in Table 4.12.

Table 4.12 Effect of absorber tube thickness on the system performance.

t_{metal} (mm)	T_e (min) (°C)	M_{ice} (kg)	COP	SCOP	ESCOP	SCP (W/kg)
1	-0.44	**0.27**	0.34	**0.083**	0.107	1.36
1.5	-0.40	**0.16**	0.32	**0.081**	0.103	1.34
2	-0.35	**0.08**	0.29	**0.079**	0.099	1.33
2.5	-0.26	**0.02**	0.28	**0.078**	0.096	1.32
3	-0.11	**0**	0.26	**0.076**	0.094	1.32
3.5	0.47	**0**	0.25	**0.075**	0.091	1.32
4	0.88	**0**	0.23	**0.074**	0.089	1.31

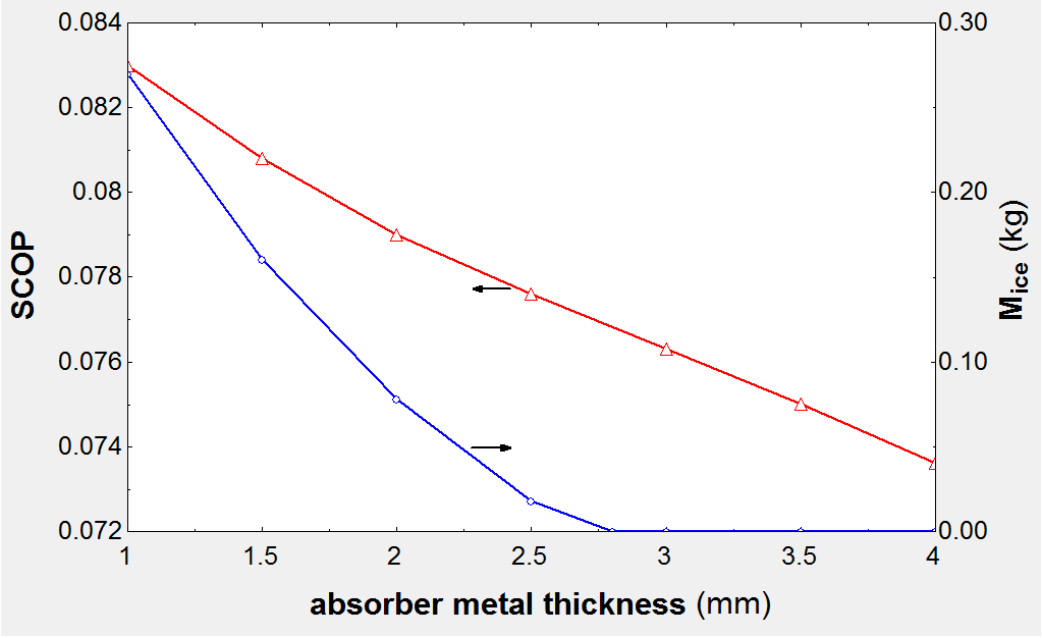

Figure 4.21 Effect of metal thickness on the performance.

Figure 4.21 represents the effect of the metal thickness on M_{ice} and SCOP as given by the result shown in Table 4.12. Thus, the metal thickness should be as small as possible to lower the thermal inertia and hence enhance the performance of the system.

The coating properties (α_{pw} and ε_{pw}) are very important in improving the system performance. Tables 4.13, 4.14, 4.15 and 4.16 present the operating and performance parameters that are affected by changing the absorptivity (α_{pw}) between 0.3 and 0.95 at constant emissivity ($\varepsilon_{pw} = 0.1$), and changing emissivity (ε_{pw}) from 0.05 to 0.9 at constant absorptivity ($\alpha_{pw} = 0.9$), respectively, while taking the metal thickness as 1 mm.

Table 4.13 The effect of absorber absorptivity on system operating parameters at $\varepsilon_{pw} = 0.1$.

α_{pw}	T_d (^oC)	T_a (^oC)	T_c (mean) (^oC)	P_c (mean) (kPa)	P_e (min) (kPa)	m_m (d) (^oC)	m_m (a) (^oC)
0.3	**69.97**	36.64	39.87	34.51	11.27	**0.19**	**0.87**
0.4	**75.78**	36.71	40.23	35.10	9.33	**0.54**	**0.96**
0.5	**81.69**	36.58	40.61	35.72	7.72	**0.89**	**1.16**
0.6	**87.75**	36.83	40.96	36.31	6.41	**1.23**	**1.35**
0.7	**93.95**	36.88	41.21	36.87	5.34	**1.56**	**1.55**
0.8	**100.35**	36.93	41.58	37.37	4.49	**1.88**	**1.74**
0.9	**106.97**	37.10	41.89	37.82	3.88	**2.18**	**1.92**
0.95	**110.03**	37.64	41.99	38.08	3.88	**2.37**	**2.06**

The absorptivity values in Table 4.13 start from 0.3 because there is no desorption can be obtained below this value. The desorbed methanol amount that is associated with $\alpha_{pw} = 0.3$ is as low as about 0.19 kg. For this almost no desorption (in case $\alpha_{pw} = 0.3$), one can find the adsorbed methanol amount during the night is 0.78 kg with SCOP = 0.033 as shown in Table 4.14. This amount of adsorbed methanol (0.78 kg) comes from about 1.47 kg remained inside the evaporator from the previous day. The increase in the absorptivity values enable adsorbent to be heated more, hence desorbs more and adsorbs good

quantities of methanol as shown in Table 4.13. Moreover, T_e, M_{ice}, SCOP, ESCOP and SCP increase with improving coating absorbance as shown in Table 4.14. COP alone shows negative impression with increases in the absorptivity values of metal surface, this is because of existing some of adsorption heat during the night due to the availability of methanol inside the evaporator from the previous day and the day generation heat is small with lower absorptivity values; the COP as defined before is the cooling effect divided by the generation heat.

Table 4.14 The effect of absorber absorptivity on performance parameters at ε_{pw} = 0.1.

α_{pw}	T_e (min) (^oC)	M_{ice} (kg)	COP	SCOP	ESCOP	SCP (W/kg)
0.3	17.80	**0**	0.45	**0.033**	0.044	0.54
0.4	14.40	**0**	0.41	**0.041**	0.054	0.66
0.5	11.10	**0**	0.38	**0.048**	0.064	0.79
0.6	7.92	**0**	0.36	**0.056**	0.074	0.92
0.7	4.91	**0**	0.35	**0.064**	0.084	1.05
0.8	2.07	**0**	0.34	**0.072**	0.094	1.18
0.9	-0.35	**0.07**	0.34	**0.080**	0.102	1.30
0.95	-0.47	**0.44**	0.34	**0.086**	0.110	1.40

Table 4.15 shows the effect of absorber emissivity on the main operating parameters of the system at α_{pw} = 0.9. Unlike effects of the metal absorptivity, the decreases in metal surface emissivity values enhance the behavior and performance of the system due to minimizing the heat losses from collector. It is obvious that, the lower surface emissivity the better is the performance. For ε_{pw} = 0.05, T_d is high as 108.88 ^oC, $m_m(d)$ is about 2.3 kg, $m_m(a)$ is 2 kg, M_{ice} is about 0.3 kg with T_e = -0.44 ^oC and SCOP is about 0.083.

Now, if the selective coating is chosen as chrome-black selective layer type AS+ (α_{pw}=0.95 and ε_{pw}= 0.07) to cover stainless steel tubes with 1 mm thick, T_d increases to about 111.22 ^oC with about 2.44 kg and 2.13 kg of desorbed and adsorbed amounts of methanol. In addition, M_{ice}, T_e, COP, SCOP, ESCOP and SCP are improved to about 0.65 kg, -0.49 ^oC, 0.35, 0.089, 0.114 and 1.46 W/kg, respectively.

Table 4.15 The effect of absorber emissivity on system operating parameters at α_{pw} = 0.9.

ε_{pw}	T_d (^oC)	T_a (^oC)	T_c (mean) (^oC)	P_c (mean) (^oC)	P_e (min) (^oC)	m_m (d) (kg)	m_m (a) (kg)
0.05	**108.88**	37.52	41.94	38.0	3.88	**2.30**	**2.0**
0.1	**106.97**	37.10	41.89	37.82	3.88	**2.18**	**1.92**
0.2	**103.66**	37.0	41.70	37.59	4.12	**2.04**	**1.83**
0.3	**100.94**	36.83	41.59	37.40	4.40	**1.92**	**1.76**
0.4	**98.53**	36.77	41.48	37.20	4.69	**1.82**	**1.67**
0.5	**96.26**	36.72	41.37	37.0	4.97	**1.71**	**1.63**
0.6	**94.01**	36.67	41.25	36.80	5.28	**1.61**	**1.56**
0.7	**91.71**	36.62	41.12	36.59	5.63	**1.49**	**1.49**
0.8	**89.27**	36.56	40.98	36.35	6.03	**1.36**	**1.42**
0.9	**86.65**	36.51	40.83	36.08	6.50	**1.22**	**1.34**

Table 4.16 The effect of absorber emissivity on system performance at α_{pw} = 0.9.

ε_{pw}	T_e (min) (^oC)	M_{ice} (kg)	COP	SCOP	ESCOP	SCP (W/kg)
0.05	-0.44	**0.27**	0.34	**0.083**	0.107	1.36
0.1	-0.35	**0.07**	0.34	**0.080**	0.102	1.30
0.2	0.70	**0**	0.34	**0.076**	0.099	1.24
0.3	1.78	**0**	0.34	**0.073**	0.096	1.19
0.4	2.77	**0**	0.34	**0.070**	0.091	1.15
0.5	3.73	**0**	0.35	**0.067**	0.089	1.11
0.6	4.72	**0**	0.35	**0.065**	0.086	1.06
0.7	5.76	**0**	0.35	**0.062**	0.083	1.02
0.8	6.89	**0**	0.36	**0.059**	0.079	0.97
0.9	8.15	**0**	0.36	**0.056**	0.075	0.91

4.2.3.5 Adsorbent Bed Thickness (Amount of Activated Carbon)

The amount of activated carbon, that fills the annular gaps between tubes, impacts strongly on the performance of the system. Large amount of activated carbon leads to slow adsorbent heating during generation and that affects negatively the performance. Similarly, a little amount of activated carbon increases the rates of heating and adsorption processes but with lower amounts of desorbed and adsorbed methanol. In order to investigate the effects of the activated carbon (NORIT RX3-Extra) amounts under the worst day of the year (19^{th} June), the diameter of the absorber tube is varied while fixing the inner pass tube diameter (D1=2 cm). The thickness of the absorber tube is taken as 1mm coated with chrome-black selective layer ($\alpha_{pw} = 0.95$ and $\varepsilon_{pw} = 0.07$) and the other system configurations are taken as mentioned in section 4.2.3.2. The internal radius of the absorber (R2) increases to increase the annular space (dR=R2-R1) from about 1 to about 4 cm for filling 1 m^2 of collector by about 8.32 to 27.39 kg of NORIT RX3-Extra and about 3.54 kg to about 11.64 kg of methanol, respectively as shown in Table 4.17.

Table 4.17 shows that increasing M_{ac} leads to a decrease in T_d (from (128.07 ^oC to 101.37 ^oC) with increases in the amount of desorbed and adsorbed methanol from about 1.71 and 1.58 kg to about 2.58 and 2.36 kg, respectively. The better performed results are obtained between dR equals 1.5 and 2.0 cm. Therefore, Tables 4.17 and 4.18 display more refined values in this range of dR with 1mm increment to show the optimum results. The results of Table 4.17 are presented in Fig. 4.22, which shows that the optimal performance results are obtained by taking M_{ac} =14.09 kg.

Table 4.17 The effect of the absorber emissivity on system operating parameters.

dR (cm)	M_{ac} (kg)	M_m (kg)	T_d (^oC)	T_a (^oC)	T_c (mean) (^oC)	P_c (mean) (kPa)	P_e (mean) (kPa)	m_m (d) (kg)	m_m (a) (kg)
1.0	**8.32**	**3.54**	**128.07**	36.95	40.95	36.30	3.91	**1.71**	**1.58**
1.5	**11.76**	**5.0**	**120.55**	37.26	41.52	37.28	3.87	**2.10**	**1.90**
1.6	**12.42**	**5.28**	**119.32**	37.15	41.60	37.40	3.87	**2.15**	**1.95**
1.7	**13.08**	**5.71**	**118.13**	37.25	41.68	37.60	3.87	**2.20**	**2.0**
1.8	**13.73**	**5.84**	**117.02**	37.33	41.75	37.67	3.87	**2.25**	**2.02**
1.9	**14.38**	**6.11**	**115.99**	37.42	41.80	37.77	3.87	**2.29**	**2.05**
2.0	**15.03**	**6.39**	**115.02**	37.50	41.85	37.86	3.87	**2.32**	**2.07**
2.5	**18.19**	**7.73**	**110.78**	37.80	42.05	38.21	3.87	**2.44**	**2.14**
3.0	**21.30**	**9.05**	**107.31**	37.79	42.17	38.40	3.87	**2.51**	**2.19**
3.5	**24.36**	**10.35**	**104.29**	37.74	42.23	38.51	3.90	**2.55**	**2.26**
4.0	**27.39**	**11.64**	**101.37**	38.73	42.27	38.57	4.18	**2.58**	**2.36**

Table 4.18 The effect of absorber emissivity on system performance parameters.

dR (cm)	M_{ac} (kg)	T_e (min) (^oC)	M_{ice} (kg)	**COP**	**SCOP**	**ESCOP**	**SCP** (W/kg)
1.0	**8.32**	-0.31	**0.04**	0.39	**0.073**	0.098	2.55
1.5	**11.76**	-0.54	**0.76**	0.39	**0.086**	0.112	2.13
1.6	**12.42**	-0.55	**0.83**	0.39	**0.087**	0.114	2.05
1.7	**13.08**	-0.54	**0.86**	0.39	**0.089**	0.115	1.97
1.8	**13.73**	-0.52	**0.88**	0.38	**0.089**	0.116	1.89
1.9	**14.38**	-0.50	**0.89**	0.38	**0.090**	0.116	1.82
2.0	**15.03**	-0.47	**0.88**	0.37	**0.090**	0.116	1.75
2.5	**18.19**	-0.50	**0.63**	0.35	**0.089**	0.114	1.42
3.0	**21.30**	-0.45	**0.27**	0.32	**0.086**	0.109	1.17
3.5	**24.36**	-0.27	**0.01**	0.30	**0.083**	0.106	1.0
4.0	**27.39**	0.94	**0**	0.28	**0.082**	0.103	0.87

Thus, for about 14.1 kg of NORIT-RX3-Extra and about 6 kg of methanol, about 0.9 kg of ice (optimum) can be produced at evaporator temperature T_e = -0.51 ^oC and the

corresponding COP, SCOP, ESCOP and SCP are 0.38, 0.09 (optimum), 0.116 (optimum) and 1.85 (kg/W), respectively.

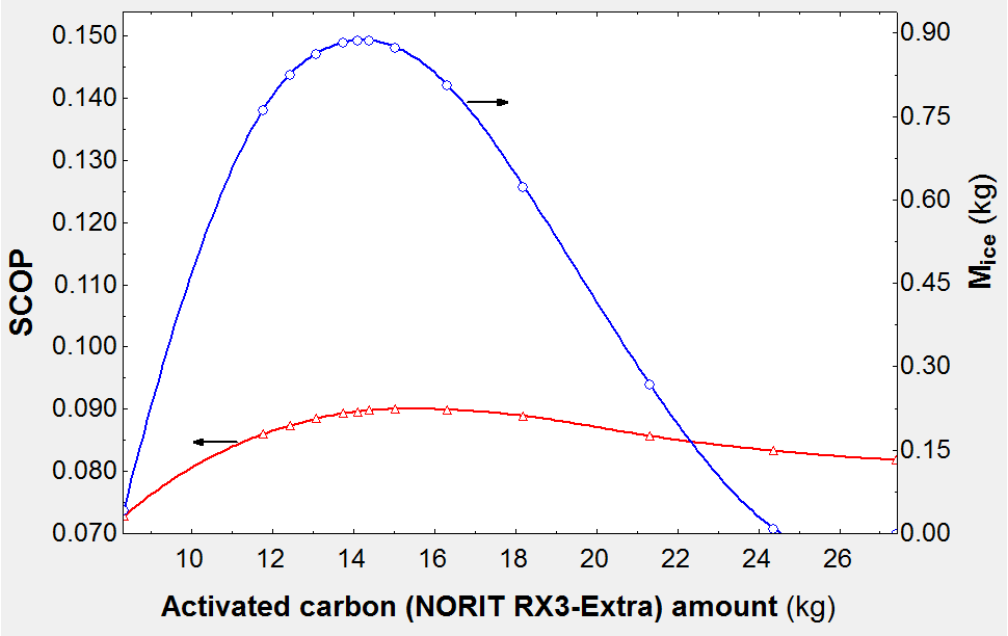

Figure 4.22 The effect of the activated carbon NORIT RX3-Exta amount (M_{ac}) on the performance.

4.2.3.6 Glazing Cover Number and Types

While the main purpose of the glazing cover is to reduce heat losses from the solar collectors, the glazing cover actually does not permit all sun radiation to reach absorber. It has a specific value of transmittance that should be as high as possible. Single glazing cover (of 3 mm thick), double glazing cover (each sheet is 3 mm thick) and transparent insulation material (TIM) are investigated in this section. The collector configuration is as obtained before (about 14.1 kg of NORIT RX3-extra, 1mm thick of stainless steel absorber with selective coating (α_{pw} = 0.95 and ε_{pw} = 0.07)).

The sheets type of single and double glazing covers is water white glass (low iron glass, $(\tau_g)_{max}$ = 0.94) while TIM is an 8 cm thick polycarbonate honeycomb with 3 cm as the

equivalent radius of the cells and 3 mm thick for the top and the bottom bases as shown in Fig. 3.3.

Figure 4.23 shows the glass transmissivity and the absorber absorptivity products ($\tau_g\alpha_{pw}$) of the three glazing cover systems on the typical hot day of 19th June. It is obvious that the single cover system has the higher value ($(\tau_g\alpha_{pw})_{max}$ = 0.86) and the second high value is for double glazing system ($(\tau_g\alpha_{pw})_{max}$ = 0.786) while the TIM has the lowest value ($(\tau_g\alpha_{pw})_{max}$ = 0.646). Correspondingly, TIM system absorbs a less radiation whereas the single cover system can absorb the best amount of solar radiation. However, the advantage of TIM is ability to minimize the heat losses.

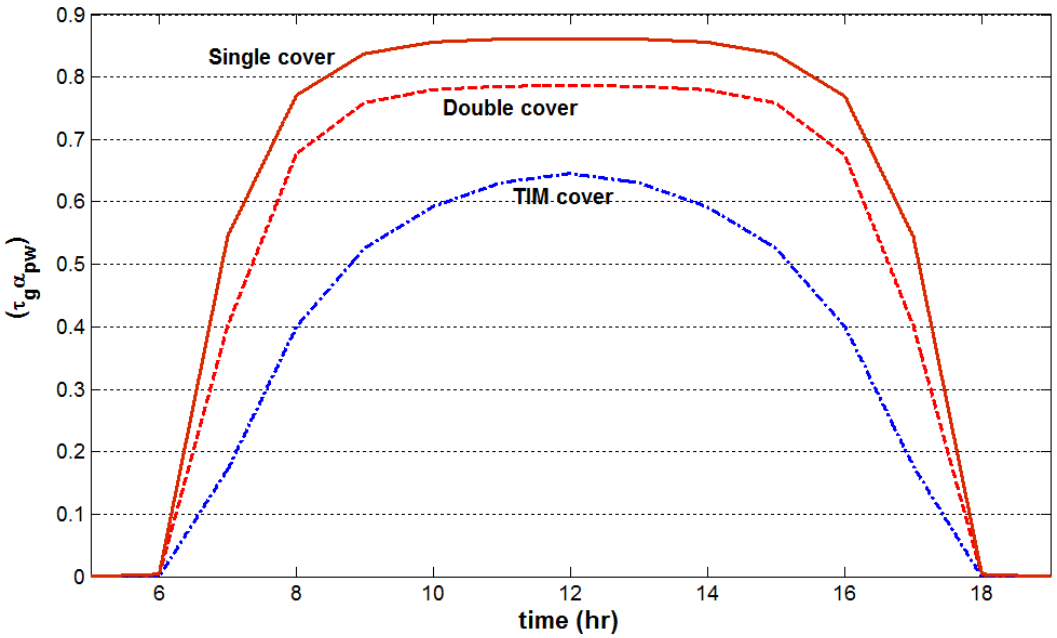

Figure 4.23 Transmissivity absorptivity product ($\tau_g\alpha_{pw}$) of the three glazing cover systems.

TIM has the lowest values of collector heat loss coefficient (U_L = 1.7 - 2.6 W/m^{2}K) compared to the single cover (U_L = 2.8 - 4.6 W/m^{2}K) and the double cover (U_L =1.8 - 3.75 W/m^{2}K) glazing systems during heating and desorption processes (generation time), as shown in Fig. 4.24.

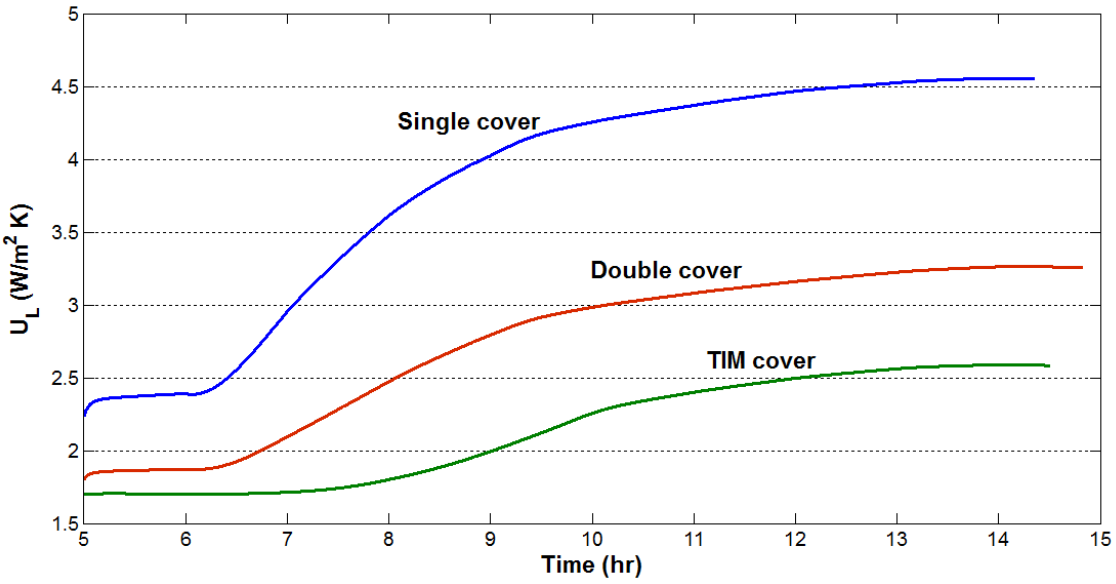

Figure 4.24 Overall collector heat loss coefficient (U_L) during heat generation time of the three glazing cover systems.

For these reasonable values of ($\tau_g\alpha_{pw}$) and U_L, the maximum temperature of adsorbent (127. 91 ^oC) can be obtained by double glazing cover system while TIM and single glazing cover systems have closed T_d values such as 118.84 and 116.41 ^oC, respectively, as shown in Fig. 4.25 and Table 4.19. For these generation temperatures, the desorbed methanol is higher by double glazing system ($m_m(d)$ = 2.76 kg) whereas $m_m(d)$ for single cover and TIM systems are 2.27 and 2.15 kg, respectively, as shown in Fig 4.26 and Table 4.19. Furthermore, adsorbed methanol amount $m_m(a)$ values indicate some advantages for the double gazing system (2.52 kg) followed by TIM (2.13 kg) and then the single cover system (2.04 kg), respectively. The corresponding amounts of the produced ice are about 2.41, 2.01 and 0.88 kg for the double glazing system, TIM and single glazing system, respectively, as shown in Fig 4.26 and Table 4.19.

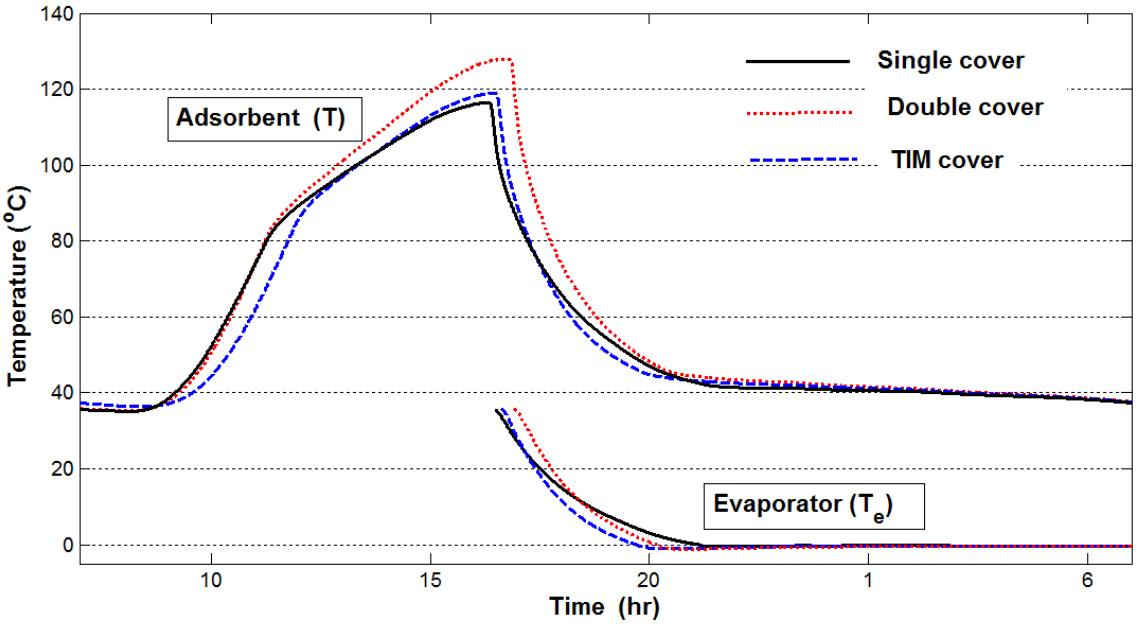

Figure 4.25 Adsorbent (T) and evaporator (T_e) temperatures of the three glazing cover systems.

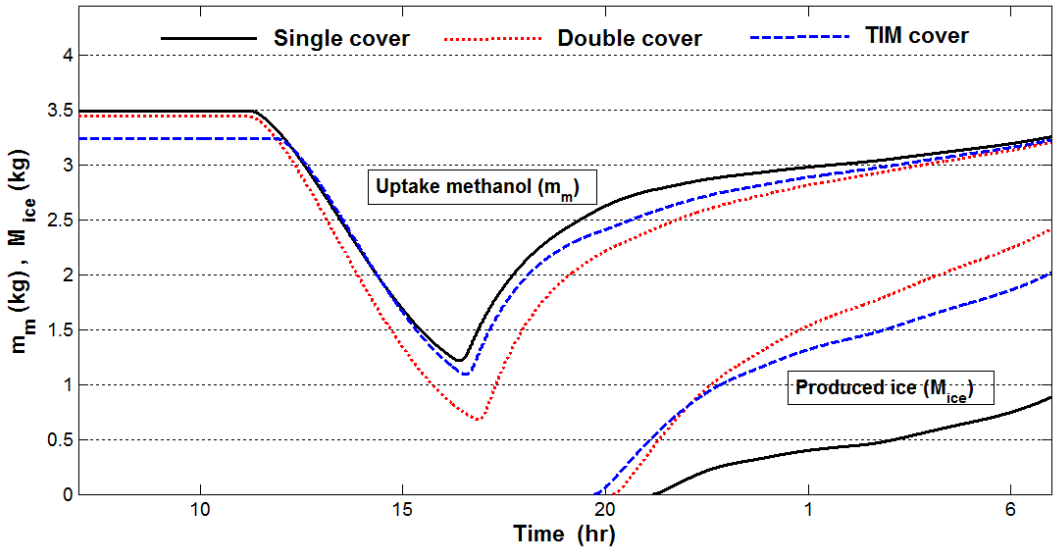

Figure 4.26 Methanol uptake (m_m) and amount of produced ice (M_{ice}) for the three glazing cover systems.

Table 4.19 shows the main operating and performance parameters, the main parameters values confirm that the double glazing system is the best type followed by TIM and then single glazing system with SCOP equals 0.112, 0.094 and 0.089, respectively.

Table 4.19 Effect of glazing cover systems on operating and performance parameters.

Parameters	Single cover	Double cover	TIM cover
T_d (^oC)	**116.41**	**127.91**	**118.84**
T_a (^oC)	37.6	37.65	37.11
$T_{c\ (mean)}$ (^oC)	41.78	42.12	42.07
$T_{e\ (min)}$ (^oC)	**-0.51**	**-1.16**	**-0.98**
$P_{c\ (mean)}$ (kPa)	37.7	38.33	38.2
$P_{e\ (mean)}$ (kPa)	3.87	3.79	3.82
m_m (d) (kg)	2.27	2.76	2.15
m_m (a) (kg)	2.04	2.52	2.13
M_{ice} (kg)	**0.88**	**2.41**	**2.01**
COP	0.38	0.40	0.41
SCOP	**0.089**	**0.112**	**0.094**
ESCOP	0.116	0.136	0.120
SCP (W/kg)	1.85	2.31	1.93

4.2.3.7 Back Insulation Thickness

As the glazing cover is used to reduce heat losses from the top side of the collector, the insulation material on the sides and the rear of collector is used for the same purpose. Fiberglass insulation is used in all previous sections to insulate the system having 10 cm thick on the rear of collector, 5 cm thick on all the collector sides and 10 cm thick for surrounding the evaporator. Fiberglass material has a low thermal conductivity (about 0.038 W/m K) and has a capability to handle temperature more than 500 ^oC. Other insulation materials such as expanded polystyrene and rigid polyurethane foam have lower thermal conductivity (about 0.034 and 0.025 W/m K), but the maximum operating temperature is as low as 75 ^oC and 120 ^oC, respectively. Polyisocyanurate insulation material (Polyiso) has lower thermal conductivity (about 0.025 W/m K) and can serve up to 150 ^oC of temperature, which is suitable for activated carbon methanol systems that

should avoid any temperature that exceeds 150 ^{o}C due to decomposition of methanol. If rigid polyisocyanurate foam boards are used to insulate the sides and rear of collector with fiberglass material remain only in the evaporator box walls, M_{ice}, T_e, SCOP and T_d are improved from 2.41 kg, -1.15 ^{o}C, 0.112 and 127.91 ^{o}C to about 2.78 kg, -1.30 ^{o}C, 0.117 and 131.50 ^{o}C, respectively, whereas use of polyisocyanurate in the evaporator box walls as well as in the collector enhances M_{ice} up to 3.11 kg at T_e = -1.35. Therefore, the effect of the collector back insulation (Polyiso) thickness on the operating and performance parameters is investigated in this section while the glazing system used is the double cover.

Table 4.20 The effect of collector back insulation thickness on system operating parameters.

t_i (m)	**T_d** (^{o}C)	**T_a** (^{o}C)	**T_c** (mean) (^{o}C)	**P_c** (mean) (^{o}C)	**P_e** (min) (^{o}C)	**m_m** (d) (kg)	**m_m** (a) (kg)
0.03	**121.32**	37.58	42.0	38.11	3.83	**2.51**	**2.26**
0.05	**126.73**	37.71	42.10	38.30	3.80	**2.72**	**2.48**
0.07	**129.36**	37.76	42.14	38.36	3.79	**2.80**	**2.57**
0.09	**130.93**	37.79	42.16	38.40	3.78	**2.85**	**2.61**
0.10	**131.50**	37.8	42.16	38.41	3.78	**2.87**	**2.63**
0.11	**131.97**	37.81	42.17	38.42	3.77	**2.88**	**2.64**
0.13	**132.72**	37.82	42.18	38.44	3.77	**2.90**	**2.67**
0.15	**133.28**	37.83	42.18	38.46	3.77	**2.92**	**2.68**
0.17	**133.72**	37.83	42.19	38.46	3.77	**2.93**	**2.69**
0.19	**134.06**	37.84	42.19	38.46	3.77	**2.94**	**2.70**
0.21	**134.34**	37.85	42.19	38.47	3.77	**2.95**	**2.71**

Table 4.20 represents the effect of the collector back insulation thickness (t_i) on the operating parameters. Increasing t_i from 0.03 m to 0.21 m increases T_d from about 121.32 ^{o}C to about 134.34 ^{o}C and the corresponding m_m(d) from 2.51 kg to 2.95 kg. Also, m_m(a) increases from about 2.26 to about 2.71 at the closed values of adsorption temperatures

(from 37.58 ^{o}C to 37.85 ^{o}C). According to these improvements in T_d and $m_{m,}$, M_{ice} increases from 1.94 to 3.36 kg with a corresponding T_e varying from -0.84 to -1.45 ^{o}C, as shown in Table 4.21. COP, SCOP, ESCOP and SCP also increase from about 0.39, 0.1, 0.124 and 2.06 (W/kg) to about 0.41, 0.12, 0.144 and 2.49 (W/kg), respectively.

Table 4.21 The effect of collector back insulation thickness on system performance parameters.

t_i (m)	**T_e** (min) (^{o}C)	**M_{ice}** (kg)	**COP**	**SCOP**	**ESCOP**	**SCP** (W/kg)
0.03	-0.84	**1.94**	0.39	**0.100**	0.124	2.06
0.05	-1.14	**2.62**	0.40	**0.110**	0.134	2.26
0.07	-1.26	**2.90**	0.41	**0.114**	0.138	2.35
0.09	-1.32	**3.06**	0.41	**0.116**	0.140	2.40
0.10	-1.35	**3.11**	0.41	**0.117**	0.140	2.41
0.11	-1.36	**3.16**	0.41	**0.118**	0.141	2.43
0.13	-1.39	**3.22**	0.41	**0.118**	0.142	2.45
0.15	-1.41	**3.27**	0.41	**0.119**	0.143	2.46
0.17	-1.43	**3.31**	0.41	**0.120**	0.143	2.47
0.19	-1.44	**3.34**	0.41	**0.120**	0.143	2.48
0.21	-1.45	**3.36**	0.41	**0.120**	0.144	2.49

Figure 4.27 shows the trend of the most two important operative parameters (M_{ice}, SCOP) with t_i varies from 3 cm to 30 cm. It is clear that both M_{ice} and SCOP increase sharply for increasing the collector back insulation thickness from 3 to 10 cm and then they rise slowly. The insulation thicknesses 5 and 10 cm are always used in the literature to avoid exaggerated thickness of the collector. For that, the back collector insulation thickness is taken as 10 cm to minimize significantly the amount of the heat losses during the generation (heating and desorption) time.

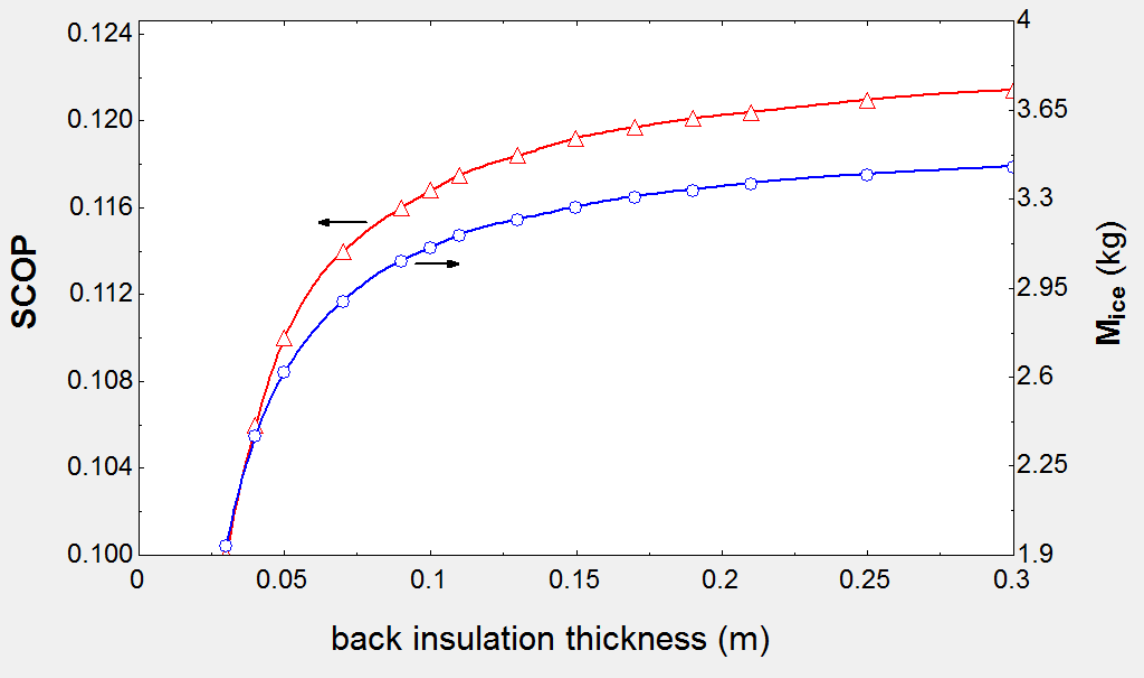

Figure 4.27 Effect of back insulation thickness (t_i) on M_{ice} and SCOP.

4.2.3.8 Other Improvements

In the previous sections, the solar collector tilt angle (β) is assumed constant at the same value of Dhahran latitude (about 26.3^o). This tilt angle is suitable to absorb maximum insolation all year days if the collector is fixed without moving during because of the heavy weight of the collector (about 55 kg without frame). However, it is more suitable to tilt the collector at least one time every month according to the tilt angle values that are proposed in Table 4.22 to minimize the solar incident angle below 6^o at noon (incident solar radiation will be almost perpendicular on the collector) for all months days.

The typical hot day on 19th June is selected to compare the effect of the tilt angle of the collector (at 26.3^o and 3.4^o) on the received solar radiation and the corresponding variation in I_T, T_d, T_e, P, M_{ice} and m_m as shown in Figures 4.28, 4.29 and 4.30.

Table 4.22 Average monthly collector tilt angle for Dhahran.

Month	1	2	3	4	5	6	7	8	9	10	11	12
Tilt angle	47.4	39.5	28.9	17.1	7.7	3.4	5.3	13.0	24.3	36.1	45.4	49.4

Figure 4.28 shows that for collector tilt equals of 26.3^{o} and 3.4^{o}, respectively, the maximum incident solar radiation rises from about 915.3 W/m^2 to about 979.1 W/m^2 and the total received radiation during a day from about 25.13 MJ/m^2 to about 27.98 MJ/m^2.

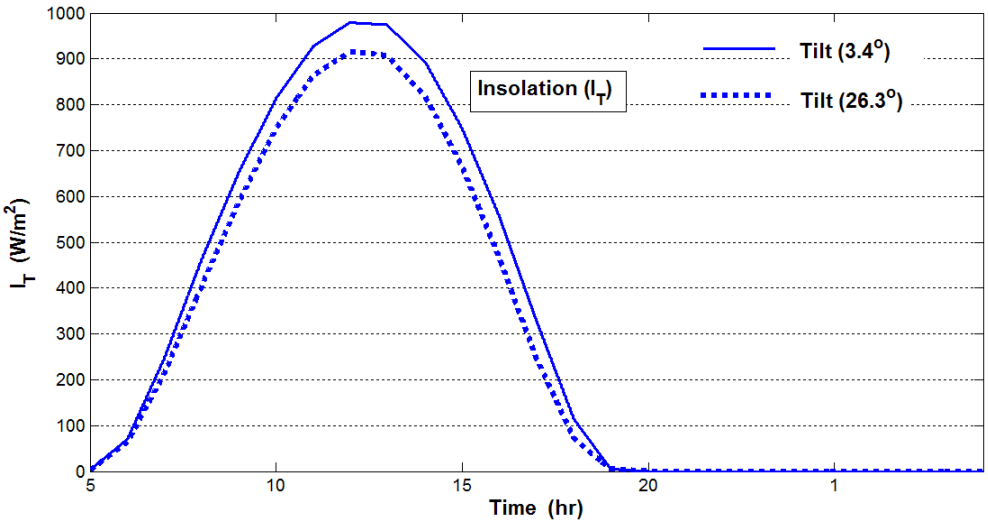

Figure 4.28 Effect of collector tilt angle on incident solar radiation on collector on 19th June.

For this increment in the solar radiation that is caused by the suitable average monthly tilt angle (of 3.4^{o} for June), the desorption temperature increases to about 143.94 ^{o}C instead of 131.5 ^{o}C (in the case of tilt = 26.3^{o}). T_e also decreases from -1.45 ^{o}C to -1.67 ^{o}C, as shown in Fig. 4.29 and 1st and 2nd columns of Table 4.23.

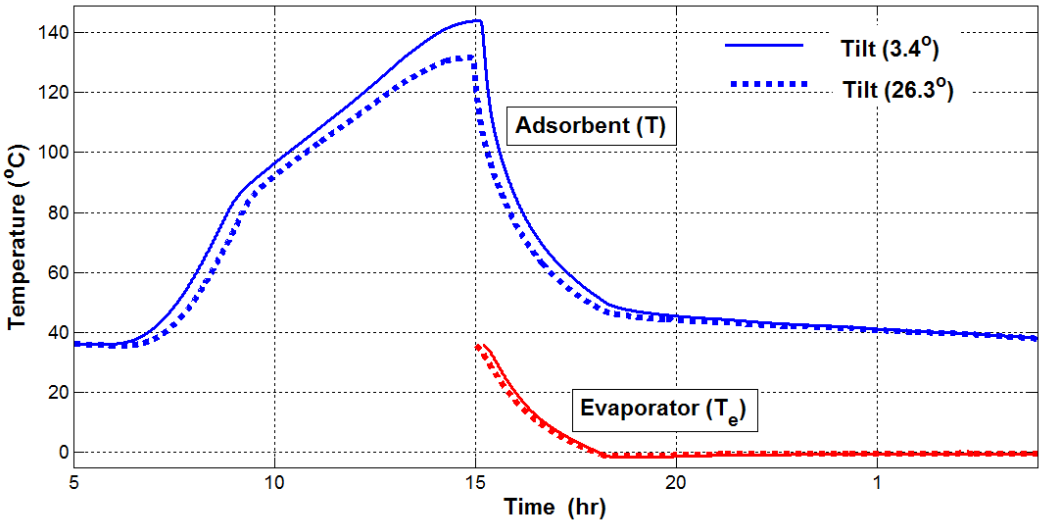

Figure 4.29 Effect of collector tilt angle on adsorbent (T) and evaporator (T_e) temperatures on 19th June.

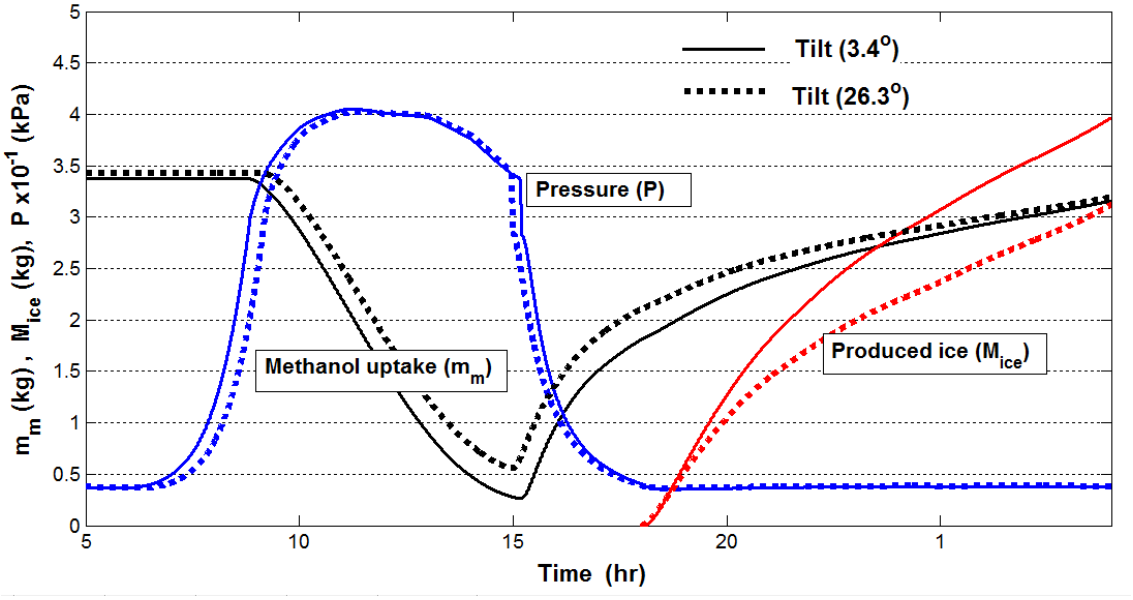

Figure 4.30 Effect of collector tilt angle on methanol uptake (T_d), pressure (P) and amount of produced ice (M_{ice}) on 19th June.

Figure 4.30 shows the effect of collector tilt angle on m_m, P and M_{ice}. Due to increasing the adsorbent temperature as shown in Fig. 4.29, the amounts of desorbed and adsorbed

methanol increase from about 2.87 kg and 2.63 kg to about 3.1 and 2.9 kg as shown in Fig 4.30 and Table 4.23. Therefore, the corresponding amount of produced ice increases from about 3.11 kg to about 3.96 kg at mean evaporator pressure equals 3.78 and 3.74 kPa for the collector tilts of 26.3^{o} and 3.4^{o}, respectively. COP, SCOP, ESCOP almost remain at the same values due to the increase in both the received heat and cooling effect while SCP increases by about 10 % as shown in 1^{st} and 2^{nd} columns of Table 4.23.

The sunset in Dhahran during the hot months such as April, May, June, July and August is between 5 and 6 (solar time) AM and there is no actual heating during this period as shown in Fig 4.31 on the typical hot day (19^{th} June). Thus, it is suitable to start the cycle at 6 AM (solar time) on the hot days and leaving the time between sunrise and 6 AM as extra time for adsorption process to the pervious cycle to improve the amount of produced ice and other performance parameters as shown in Fig 4.32 and 3^{rd} column in Table 4.23. In winter days the heating starts at the sunrise time (usually after 6 AM) due to the increase in solar zenith angle, so there is no need to shifting starting time.

Figures 4.31 and 4.32 and Table 4.23 show that these are no significant changes in the operative parameters due to this time offset. However the amount of ice produced increases from 3.96 to 4.24 kg and SCOP is 0.119 instead of 0.116 (in case of no time offset).

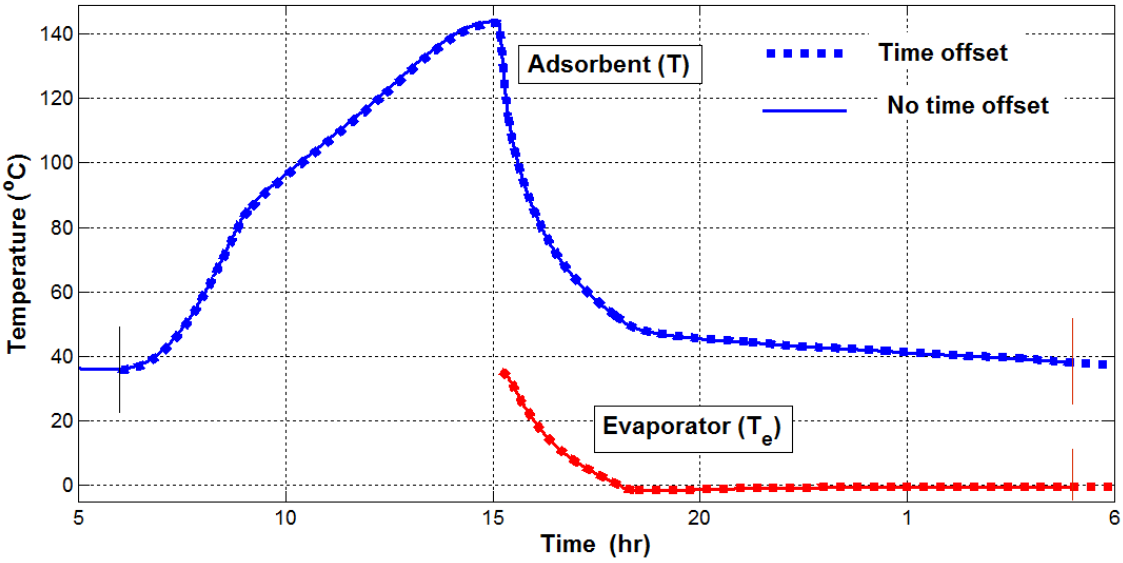

Figure 4.31 Effect of time offset on adsorbent (T) and evaporator (T_e) temperatures at Tilt = 3.4^o on 19th June.

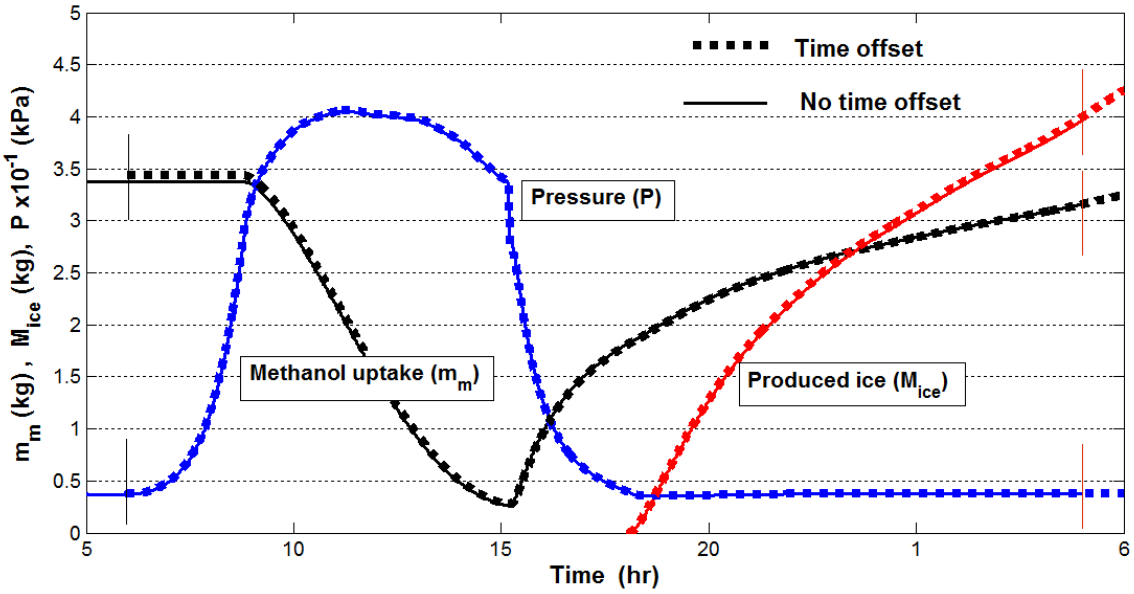

Figure 4.32 Effect of time offset on methanol uptake (m_m), pressure (P) and produced ice (M_{ice}) at Tilt = 3.4^o on 19th June.

Table 4.23 Effect of collector tilt angle and time offset on operating and performance parameters.

Parameters	Tilt = 26.3°	Tilt = 3.4°	Tilt = 3.4° with time offset
T_d (°C)	**131.5**	**143.94**	**143.4**
T_a (°C)	37.8	38.01	37.3
$T_{c\ (mean)}$ (°C)	42.16	42.02	42.05
$T_{e\ (min)}$ (°C)	**-1.35**	**-1.67**	**-1.68**
$P_{c\ (mean)}$ (kPa)	38.41	38.17	38.2
$P_{e\ (mean)}$ (kPa)	3. 78	3.74	3.74
m_m (d) (kg)	2.87	3.1	3.17
m_m (a) (kg)	2.63	2.89	2.97
M_{ice} (kg)	**3.11**	**3.96**	**4.25**
COP	0.41	0.41	0.42
SCOP	**0.117**	**0.116**	**0.119**
ESCOP	0.140	0.139	0.143
SCP (W/kg)	2.41	2.66	2.74

The next section concerns with these improvements (collector tilt angle and starting time offset) and all the previous improvements to show the enhanced behavior and the performance of the system.

4.2.3.9 Actual System Behavior after Improving the Main Collector Parameters.

After all the previous suggested improvements, the system is simulated during ten consecutive days for both summer and winter to show its actual behavior and performance. The proposed collector (1 m^2) consists of 17 stainless steel tubes (1mm thick, about 59.3 mm outer diameter and 1m long) with 2 cm outer diameter of inner perforated pass steel tubes to handle the optimum mass of about 14.1 kg of NORIR RX3-Extra; the corresponding methanol is about 6 kg. The tubes are covered by chrome-black selective layer (α_{pw} = 0.95 and ε_{pw} = 0.07); the double glazing system is selected. Rigid polyisocyanurate foam insulation is used on the sides (5 cm thick) and back (10 cm thick)

of the collector as well as on the box that surrounds the evaporator (10 cm thick). The other system components data are shown in Fig 4.33. The solar collector tilt angles are taken corresponding to those values shown in Table 4.22; the offset starting operating time is taken into consideration.

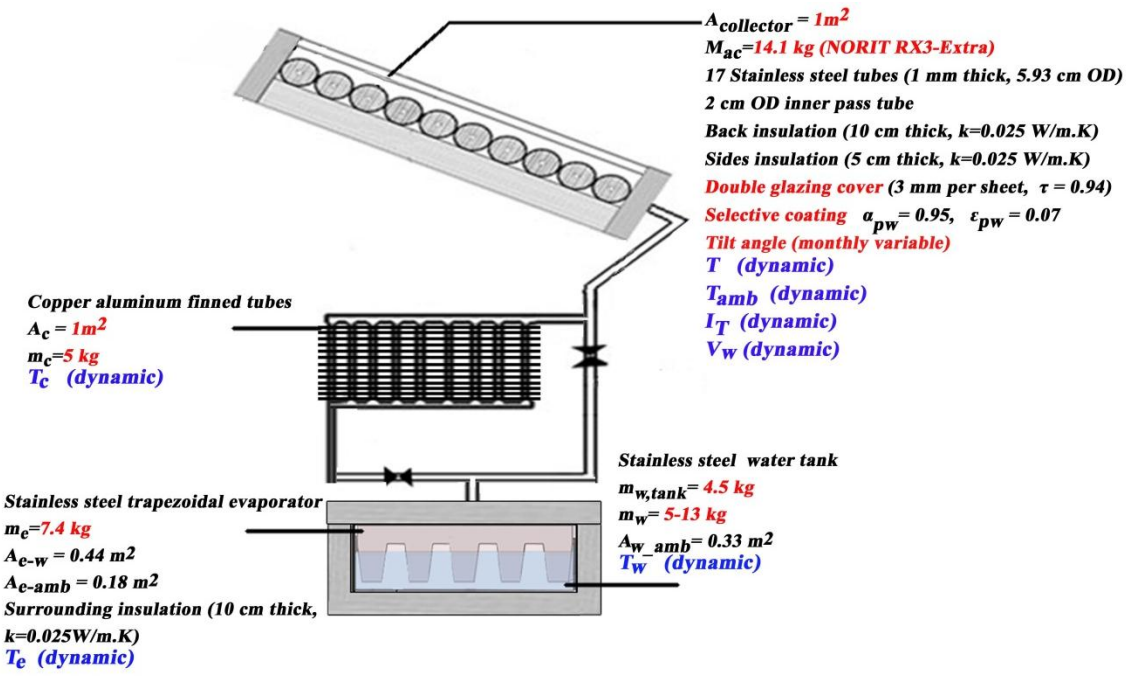

Figure 4.33 System configuration details after the improvements

The system behavior and performance are estimated under Dhahran hot climate conditions during 10 consecutive days (from 14th to 23th of June 2011), as shown in Figures 4.34, 4.35 and 4.36 and Table. 4.24.

Figure 4.34 shows the incident solar radiation on suitable collector tilt (Tilt = 3.4^{o}) from 14th to 23rd of June. Comparing the I_T values shown in Fig. 4.34 to those described in section 4.2.3.2 for collector tilt angle = 26.3^{o} during the period between 14th and 20th

June affirms some increases in I_T values from about 904.4 W/m^2 as minimum on 18th June to about 1016 W/m^2 on 15th June as maximum instead of about 850 W/m^2 as a minimum to 950 W/m^2 as a maximum for the same two days. The corresponding solar radiations received during these two days times are 26.39 and 29.3 MJ/m^2 instead of 26.28 and 23.88 MJ/m^2, thus improved about 10.5% and 11.5 % for the two days (18th and 15th June), respectively.

The overall adsorbent temperatures increase as shown in Fig 4.35; the maximum desorption temperature (T_d) is 135^{o}C instead of 102.23 ^{o}C on 14th June as a minimum and T_d = 147.7 ^{o}C instead of 112.37 ^{o}C on 20th June as the maximum at the same period. Recalling that T_d should be below 150 ^{o}C, for this reason, the previous improvements take that into consideration as shown in Fig 4.35; the highest value of T_d is 147.7 ^{o}C on 20th June and the others days have lower than this value. Notice that T_c values are not changed much while T_e values go slightly below 0^{o}C (-2.5 ^{o}C $\leq$ T_e (min) $\leq$ -1.3 ^{o}C) during all considered days for cooling and solidifying about 7 kg of water.

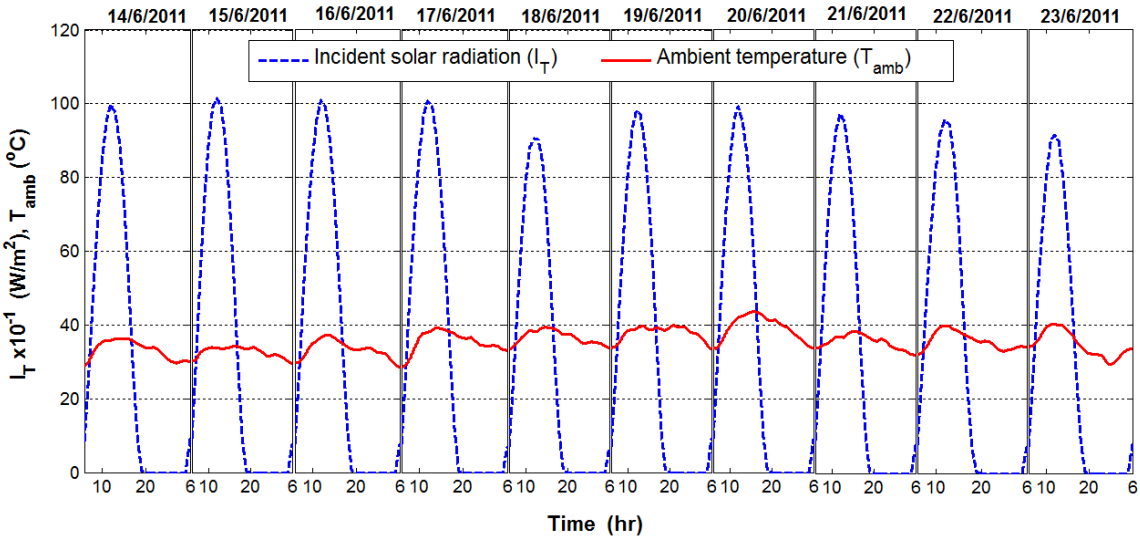

Figure 4.34 Solar radiation on collector (I_T) and ambient temperature (T_{amb}) recorded during June 14-23, 2011.

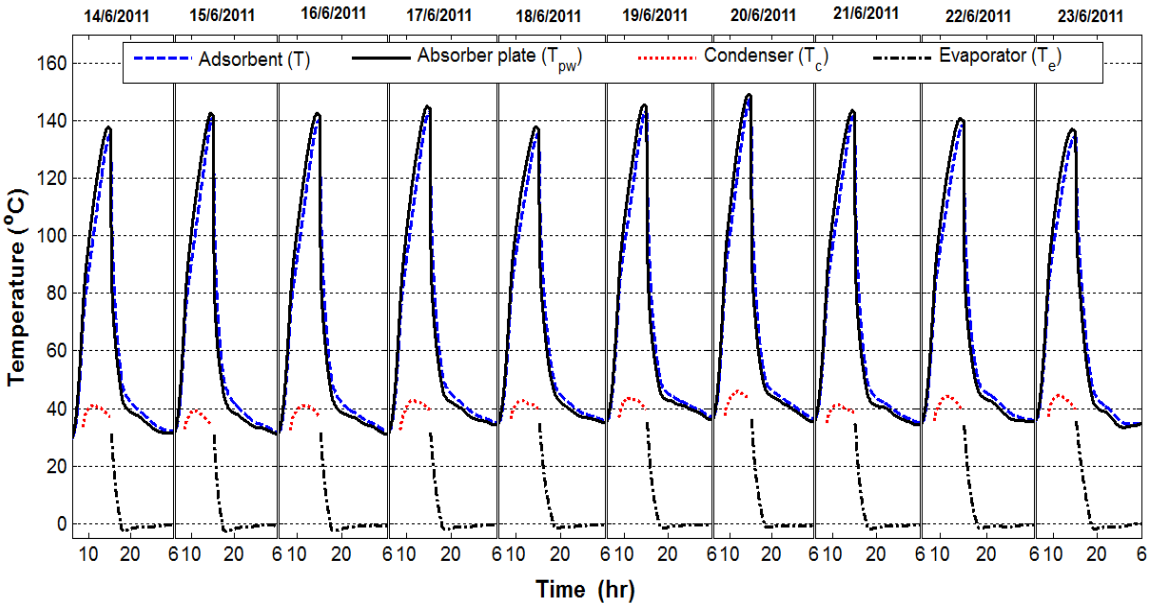

Figure 4.35 Collector absorber (T_{pw}), adsorbent bed (T), condenser (T_c) and evaporator (T_e) temperatures calculated for June 2011.

.

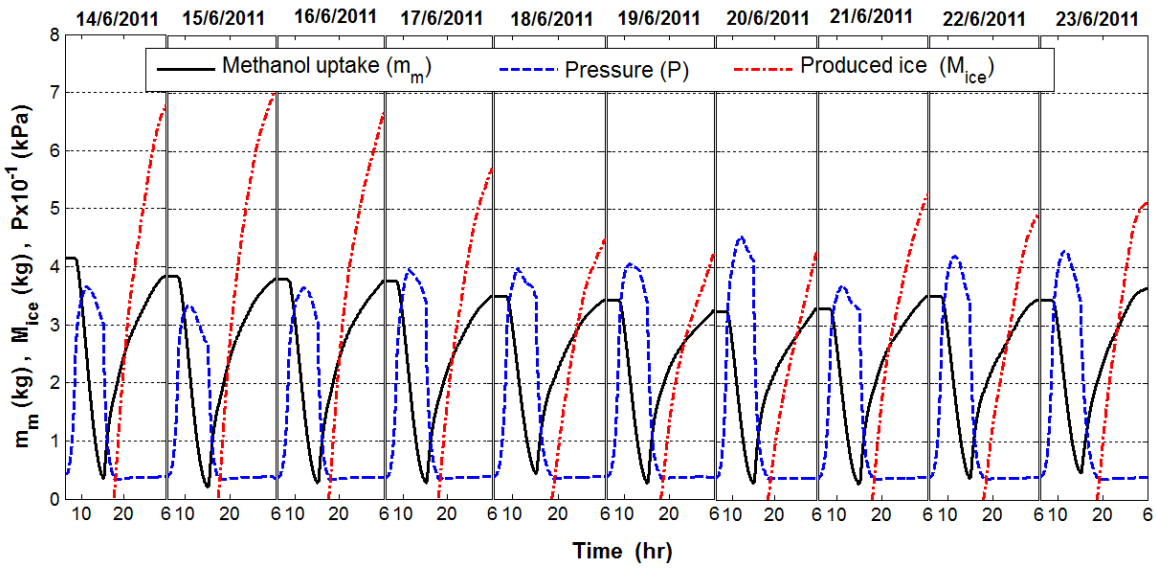

Figure 4.36 Methanol uptake (m_m), adsorbent bed pressure (P) and amount of produced ice (M_{ice}) calculated for June 2011.

The methanol uptake (m_m) shown in Fig 4.36 varies between about 4.2 kg on 14th June as a maximum and 0.27 kg on 19th June as a minimum out of the 5.99 kg (the maximum methanol that can be adsorbed into the system (M_m)). From 14th to 23rd of June, the

average desorbed methanol amount (m_m (d)) is 3.275 kg out of the corresponding M_m = 5.99 kg (for NORIT RX3-Extra) compared to 2.25 kg out of M_m= 6.6 kg (for AC-35) from 14th to 20th June as mentioned in section 4.2.3.2. The average desorption ratio (m_m(d)/M_m) after the improvements is 54.67% while it equals 34.1% in section 3.2.3.2, thus enhanced by about 62.40 %. Also m_m(a) increases to about 3.223 kg (as average m_m(a) for 10 days from 14th to 20th June) compared to the value of 2.13 kg before the previous improvements. The corresponding adsorption ratio (m_m(a)/M_m) increases about 60 %. Therefore, the amount of produced ice increases from 0 kg in the worst day (19th June) and 2.35 kg on 15th June to about 4.25 and 7 kg, respectively.

The lowest values of COP, SCOP, ESCOP and SCP are 0.42. 0.119, 0.143 and 2.74 on the typical bad conditions day (19th June) as shown in Table 4.24. Thus, the corresponding improvements are 50%, 54.5%, 50% and 144.6% of COP, SCOP, ESCOP and SCP, respectively.

Table 4.24 System performance for June 2011.

Date	**14/6**	**15/6**	**16/6**	**17/6**	**18/6**	**19/6**	**20/6**	**21/6**	**22/6**	**23/6**
COP	0.44	0.47	0.46	0.42	0.44	0.42	0.44	0.47	0.44	0.48
SCOP	**0.140**	**0.139**	**0.137**	**0.125**	**0.127**	**0.119**	**0.120**	**0.131**	**0.130**	**0.137**
ESCOP	0.165	0.165	0.164	0.150	0.152	0.143	0.143	0.157	0.154	0.164
SCP (W/kg)	3.25	3.33	2.24	2.98	2.76	2.74	2.77	2.99	2.85	2.93
M_{ice} (kg)	**6.77**	**7**	**6.67**	**5.69**	**4.47**	**4.25**	**4.25**	**5.26**	**4.91**	**5.1**
m_m(d) (kg)	3.8	3.63	3.51	3.48	3.05	3.16	2.96	3.03	3.14	2.99
m_m(a) (kg)	3.48	3.58	3.49	3.21	2.99	2.97	3.01	3.03	3.10	2.99
P_e (kPa)	3.65	3.64	3.66	3.67	3.72	3.74	3.73	3.70	3.72	3.70
P_c (kPa)	33.72	30.5	33.60	36.20	37.01	38.20	41.95	39.38	38.32	39.36

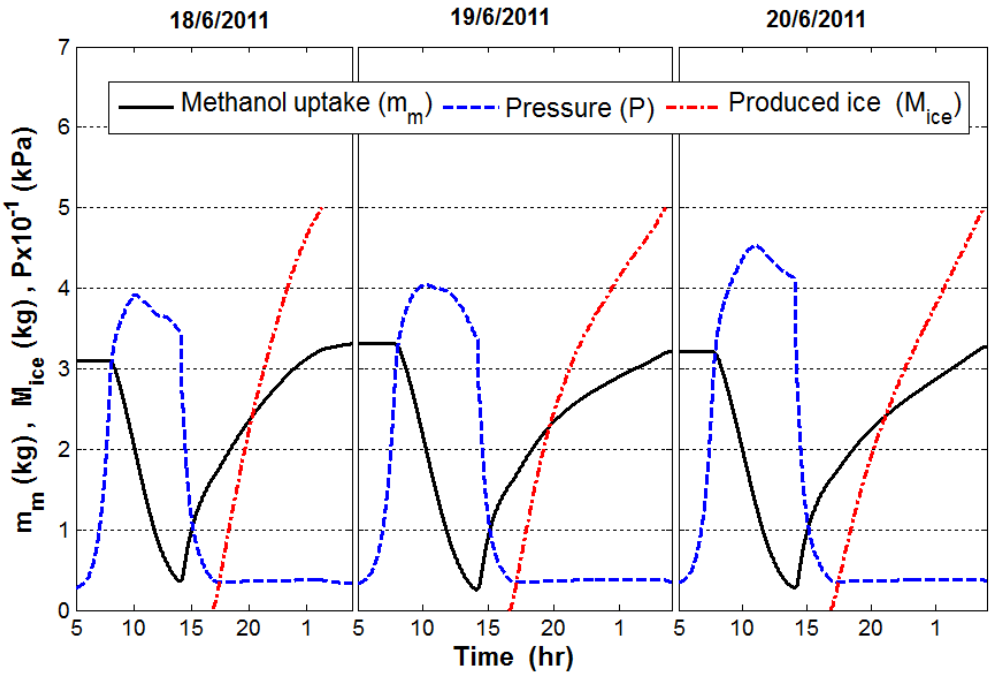

Figure 4.37 Methanol uptake(m_m), adsorbent bed pressure (P) and amount of produced ice (M_{ice}) calculated for 18th, 19th and 20th June 2011 (for m_w=5 kg).

It is obvious from Fig. 4.36 and Table 4.24 that M_{ice} is between 4 and 5 kg such as on 18th, 19th and 20th June while the main objective of this investigation is to produce 5 kg or more of ice. Thus results is because of the mass of water (m_w) in the evaporator is 7 kg. If m_w is reduced by 2 kg, i.e. to be 5 kg, the produced ice will be 5 kg on 18th, 19th and 20th June, as shown in Fig 4.37, at T_e (min) equals -2.48, -1.95 and -1.58 ^oC with corresponding SCOP equals 0.126, 0.119 and 0.119, respectively.

In cold days (from 17th to 26th December), the system is also modeled to show the best performance that can be obtained after taking into consideration the previous improvements. For this reason, the amount of water is increased up to 13 kg to show the maximum capability of the system for ice production. Figures 4.38, 4.39 and 4.40 and Table 4.25 represent the important operating and performance parameters.

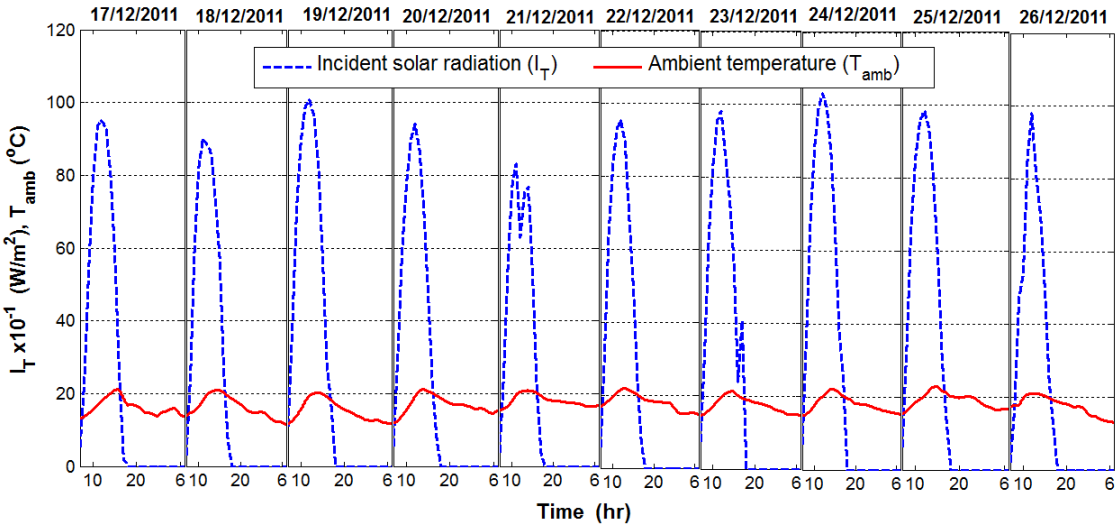

Figure 4.38 Incident solar radiation on collector (I_T) and ambient temperature (T_{amb}) recorded during December 17-26, 2011.

Incident solar radiation (I_T) from 17th to 26th December on the tilted collector (Tilt=49.4^o) is presented in Fig. 4.38. The highest and lowest I_T (max) are about 1030 and 831 W/m^2, corresponding to total received solar energies of about 25.83 and 19.26 MJ/m^2 on 24th and 21st December, respectively. On 19th June, the total incident solar radiation is about 24.84 MJ/m^2 instead of about 22.2 MJ/m^2 at the same day as was given in section 4.2.3.2; the increase is about 11.9 %.

The maximum adsorbent temperature (T_d) increases to be between 92.55 ^{o}C and 118.7 ^{o}C during these 10 cold days (from 17th to 26th December) as shown in Fig. 4.39. In the best weather condition day (19th December) T_d = 108.72 ^{o}C instead of 78.03 ^{o}C (before the collector improvements). T_e (min) varies between -2.97 (on 17th December) ^{o}C and -4 ^{o}C (on 19th December); it does not go below -4 ^{o}C due to the large amount of water (m_w = 13 kg).

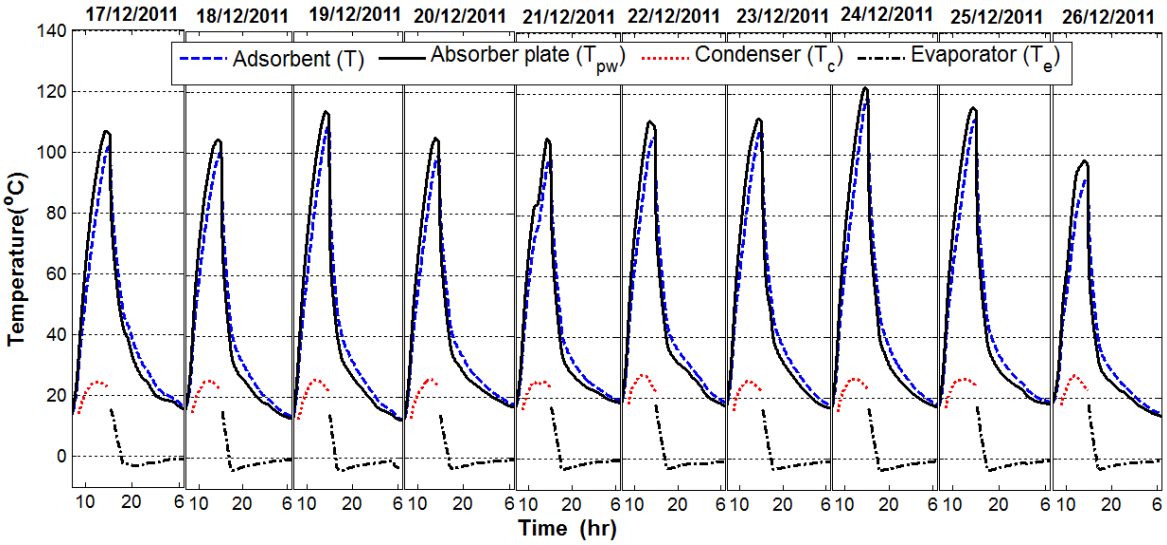

Figure 4.39 Collector absorber (T_{pw}), adsorbent bed (T), condenser (T_c) and evaporator (T_e) temperatures calculated for the period 17-26 December 2011.

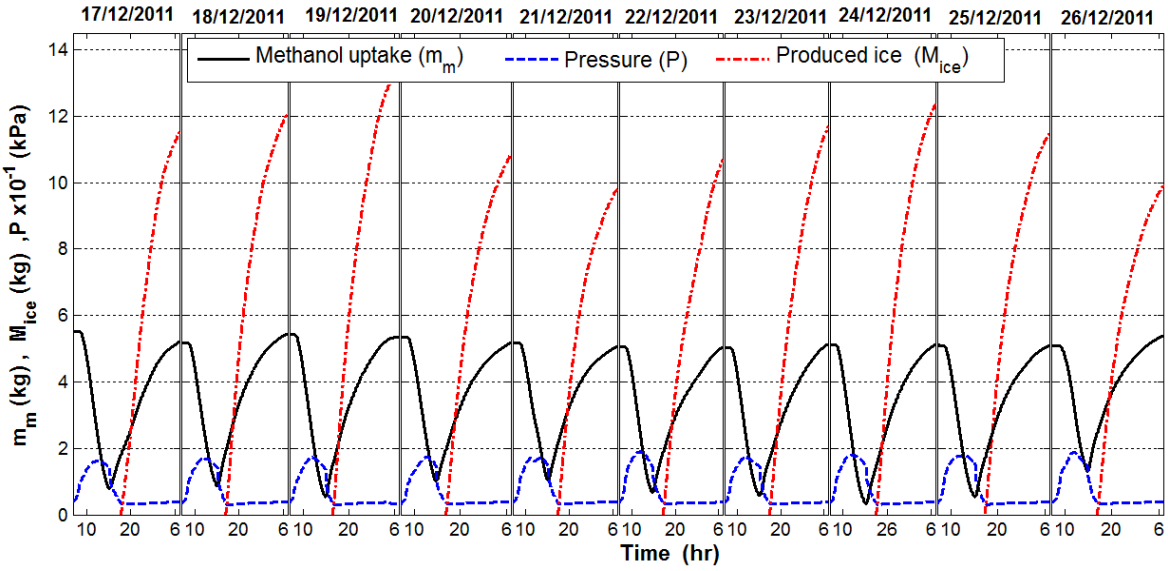

Figure 4.40 Methanol uptake(m_m), adsorbent bed pressure (P) and amount of produced ice (M_{ice}) calculated for the period 17-26 December 2011.

Figure 4.40 and Table 4.25 show the important performance parameters during the cold days. m_m varies between about 5.5 kg as a maximum and about 0.34 as a minimum; the average desorbed and adsorbed amounts of methanol during those 10 days (from 17th to

26th December) are about 4.439 and 4.422 kg with the average desorption ($m_m(d)/M_m$) and adsorption ratios ($m_m(a)/M_m$) equal 74.1 % and 73.82%, respectively. M_{ice} increases to an excellent value that reaches 13 kg on 19th December; the minimum M_{ice} is about 9.8 out of 13 kg on 21st December as shown in both Fig 4.40 and Table 4.25 because of the higher minimum adsorbent temperature at the end of 21st December cycle (T_a=19.4 ^oC) as shown in Fig 4.39.

Fig 4.40 and Table 4.25 also show the system operative pressure is between 3.5 and about 17 kPa (absolute pressure) for December 2011.

Table 4.25 System performance for December 2011.

Date	17/12	18/12	19/12	20/12	21/12	22/12	23/12	24/12	25/12	26/12
COP	0.52	0.59	0.54	0.52	0.53	0.54	0.56	0.54	0.54	0.59
SCOP	**0.232**	**0.245**	**0.224**	**0.226**	**0.239**	**0.228**	**0.221**	**0.212**	**0.220**	**0.241**
ESCOP	0.251	0.265	0.254	0.258	0.264	0.258	0.255	0.241	0.246	0.279
SCP (W/kg)	4.16	4.33	4.56	3.92	3.78	4.1	4.29	4.50	4.29	3.85
M_{ice} (kg)	**11.52**	**12.1**	**13.0**	**10.83**	**9.80**	**10.66**	**11.67**	**12.35**	**11.46**	**9.89**
$m_m(d)$ (kg)	4.73	4.32	4.90	4.33	4.13	4.37	4.46	4.79	4.57	3.79
$m_m(a)$ (kg)	4.39	4.58	4.81	4.41	4.01	4.35	4.55	4.76	4.55	4.08
P_e (kPa)	3.50	3.51	3.42	3.55	3.58	3.55	3.51	3.48	3.52	3.58
P_c (kPa)	14.45	15.14	14.72	14.79	15.64	16.91	15.41	16.01	16.41	16.38

These new June and December results according to the pervious collector improvements may denote that the performance of the system during any day in a whole year is in between the values corresponding to m_w = 7 kg for June and m_w = 13 kg for December, as given in Table 4.26.

Table 4.26 System predicted performance data for both Jnne and December of 2011.

M_{ice} (kg)	COP	SCOP	ESCOP	SCP (W/kg)	T_e (^oC)
4.25 – 13	0.42 – 0.59	**0.119 – 0.245**	0.143 – 0.279	2.7 – 4.6	(-1.3) – (-4)

Finally, the comparison between the thermodynamic analysis and modeling results are presented in Table 4.27. Values of T_d, T_a, T_c, T_e and I_T on 19th June and 19th December are obtained from the modeling results and inserted into the thermodynamic analysis code to obtain and compare the performance results. It is obvious that the results of M_{ice}, COP, SCOP, ESCOP and SCP are close to each other.

Table 4.27 Comparsion betwteen thermodynaic analysis and modeling performance results.

Study		M_{ice} (kg)	COP	SCOP	ESCOP	SCP (W/kg)
19th June (m_w=7 kg)	**Thermodynamic analysis results**	**4.64**	**0.44**	**0.120**	**0.144**	**2.75**
	Modeling results	**4.25**	**0.42**	**0.119**	**0.143**	**2.74**
19th December (m_w=14 kg)	**Thermodynamic analysis results**	**13.70**	**0.57**	**0.239**	**0.272**	**4.88**
	Modeling results	**13.35**	**0.55**	**0.228**	**0.259**	**4.64**

CHAPTER 5

CONCLUSIONS

In this study, the operating and performance parameters of an intermittent solar thermal powered activated carbon/methanol adsorption cooling system are presented using the thermodynamic analysis and weather data for Dhahran. Thermodynamic analysis gives a primary vision of predicting the performance while the modeling under Dhahran climate conditions presents the actual performance of the solar cooling systems that strongly depends on local climate conditions.

According to the obtained results of both the thermodynamic analysis and the modeling study, to have high performance in terms of the amount of ice production and the coefficients of performance, the following operating parameters and collector configuration are preferred,

- Thermodynamic analysis indicates that the optimal results of COP can be obtained for lower condensation temperatures ($T_c \leq 30$ for $80\ ^oC \leq T_d \leq 100\ ^oC$). For higher condenser temperature, the collector should be heated to higher adsorbent temperatures with concentrating means to a maximum allowable temperature of 150 ^{o}C. Furthermore, the amount of produced ice could be greater than 5 kg out of 7 kg of water for high adsorbent temperature and low condenser temperature ($T_d \geq 105\ ^oC$ and $T_c \leq 35\ ^oC$). On the other hand, the optimal result could be achieved for freezing

purposes if the evaporator temperature is close to zero (-4 ^{o}C $\leq T_e \leq$ 0 ^{o}C) for lower minimum adsorbent temperatures (T_a < 30 ^{o}C). Consequently, the optimum values of the condenser and evaporator pressures are lower than 25 kPa and greater than 3 kPa, respectively. Finally, the amount of produced ice increases with decreasing the initial water temperature.

- Thin stainless steel absorber tubes should be selected with suitable selective coating to improve both operative and performance parameters.
- Activated carbon NORIT RX3-Extra is more convenient for improving a solar adsorption ice-maker performance than the other known types; about 14 .1 kg of NORIT RX3-Extra per m^2 of collector is the optimal mass for these improvements.
- In order to increase the desorption temperature and the amount of desorbed methanol for producing high amount of ice and improving the performance, the double glazing system should be chosen rather than TIM (Transparent Insulation Material) and single cover systems.
- Thermal insulation material used in the system is preferred to have quite low thermal conductivity. In addition, the increase of rear insulation of the collector enhances the performance. However the recommended thickness is 10 cm to avoid an exaggerated thickness of the collector.
- The collector tilt angle should be changed monthly to the suitable angle for collecting higher solar radiation. Furthermore, it is suitable to delay the start of heating time to be at 6 AM in summer days to give some extra minutes for enhancing cooling effect.

Finally, the results show that the system can produce from 5 kg of ice up to 13 kg by m^2 of collector under Dhahran climate conditions. Coefficient of performance (COP) and solar coefficient of performance (SCOP) are improved from about 0.42 and 0.12 as the minimum in the hot days to about 0.59 and 0.24 as the maximum in the cold days, respectively. It is believed that this study forms a basic guideline for constructing a good solar adsorption ice-maker that will be operating almost on its own for remote areas.

References

[1] Sasmaz, T. Thermodynamic Analysis of Assisted Adsorption Cooling System. M.Sc. Thesis, Near East University, Nicosia 2011.

[2] Wimolsiri Pridasawas, and Teclemariam Nemariam. (2003), Solar cooling, Assignment for Ph.D. Course: Solar Heating, Technical University of Denmark (DTU).

[3] Critoph, R. E.:1988, Performance limitations of adsorption cycles for solar cooling. *Solar Energy*, 41(1), 21-31.

[4] San, J.-Y. and Lin, W.-M.:2008, Comparison among three adsorption pairs for using as the working substances in a multi-bed adsorption heat pump. *Applied Thermal Engineering*, 28 (8-9), 988-997.

[5] Wang, L. W., Wang, R. Z. and Oliveria, R. G.:2009, A review on adsorption working pairs for refrigeration. *Renewable and Sustainable Energy Reviews*, 13(3), 518-534.

[6] Askalanya, Ahmed A. M., Ismail, Salema I.M., Ali, Ahmed Hamza H. and Morsyb, M.G.:2012, A review on adsorption cooling systems with adsorbent carbon. *Renewable and Sustainable Energy Reviews*, 16, 493– 500

[7] Alghoul M A, Sopian K, Sulaiman M Y, Azmi B Z, Wahab M A, (2007) "Review of materials for adsorption refrigeration technology," Vol. Iss: , pp.225 – 229

[8] Srivastava NC, Eames IW. A review of adsorbents and adsorbates in solid–vapour adsorption heat pump systems. Appl Therm Eng 1998; 18:707–14.

[9] Wang LW, Wang RZ, Lu ZS, Chen CJ, Wang K, Wu JY. The performance of two adsorption ice making test units using activated carbon and a carbon composite as adsorbents. Carbon 2006; 44:2671–80.

[10] Eric JHU. A study of thermal decomposition of methanol in solar powered adsorption refrigeration systems. Sol Energy 1998; 52(5):325–9.

[11] Vasta, S., Maggio, G., Santori, G., Freni, A., Polonara, F. and Restuccia, G., An adsorptive solar ice-maker dynamic simulation for north Mediterranean climate, Energy Conversion & Management, accepted for publication 2008.

[12] Zhao H, Zhang M, Liu Z, Liu Y, Ma X. Mechanical and experimental study on freeze proof solar powered adsorption cooling tube using active carbon/ methanol working pair. Energy Convers Manage 2008; 49:2434–8.

[13] Hassan H.Z., A.A. Mohamad and R. Bennacer, "Simulation of an adsorption solar cooling system." *Elsevier, Energy 36*. 2011.P: 530-537.

[14] Leite, A. P. F., Grilo, M. B., Andrade, R. R. D., Belo, F. A. & Meunier, F. (2007). Experimental thermodynamic cycles and performance analysis of a solar-powered adsorptive icemaker in hot humid climate. Energy Renewable, Vol. 32, pp. 697-712

[15] Medini N, Marmottant B, Golli ES, Grenier Ph. Study of a solar icemaker machine. Int J Refrigerate 1991;14:363–7

[16] Ogueke, V. and Anyanwu E E. *"The* performance analysis of a solid adsorption solar refrigerator during collector cool-down and refrigerant evaporation/re-adsorption phase*." Journal of Process Mechanical Engineering* 223 February 1, 2009: 11-19

[17] Li, M. and R.Z. Wang, "Heat and Mass Transfer in a Flat Plate Solar Solid Adsorption Refrigeration Ice Maker", *Renewable Energy* 28 (2003):613–622.

[18] Chekirou, W., Boukheit, N., Kerbache, T., Numerical Modeling of Combined Heat and Mass Transfer in a Tubular Adsorber of a Solid Adsorption Solar Refrigerator. Revue des Energies Renouvelables Vol. 10 No.3 (2007) 367-379.

[19] Critoph, R. E. and Tamainot-Telto, Z., "Solar Adsorption Refrigeration." *Renewable Energy* 12 (4). 1997: 409-417.

[20] Anyanwu, E.E. and N.V. Ogueke, "Thermodynamic Design Procedure for Solid Adsorption Solar Refrigerator." *Renewable Energy* 30 (2005): 81–96.

[21] Tamainot-Telto, Z., Critoph, S.J. Metcalf, Zhong, R.E., Thorpe, Y., 2009. "Carbon-ammonia pairs for adsorption refrigeration applications: ice making, air

conditioning and heat pumping." *International Journal of Refrigeration* 32(6):1212 – 1229.

[22] Critoph RE, Metcalf SJ. Specific cooling power intensification limits in ammonia carbon adsorption refrigeration systems. Applied Thermal Engineering 2004; 24:661–78.

[23] Critoph, R.E., Multiple bed regenerative adsorption cycle using the monolithic carbon–ammonia pair, Appl.Therm. Eng. 22 (2002): 667–677.

[24] Zhang YH. Adsorption function. Shanghai, China: Publishing House of Scientific and Technological Literature in Shanghai; 1989.

[25] Poyelle F, Guilleminot J-J, Meunier F. Experimental tests and predictive model of an adsorptive air conditioning unit. Industrial & Engineering Chemistry Research 1999; 38(1):298–309.

[26] Jones JA. Sorption refrigeration research at JPL/NASA. Heat Recovery Systems & CHP 1993; 13(4):363–71.

[27] Zhu RQ, Han BQ, Lin MZ, Yu YZ. Experimental investigation on an adsorption system for producing chilled water. International Journal of Refrigeration 1992; 15(1):31–4.

[28] Yang RT. Gas separation by adsorption methods. Beijing, China: Publishing House of Chemical Industry; 1991

[29] http://www.greenchiller.biz

[30] Demir, Hasan, Moghtada Mobedi, and Semra Ülkü. "Effects of porosity on heat and mass transfer in a granular adsorbent bed." International Communications in Heat and Mass Transfer 36.4 (2009): 372-377.

[31] R.P. Kluppel and J.M. Gurgel, Solar adsorption cooling using silica gel/water, Advances in Solar Energy Technology, vol. 3, pp. 2627-2631, 1988

[32] Alam KCA, Saha BB, Kang YT, Akisawa A, Kashiwagi T. Heat exchanger design effect on the system performance of silica gel adsorption refrigeration machines. International Journal of Heat and Mass Transfer 2000; 43(24): 4419–31.

[33] Wang DC, Li YH, Li D, Xi YZ, Zhang JP. A review on adsorption refrigeration technology and adsorption deterioration in physical adsorption systems. Renewable and Sustainable Energy Reviews 2010; 14(1):344e53.

[34] Wang K, Wu JY, Xia ZZ, Li SL, Wang RZ. Design and performance prediction of a novel double heat pipes type adsorption chiller for fishing boats. Renewable Energy 2008; 33(4):780–90.

[35] El-Sharkawy II, Saha B B, Koyama S, He J, Ng KC, Yap C. Experimental investigation on activated carbon–ethanol pair for solar powered adsorption cooling applications. Int J Refrig 2008; 31:1407–13.

[36] El-Sharkawy II, Kuwahara K, Saha BB, Koyama S, Ng KC. Experimental investigation of activated carbon fibers/ethanol pairs for adsorption cooling system application. Appl Therm Eng 2006; 26:859–65.

[37] Saha BB, El-Sharkawy II, Chakraborty A, and Koyama S. Study on an activated carbon fiber ethanol adsorption chiller: Part I e system description and modeling. Int J Refrig 2007; 30:86–95.

[38] Saha BB, El-Sharkawy II, Chakraborty A, Koyama S. Study on an activated carbon fiber ethanol adsorption chiller: Part II e performance evaluation. Int J Refrig 2007; 30:96–102.

[39] Y. Zhong, R.E. Critoph, R.N. Thorpe, Z. Tamainot-Telto, Dynamics of BaCl2 – NH3 Adsorption Pair, Applied Thermal Engineering (2008), doi: 10.1016/j.applthermaleng.2008.06.015

[40] Wang, R.Z., R.G. Oliveira. 2006. "Adsorption refrigeration-An efficient way to make good use of waste heat and solar energy." Progress in Energy and Combustion Science 32(4):424-458.

[41] Guilleminot JJ, Choisier A, Chalfen JB, Nicolas S, Reymoney JL. Heat transfer intensification in fixed bed adsorbers. Heat Recov Syst CHP 1993; 13(4):297–300.

[42] Elton IM, Saying AAM. A simple method to enhance thermal conductivity of using some additives. Renewable Energy 1994; 4(1):111–5.

[43] Restuccia, G., Freni, A., Vasta, S., and Aristov, Y., "Selective Water Sorbent for Solid Sorption Chiller: Experimental Results and Modeling," *International Journal of Refrigeration*, vol. 27, no. 3, pp. 284-293, 2004.

[44] Munyebvu E. Heat transfer in monolithic charcoals for use in adsorption refrigeration systems. M.Sc. Thesis University of Warwick, Coventry 1994.

[45] Tamainot-Telto, Z. and Critoph, R. E.:2000, Thermophysical properties of monolithic carbon. *International Journal of Heat and Mass Transfer*, 43(11), 2053-2058.

[46] Guilleminot JJ, Meunier F, Paklesa J. Heat and mass transfer in a non-isothermal fixed bed solid adsorbent reactor: a uniform pressure-non-uniform temperature case. Int J Heat Mass Transfer 1987; 30(8):1595–606.

[47] Liu, Y. L., Wang, R. Z. and Xia, Z. Z.:2005, Experimental study on a continuous adsorption water chiller with novel design. International Journal of Refrigeration, 28 92), 218-230.

[48] Xia, Z. Z., Chen, C. J., Kiplagat, J. K., Wang, R. Z. and Hu, J. Q.:2008b, Adsorption Equilibrium of water on silica gel. Journal of Chemical & Engineering Data, 35 (10), 2462-2465.

[49] Hassan, H.Z., Mohamad, A.A. and Al-Ansary, H.A.:2012, Development of a continuously operating solar-driven adsorption cooling system: Thermodynamic analysis and parametric study. Applied Thermal Engineering, doi: 10.1016/j.applthermaleng.2012.04.040.

[50] Uyan, A. S., Akrisawa, A., Miyazaki, T., Ueda, Y. and Kashiwagi, T.:2009, Numerical analysis of an advanced three bed mass recovery adsorption refrigeration cycle. Applied Thermal Engineering, 29 (14-15), 2876-2884.

[51] Miyazaki, T., Akrisawa, A. and Saha, B. B.:2010, The performance analysis of novel dual evaporator type three-bed adsorption chiller. International Journal of Heat Recovery Systems, 5 (2), 133-141.

[52] Sato, K., Tanaka, S., Honda, K. Y. and Fujiwara: US5775126 (1998) and JP9303900 (1997).

[53] Alam, K. C. A., Akahira, A., Hamamoto, Y., Akrisawa, A. and Kashiwagi, T.:2004, A four-bed mass recovery adsorption refrigeration waste/renewable heat source. Renewable Energy, 29 (9), 1461-1475.

[54] K. Sato, H. Ishii, Y. Nagashima, S. Tanaka, S. Inoue,: JP2001215068 (2001).

[55] Critoph, R. E.:2001, Simulation of a continuous multiple-bed regenerative adsorption cycle. International Journal of Refrigeration, 24 (5), 428-437.

[56] Wang, R. Z.:2001, Performance improving of adsorption cooling by heat and mass recovery operation. International Journal of Refrigeration, 24 (7), 602-611.

[57] Sumathy, K., Yeung, K.H. and Yong, L.:2003, Technology development in the solar adsorption refrigeration system. Progress in Energy and Combustion Science, 29 (4), 301-327.

[58] Shelton SV. Ramp wave analysis of the solid/vapor heat pump. ASME Journal of Energy Resource Technology 1990; 112(3):69–78.

[59] Critoph, R.E., A forced convection regenerative cycle using the ammonia-carbon pair. In proceedings of Solid Sorption Refrigeration, Paris, 11R, 1992, pp. 80 85.

[60] Lai Hai-Ming. An enhanced adsorption cycle operated by periodic reversal forced convection. Applied Thermal Engineering 2000; 20:595–617.

[61] Critoph RE. Forced convection adsorption cycle with packed bed heat regeneration. International Journal of Refrigeration 1999; 22:38–46.

[62] Tierney, M. J.:2002, Feasibility of driven convective thermal wave chiller with low-grade heat. Renewable Energy, 33 (9), 2097-2108.

[63] Meunier, F.:1985, Second law analysis of a solid adsorption heat pump operating on reversible cascaded cycles; Application to the Zeolite-water pair. Journal of Heat Recovery System, 5 (2), 133-141.

[64] Liu, Y and Leong, K. C.:2006, Numerical study of a novel Cascaded adsorption cycle. International Journal of Refrigeration, 29 (2), 250-259.

[65] Leite APF, Daguenet M. Performance of a new solid adsorption ice maker with solar energy regeneration. Energy Convers Manage 2000; 41:1625–47.

[66] Anyanwu, E. E., & Ezekwe, C. I. 2003. Design, construction and test run of a solid adsorption solar refrigerator using activated carbon/methanol, as adsorbent/adsorbate pair. Energy Conversion and Management, 44(18), 2879-2892.

[67] Li M, Sun CJ, Wang RZ, Ca WD. Development of no valve solar ice maker. Appl Therm Eng 2004; 24:865–72.

[68] Passos FP. Etude des couples charbon actif/methanol et de leur application a la refrigerations solaire [Ph.D.] Lausanne: Ecole Polytechnique Federale de Lausanne; 1986. 101p.

[69] Nwamba, J. K., C. F. Meyer, and M. Mbarawa. "The Design and Evaluation of a Solarpowered Adsorption Refrigerator for African Conditions [Ms.]." Tshwane University of Technology, 2008.

[70] Critoph, R. E.:1999, Adsorption refrigerators and heat pump. Carbon Materials for Advanced Technologies, Edited by Timothy D. Burchell, Chap. 10, pp. 303-340, ISBN 0-08-042683-2.

[71] Jufang Wu, Marianne E. Stro¨mqvist, Ola Claesson, Ingrid E. Fa¨ngmark, and Lars-Gunnar Hammarstro¨m , "A Systematic Approach for Modelling the Affinity Coefficient in the Dubinin–Radushkevich Equation." Carbon 40 (2002) 2587–2596.

[72] Demir, H., Mobedi, M. and Ulku S., A review on adsorption heat pump: Problems and solutions. Renewable and Sustainable Energy Reviews (2008); 12: 2381–2403.

[73] Eckenfelder, W. W., Industrial Water Pollution Control, 3rd edition (1999); McGraw-Hill Science.

[74] Leite A.P.F., Grilo M.B., Andrade R.R.D., Belo F.A., 2004. Dimensioning, thermal analysis and experimental heat loss coefficients of an adsorptive solar icemaker. Renewable Energy 29, 1643-1663.

[75] J.A. Duffie and W. Beckman, 'Solar Energy Thermal Processes', John Wiley& Sons, Inc., 2006.

[76] Rommel M,Wagner A. Application of transparent insulation materials in improved flat-plate collectors and integrated collector storages. Solar Energy 1992;49:371–80.

[77] E.F. Passos, J.F. Escobedo, F. Meunier, Simulation of an intermittent adsorptive solar cooling system, Solar Energy 42 (2) (1989) 103-111.

[78] Li Yong and Sumathy, K., Review of Mathematical Investigation on the Closed Heat of Adsorption Pump and Cooling Systems, Renewable Sustainable Energy Rev., 2002, vol. 6, p. 305.

[79] Zhao Y, Hu E. and Blazewicz A., "Dynamic Modeling of an Activated Carbon–Methanol Adsorption Refrigeration Tube with Considerations of Interfacial Convection and Transient Pressure Process." Applied Energy 95 (2012): 276–284.

[80] E. E. Anyanwu, U. U. Oteh, and N. V. Ogueke, "Simulation of a solid adsorption solar refrigerator using activated carbon/methanol adsorbent/refrigerant pair," Energy Conversion and Management, vol. 42, no. 7, pp. 899–915, 2001.

[81] R.Z. Wang, M. Li, Y.X. Xu and J.Y. Wu, An energy efficient hybrid system of solar powered water heater and adsorption ice maker, Solar Energy, vol. 68, pp. 189- 195, 2000.

[82] Watmuff, J.H., Charters, W.W.S., Proctor, D., 1977. Solar and wind induced external coefficients for solar collectors. International Revued'Heliotechnique 2, 56.

[83] Zhao Y, Hu E. and Blazewicz A., "A Comparison of Three Adsorption Equations and Sensitivity Study of Parameter Uncertainty Effects on Adsorption Refrigeration Thermal Performance Estimation." *Heat Mass Transfer* (2012) 48:217–226.

[84] El-Sharkawy, I.I., Hassan, M., Saha, B.B., Koyama, S., Nasr, M.M., Study on adsorption of methanol onto carbon based adsorbents. *Int. J. Refrigeration* 32 .7 (2009), 06-011.

[85] Henninger, S.K., Schicktanz, M., Hugenell, P.P.C., Sievers, H., and Henning, H.-M., "Evaluation of methanol adsorption on activated carbons for thermally driven chillers part I: Thermophysical characterization." *International Journal of Refrigeration* 35.3 (2012), 543-553.

VITA

Name	: Naef Abduljalil Abdulrahman Qasem
Nationality	: Yemeni
Date of Birth	: 29/8/1983
Email	: naifaglil2002@yahoo.com
Permanent Address	: Taiz University - Taiz - Yemen
Present Address	: King Fahd University of Petroleum and Minerals –Dhahran – Saudi Arabia.
Tel.	: +966 535483440
	: +967 71179840
Academic Background	: Bachelor of Mechanical Engineering – King Khalid University (KKU) – Abha, Saudi Arabia - February, 2008